

**BENZOTHAZOLE MOIETY LIQUID CRYSTALLINE
MONOMERS CONTAINING SCHIFF BASE-ESTER:
THERMAL, MESOMORPHIC AND OPTICAL PROPERTIES**

NUR SYAFIQAH FARHANAH BINTI DZULKHARNIEN

**FACULTY OF SCIENCE
UNIVERSITY OF MALAYA
KUALA LUMPUR**

2018

**BENZOTHAIAZOLE MOIETY LIQUID CRYSTALLINE
MONOMERS CONTAINING SCHIFF BASE-ESTER:
THERMAL, MESOMORPHIC AND OPTICAL
PROPERTIES**

NUR SYAFIQAH FARHANAH BINTI DZULKHARNIEN

**DISSERTATION SUBMITTED IN FULFILMENT OF THE
REQUIREMENTS FOR THE DEGREE OF MASTER OF
SCIENCE (EXCEPT MATHEMATICS & SCIENCE
PHILOSOPHY)**

**DEPARTMENT OF CHEMISTRY
FACULTY OF SCIENCE
UNIVERSITY OF MALAYA
KUALA LUMPUR**

2018

UNIVERSITY OF MALAYA
ORIGINAL LITERARY WORK DECLARATION

Name of Candidate: **NUR SYAFIQAH FARHANAH BINTI DZULKHARNIEN**

Matric No: **SGR150047**

Name of Degree: **DEGREE OF MASTER OF SCIENCE (EXCEPT
MATHEMATICS & SCIENCE PHILOSOPHY**

Title of Project Paper/Research Report/Dissertation/Thesis (“this Work”):

**BENZOTHAZOLE MOIETY LIQUID CRYSTALLINE MONOMERS
CONTAINING SCHIFF BASE-ESTER: THERMAL, MESOMORPHIC AND
OPTICAL PROPERTIES**

Field of Study: **POLYMER CHEMISTRY**

I do solemnly and sincerely declare that:

- (1) I am the sole author/writer of this Work;
- (2) This Work is original;
- (3) Any use of any work in which copyright exists was done by way of fair dealing and for permitted purposes and any excerpt or extract from, or reference to or reproduction of any copyright work has been disclosed expressly and sufficiently and the title of the Work and its authorship have been acknowledged in this Work;
- (4) I do not have any actual knowledge nor do I ought reasonably to know that the making of this work constitutes an infringement of any copyright work;
- (5) I hereby assign all and every rights in the copyright to this Work to the University of Malaya (“UM”), who henceforth shall be owner of the copyright in this Work and that any reproduction or use in any form or by any means whatsoever is prohibited without the written consent of UM having been first had and obtained;
- (6) I am fully aware that if in the course of making this Work I have infringed any copyright whether intentionally or otherwise, I may be subject to legal action or any other action as may be determined by UM.

Candidate’s Signature

Date:

Subscribed and solemnly declared before,

Witness’s Signature

Date:

Name:

Designation:

**BENZOTHAZOLE MOIETY LIQUID CRYSTALLINE MONOMERS
CONTAINING SCHIFF BASE-ESTER: THERMAL, MESOMORPHIC AND
OPTICAL PROPERTIES**

ABSTRACT

A series of Schiff base ester chromophore based liquid crystalline monomers with rigid core benzothiazole ring and methacrylate group as terminal groups was designed and synthesized via Schiff base formation reaction followed by Williamson etherification and esterification reactions. These monomers were differentiated from each other by varying the substituents (-CH₃, -OCH₃ and -OCH₂CH₃) at the sixth position on benzothiazole moiety. The chemical structures of the synthesized monomers were characterized and confirmed by spectroscopic techniques such as FTIR, ¹H NMR and ¹³C NMR. Thermogravimetric analysis (TGA) was used to study the thermal stability as well as thermal properties of the synthesized monomers. The monomer with ethoxy substituent (**M4**) showed the highest thermal stability compared to other monomers by comparing the decomposition temperatures corresponding to 5% weight loss for each of the monomers. The mesomorphic behavior for all liquid crystalline monomers was studied by using differential scanning calorimetry (DSC) and polarized optical microscopy (POM). POM studies revealed that monomer with no substituent at the sixth position of benzothiazole ring exhibited nematic and smectic mesophases at 120.7 °C and 74.2 °C respectively, upon cooling. Meanwhile, monomers with -CH₃, -OCH₃ and -OCH₂CH₃, revealed only nematic mesophase at 108.4 °C, 109.1 °C and 119.8 °C accordingly, during heating scan. The mesophase textures from POM observation are supported by corresponding DSC results. These results suggest that the formation of mesophases and that the mesophase stability of monomers **M1** - **M4** were influenced by the terminal substituents. The effects of substituents, solvent polarity and temperature on the optical

properties of monomers **M1** - **M4** were evaluated with UV-Vis and fluorescence spectroscopies. It was found that the absorption and emission maxima of the monomers were red-shifted by the influence of various strength of electron-donating groups on the sixth position of benzothiazole moiety. The fluorescence studies showed that the monomers **M1** - **M4** exhibited a range of emission band at 401-500 nm which can be categorized as violet-blue emission. Furthermore, an investigation on the effect of different solvents showed that all the monomers exhibited a polytonic behavior upon increasing solvent polarity for absorption spectra. This result was further discussed using Reichardt-Dimroth solvent scales, $E_T(30)$ and Kamlet-Taft solvent scales. The thermochromic behavior of these monomers was evaluated using fluorescence spectroscopy from 20 °C to 55 °C. The fluorescence intensity for all monomers was decreased with respect to increase in temperature without shifting their emission band.

Keywords: Schiff base-ester; benzothiazole; monomer; mesomorphic behavior, thermal and optical properties.

**MOEITI BENZOTHIAZOLE MONOMER CECAIR KRISTAL
MENGANDUNGI ASAS SCHIFF ESTER: CIRI-CIRI TERMA, MESOMORFIK
DAN OPTIKAL**

ABSTRAK

Satu siri monomer cecair kristal yang berasaskan kromofor Schiff dan ester bersama teras cincin benzothiazole dan kumpulan metakrilat telah direka dan disintesis melalui pembentukan yang berasaskan Schiff diikuti dengan pengetheran Williamson dan tindak balas pengesteran. Monomer-monomer ini dibezakan antara satu sama lain dengan mempelbagaikan unit gantian (-CH₃, -OCH₃, -OC₂H₅) pada kedudukan ke-enam pada rangka benzothiazole. Struktur kimia kesemua monomer yang telah disintesis disahkan melalui teknik spektroskopi seperti FTIR, ¹H NMR dan ¹³C NMR. Analisis thermogravimetrik (TGA) telah digunakan untuk mengkaji kestabilan terma dan juga ciri-ciri terma yang ada pada monomer-monomer yang disintesis. Monomer yang mempunyai unit gantian etoksi (M4) menunjukkan kestabilan terma yang paling tinggi berbanding monomer-monomer yang lain dengan membandingkan suhu penguraian yang merujuk kepada 5% kehilangan berat dalam julat untuk setiap monomer. Ciri-ciri mesomorfik untuk kesemua monomer cecair kristal telah dikaji dengan menggunakan DSC dan POM. Kajian POM menunjukkan monomer yang tidak mempunyai unit gantian pada kedudukan ke-enam cincin benzothiazole mempamerkan mesofasa smektik dan nematik pada suhu 120.7 °C dan 74.2 °C masing-masing, semasa penyejukan. Manakala, monomer-monomer dengan unit gantian -CH₃, -OCH₃ dan -OCH₂CH₃, menunjukkan mesofasa nematik sahaja pada suhu 108.4 °C, 109.1 °C dan 119.8 °C mengikut turutan, ketika pemanasan. Tekstur mesofasa daripada pemerhatian POM disokong oleh keputusan DSC masing-masing. Ini menunjukkan bahawa pembentukan mesofasa serta kestabilan mesofasa untuk setiap monomer dipengaruhi oleh unit gantian. Kesan perbezaan unit gantian, pelarut dan suhu pada ciri-ciri optikal monomer-monomer M1 - M4 dinilai dengan

menggunakan spektroskopi UV-Vis dan pendarfluor. Keputusan menunjukkan penyerapan dan pelepasan maksima mengalami peralihan merah dengan dipengaruhi oleh pelbagai kekuatan kumpulan penderma pada kedudukan ke-enam rangka benzothiazole. Kajian terhadap pelepasan menunjukkan bahawa monomer-monomer **M1** - **M4** mempamerkan kumpulan pelepasan dengan jarak 401-500 nm yang boleh dikategorikan sebagai cahaya violet-biru. Selain itu, kajian tentang kesan perbezaan pelarut menunjukkan kesemua monomer mempamerkan sifat politonik dengan penambahan kekutuban pelarut pada penyerapan maksima. Keputusan ini dikaji dengan lebih mendalam menggunakan skala pelarut Reichardt-Dimroth, $E_T(30)$ and skala pelarut Kamlet-Taft. Ciri-ciri termokromic pada monomer-monomer ini dinilai dengan spektroskopi pendarfluor dari 20 °C sehingga 55 °C. Keamatan pendarfluor untuk kesemua monomer berkurangan dengan penambahan suhu tanpa mengubah kedudukan pelepasan.

Kata kunci: Asas Schiff-ester; benzothiazole; monomer; sifat mesomorfik, ciri-ciri terma dan optikal.

ACKNOWLEDGEMENTS

Firstly, I would like to express my gratitude to my supervisors, Dr. Noordini Binti Mohamad Salleh and Prof. Dr. Rosiyah Yahya for their sincere support, encouragement and valuable advices that helped me a lot throughout my research period. I would like to thank to the technical staff especially to Mr. Zulkifli Abu Hasan for the continuous help in setting up the lab equipment and all the Chemistry Department staff who are directly or indirectly involved in my research work.

My sincere thanks and appreciation to all, who have provided assistance throughout the course of the research, particularly to Dr. Mehran Fadaeinasab, Madam Dara Fiona Binti Mohamad and Mr. Zakaria bin Ahmat for helping me out on running ^1H NMR and ^{13}C NMR instruments. Many thanks also to Prof. Dr. Aziz bin Hassan for allowing me to use DSC instrument and Dr. Nor Mas Mira Abd. Rahman as well as Dr. Rabiul Mohd. Karim for their support and advices regarding on my research work.

I would like to express my utmost gratefulness to my beloved parents, Mr. Dzulkharnien Bin Osman and Mrs. Rashidah Binti Ibrahim as well as my siblings and friends for their constant support, understanding, and prayers. Without their support, I think I might not be able to complete my thesis as well. Finally, I also would like to acknowledge the financial support from University of Malaya (Grant No.: FP043-2016) during the whole candidature time.

TABLE OF CONTENTS

Abstract	iii
Abstrak	v
Acknowledgements	vii
Table of Contents	viii
List of Figures	xii
List of Tables	xvi
List of Schemes	xvii
List of Symbols and Abbreviations	xviii
List of Appendices	xx
CHAPTER 1: INTRODUCTION	1
1.1 Fundamental of liquid crystals	1
1.2 History of liquid crystals	3
1.3 Classification of liquid crystals	5
1.4 Calamitic liquid crystals	7
1.5 Basic types of liquid crystals	8
1.5.1 Nematic mesophase	9
1.5.2 Smectic mesophase	10
1.5.3 Cholesteric mesophase	11
1.6 Problem statement	12
1.7 Objectives	13
1.8 Thesis outline	14
CHAPTER 2: LITERATURE REVIEW	16
2.1 Liquid crystalline compound bearing heterocyclic moiety	16

2.2	Schiff base ester based liquid crystals	19
2.3	Schiff base-benzothiazole moiety based compounds	23
2.4	Structure-mesomorphic properties relationship.....	25
2.4.1	Effect of mesogenic core in mesomorphic behavior	26
2.4.2	Effect of linking group on mesomorphic behavior.....	28
2.4.3	Effect of length of flexible spacer on mesomorphic behavior	31
2.4.4	Effect of terminal substituents on mesomorphic behavior	33
2.5	Effect of environment on liquid crystal compounds.....	35
2.5.1	Influence of solvents on liquid crystalline compounds	35
2.5.2	Influence of temperature on liquid crystal compounds	38
CHAPTER 3: EXPERIMENTAL		40
3.1	Materials and reagents	40
3.2	Synthesis of liquid crystal monomers.....	40
3.2.1	Synthesis of monomer M1	41
3.2.2	Synthesis of monomer M2	46
3.2.3	Synthesis of monomer M3	48
3.2.4	Synthesis of monomer M4	50
3.3	Characterization methods and instrumentations.....	52
3.3.1	Nuclear Magnetic Resonance Spectroscopy (NMR).....	52
3.3.2	Fourier Transform Infrared Spectroscopy (FTIR).....	53
3.3.3	CHN Analysis.....	53
3.3.4	Differential Scanning Calorimetry (DSC).....	53
3.3.5	Polarized Optical Microscopy (POM).....	54
3.3.6	Thermogravimetric Analysis (TGA).....	54
3.3.7	UV-Visible (UV-Vis) and Photoluminescence Spectrometry.....	55

CHAPTER 4: RESULTS AND DISCUSSION	56
4.1 LC monomers and mechanism	56
4.1.1 Schiff base formation	58
4.1.2 Williamson etherification reaction	59
4.1.3 Steglich esterification reaction	60
4.2 Structural determination	61
4.2.1 ¹ H NMR spectra	62
4.2.2 ¹³ C NMR spectra	65
4.2.3 FTIR spectra	67
4.3 Solubility behavior.....	69
4.4 Thermal properties of M1 – M4	69
4.5 Mesomorphic behavior of M1 – M4	72
4.5.1 Effect of thermal substituents on mesogenic unit.....	72
4.5.2 Structural-mesomorphic relationship	81
4.6 Optical properties of M1 – M4	84
4.6.1 Effect of different solvents on monomers	84
4.6.2 Correlation by solvent polarity scales	87
4.6.2.1 Reichardt-Dimroth solvent scale	88
4.6.2.2 Kamlet-Taft solvent scale.....	89
4.6.3 Effect of different strengths of electron-donating groups	92
4.6.4 Effect of temperature on monomers	94
 CHAPTER 5: CONCLUSIONS & SUGGESTIONS FOR FUTURE STUDIES ...	96
5.1 Conclusions	96
5.2 Suggestions for future studies.....	97
 References	99

List of Publications and Papers Presented	110
Appendix	112

University of Malaya

LIST OF FIGURES

Figure 1.1: Arrangements of molecules in the solid, liquid crystals and liquid Adopted from (Hoogboom et al., 2007).....	1
Figure 1.2: Structure of the first liquid crystalline compound, cholesteryl benzoate Redrawn from (Ermakov et al., 2016).	3
Figure 1.3: Molecular structures of (a) calamitic (b) discotic (c) bent-shaped liquid crystals. Redrawn from (Senyuk, 2011).....	6
Figure 1.4: General structure template of calamitic liquid crystal. Adopted from (Hudson & Maitlis, 1993).	7
Figure 1.5: Illustration of molecular orientation in (a) SmA and (b) SmC mesophases. Adopted from (Dierking & Al-Zangana, 2017).	10
Figure 1.6: Molecular arrangement of chiral nematic mesophase. Adopted from (Dumanli & Savin, 2016).	12
Figure 1.7: Molecular structure of a series of benzothiazole liquid crystalline monomers containing Schiff base-ester group.....	13
Figure 2.1: A series of azo-benzothiazole compounds (Karim et al., 2013).	16
Figure 2.2: Liquid crystalline compounds bearing benzothiazole (Dutta et al., 2010).	17
Figure 2.3: Four series of new liquid crystalline compounds (Chia & Lin, 2013).	19
Figure 2.4: Schiff base ester group with fluorinated group (Ha & Lee, 2014).	20
Figure 2.5: 5-chloro-2-(4-alkanoyloxybenzylidenamino)benzoxazoles (Ha et al., 2011).	21
Figure 2.6: Molecular structures of intermediate and final product of trimeric star shaped LC compounds (Ooi et al., 2013).	22
Figure 2.7: 6-methoxy-2-(4-alkanoyloxybenzylidenamino)benzothiazoles liquid crystal compounds (Ha et al., 2010).	24

Figure 2.8: Liquid crystalline dimers containing Schiff base benzothiazole moiety (Foo et al., 2015).	24
Figure 2.9: 2-[4-(4- <i>n</i> -alkoxybenzoyloxy) phenylazo]-6-fluorobenzothiazoles (Series 1) and 2-[4-(4- <i>n</i> -alkoxybenzoyloxy) naphtha-1-ylazo]-6-fluorobenzothiazoles (Series 2) (Thaker et al., 2013).	26
Figure 2.10: Liquid crystalline compounds containing different mesogenic groups (Yeap et al., 2010).	27
Figure 2.11: Two series of liquid crystalline compounds with chalcone as central linkage (Thaker & Kanojiya, 2011).	28
Figure 2.12: Azo substituted bent-core compounds (Nagaveni et al., 2012).	30
Figure 2.13: A series of non-symmetric liquid crystal dimers (Seou et al., 2014).	31
Figure 2.14: Series of calamitic isoflavone ester with different length of alkanoyloxy chain (Yam & Yeap, 2011).	32
Figure 2.15: Azo ester based liquid crystalline compounds (Naoum et al., 2011).	33
Figure 2.16: a) Liquid crystalline compounds containing imine and ester linker b) a series of LC compounds with imine group (Yeap et al., 2015).	34
Figure 2.17: A series of 4-alkoxybenzoic acid liquid crystalline derivatives (Sıdır et al., 2015).	36
Figure 2.18: Liquid crystalline compound with different fluoro substituents (Praveen & Ojha, 2012).	37
Figure 3.1: ¹ H NMR spectra of M1	46
Figure 3.2: ¹ H NMR spectra of M2	47
Figure 3.3: ¹ H NMR spectra of M3	49
Figure 3.4: ¹ H NMR spectra of M4	51
Figure 4.1: Mechanism of Schiff base reaction. Redrawn from (Islam et al., 2018).	58

Figure 4.2: Reaction mechanism of Williamson etherification. Redrawn from (Solomons & Fryhle, 2000).	59
Figure 4.3: Early stage of Steglich esterification reaction. Adopted from (Yan et al., 2012).	60
Figure 4.4: Role of DMAP in Steglich esterification reaction. Adopted from (Tsakos et al., 2015).	61
Figure 4.5: ^1H NMR spectra of M1	63
Figure 4.6: ^{13}C NMR spectra of M1	65
Figure 4.7: FTIR spectra for M1	68
Figure 4.8: TG traces of M1 - M4	70
Figure 4.9: DTG curves of LC monomers.	70
Figure 4.10: DSC thermograms of (a) M1 (b) M2 - M4	74
Figure 4.11: Optical photomicrographs (magnification $\times 50$) of M1 observed under POM upon cooling cycle: (a) nematic droplets texture at 120.7 $^{\circ}\text{C}$ (b) marble texture of nematic phase at 113.7 $^{\circ}\text{C}$ and (c) smectic phase showing schlieren texture at 74.2 $^{\circ}\text{C}$	75
Figure 4.12: The optical textures (magnification $\times 50$) of M2 observed under POM. (a) crystalline texture at room temperature and (b) schlieren texture of nematic phase at 108.4 $^{\circ}\text{C}$	76
Figure 4.13: The optical textures (magnification $\times 50$) of M3 observed under POM. (a) large nematic droplets at 113.2 $^{\circ}\text{C}$, (b) fine grain texture of nematic phase at 103.3 $^{\circ}\text{C}$ and (c) nematic droplets with thread-like texture at 109.1 $^{\circ}\text{C}$	77
Figure 4.14: The optical textures (magnification $\times 50$) of M4 observed under POM. (a) schlieren texture of nematic phase at 118.9 $^{\circ}\text{C}$, (b) schlieren texture with four-dark brushes of nematic phase at 114.9 $^{\circ}\text{C}$ and (c) schlieren texture of nematic phase at 119.8 $^{\circ}\text{C}$	78

Figure 4.15: Molecular structures and molecular lengths of monomers M1 – M4 . The molecular lengths of the studied compounds were calculated from the most extended conformation with optimized energy level by simple molecular modelling (MM2 energy parameters derived from ChemBio3D Ultra 11.0 software).	80
Figure 4.16: A series of azo-ester based liquid crystalline monomers (Karim et al., 2013).	81
Figure 4.17: UV-Vis absorption spectra for M1 - M4 in different solvents.	85
Figure 4.18: Photoluminescence emission spectra of M1 - M4 in various solvents.	86
Figure 4.19: Plot of absorption frequency (ν_{\max} in 10^{-3} cm^{-1}) of M1 - M4 versus the E_T (30) values in various solvents.	88
Figure 4.20: Experimental versus calculated values of ν_{\max} for all investigated monomers using (a) Reichardt-Dimroth and (b) Kamlet Taft solvent scales.	91
Figure 4.21: (a) Absorption and (b) emission spectra for M1 - M4 in dilute THF.	92
Figure 4.22: Emission fluorescence spectra of M1 – M4 in THF at different temperatures.	94

LIST OF TABLES

Table 4.1: Molecular structure and yield of synthesized LC monomers.	56
Table 4.2: ^1H NMR chemical shifts of different types of protons present in M1 - M4 . ..	64
Table 4.3: ^{13}C NMR chemical shifts of various types of carbons present in M1 - M4 . ..	66
Table 4.4: General FTIR absorption spectra for M1 - M4	68
Table 4.5: Thermal analysis data for M1 - M4	71
Table 4.6: Mesophase length, phase transitions, and enthalpy changes for M1 - M4 upon heating and cooling scans.....	73
Table 4.7: Comparison on thermal, mesomorphic and optical properties M1 - M4 and M5 - M8	82
Table 4.8: Absorption and PL emission maxima spectra M1 - M4 in selected solvents.	84
Table 4.9: Data of linear correlations between the absorption wavenumbers ν_a (cm^{-1}) of M1- M4 and $E_T(30)$ values (cm^{-1}) for n different solvents, according to $\nu_a = \nu_0 + S \cdot E_T(30)$ as Eq. 1, with r as correlation coefficient.	88
Table 4.10: Solvatochromic parameters for M1 - M4 using Kamlet-Taft approach.	90
Table 4.11: Observed and calculated absorption maxima for all monomers in various solvents.	92

LIST OF SCHEMES

Scheme 3.1: Synthesis of 4-(benzothiazol-2-yliminomethyl)-phenol (1a).	41
Scheme 3.2: Synthesis of 4-(6-hydroxyhexyloxy)benzoic acid (2).	42
Scheme 3.3: Synthesis of 4-(6-methacryloxyhexyloxy)benzoic acid (3).	43
Scheme 3.4: Synthesis of 4-[6-(2-Methyl-acryloyloxy)-hexyloxy]-benzoic acid 4-(benzothiazol-2-yliminomethyl)-phenyl ester (M1).	44
Scheme 4.1: Synthetic route of LC monomers, M1 - M4	57

University of Malaya

LIST OF SYMBOLS AND ABBREVIATIONS

ATR	:	Attenuated total reflectance
CDCl ₃	:	Deuterated chloroform
CHCl ₃	:	Chlorofom
D-A	:	Donor-acceptor
DCC	:	<i>N,N'</i> -dicyclohexylcarbodiimide
DCM	:	Dichloromethane
DHU	:	Dicyclohexylurea
DMAP	:	<i>p</i> -Dimethylaminopyridinie
DMF	:	<i>N,N</i> -dimethylformamide
DMSO- <i>d</i> ₆	:	Deuterated dimethylsulfoxide
DSC	:	Differential Scanning Calorimetry
DTG	:	Derivative thermogravimetric
E _T (30)	:	Reichardt-Dimroth solvent scale parameter
FLC	:	Ferroelectric liquid crystal
FTIR	:	Fourier Transform Infrared Spectroscopy
GM	:	Goldstone mode
LCD	:	Liquid crystal display
LCs	:	Liquid crystals
MBBA	:	<i>N</i> -(<i>p</i> -methoxybenzylidene)- <i>p-n</i> -butylaniline
NMR	:	Nuclear Magnetic Resonance Spectroscopy
OSC	:	Organic semiconductor
PAA	:	Para-azoxyanisole
PC	:	Personal computer
PL	:	Photoluminescent

PLCs	:	Polymer liquid crystals
POM	:	Polarized Optical Microscopy
Ppm	:	parts per million
PXRD	:	Powder X-ray diffraction
SAXS	:	Small angle X-ray scattering
SmA	:	Smectic A
SmC	:	Smectic C
T _d	:	Decomposition temperature
T _g	:	Glass transition temperature
T _m	:	Melting temperature
T _{NI}	:	Nematic-isotropic temperature
TGA	:	Thermogravimetric Analysis
THF	:	Tetrahydrofuran
UV	:	Ultra-violet
XRD	:	X-ray diffraction
%T	:	Transmittance
λ _{max}	:	Maxima wavelength
π*	:	Dipolarity/polarizability
A	:	Hydrogen bond donor acidities
B	:	Hydrogen bond acceptor basicities
ν _(max)	:	Maxima frequency
ν _R	:	Relaxation frequency

LIST OF APPENDICES

Appendix A: FTIR Figures.	112
Appendix B: ^1H NMR Figures.....	117
Appendix C: ^{13}C NMR Figures.....	120
Appendix D: TGA Figures.....	123

University of Malaya

CHAPTER 1: INTRODUCTION

1.1 Fundamental of liquid crystals

Solids and liquids are the most common states of matter and can be differentiated with each other easily as their molecules possess different amount of order. The molecules in crystalline solids are arranged themselves by occupying a specific position as well as oriented in a specific way (Müller & Chentanez, 2011). On the contrary, for liquid state, molecules possess neither long-range positional order nor orientation order. Another type of matter, which is known as liquid crystal phase, was discovered by Lehmann in 1888 and had been studied extensively among the researchers in the past several decades due to its fascinating properties for various applications. This phase can be categorized as an intermediate state of matter, in between the liquid phase and the crystal solid phase.

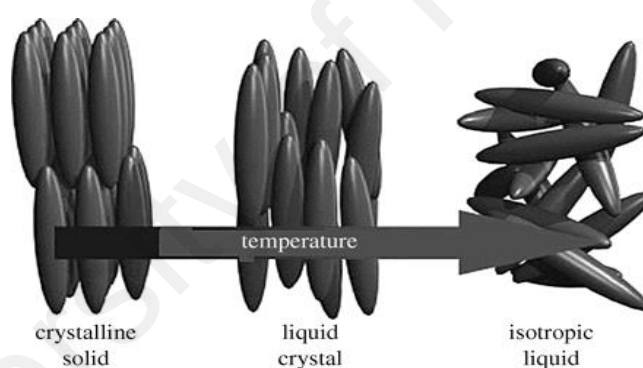


Figure 1.1: Arrangements of molecules in the solid, liquid crystals and liquid Adopted from (Hoogboom et al., 2007).

Figure 1.1 shows a schematic representation of molecular arrangements in the solid, liquid crystal and liquid phases. Solids are well known for their rigidity, incompressibility and mechanical strength ability. These features are mostly due to their molecules being closely packed and rigidly held together by intermolecular bonds giving rise to a highly ordered crystalline form. The molecules in solid are able to occupy certain position and each molecule must maintain a specific orientation, namely the positional and orientational order, respectively. In addition, the molecules in solids possess long-

range order as the center mass of the molecules are located on a three-dimensional periodic lattice. Consequently, the X-ray diffraction patterns show sharp Bragg peaks (Vertogen & de Jeu, 2012). This type of matter is called anisotropic as the properties of materials are much dependable on the crystallographic orientation direction.

Increasing the temperature to melting temperature, the crystalline form melts as the thermal energy causes the intermolecular bonding in the molecules to break down. Thus, both the positional and orientation orders are lost. The molecules are free to diffuse in a random fashion, constantly bumping into each other and abruptly changing their direction of motion. This describes that the material is in the liquid state. Due to the randomness of molecular orientation in the liquid state, the material could exhibit fluidic properties such as ability to flow and change their shapes in response to weak outside forces (Kumar, 2016). The liquid state is also called isotropic because the properties of the material are the same in all directions. In contrast to solid state, the X-ray diffraction patterns show broad reflections corresponding to short-range structure.

In between solid and liquid phases, there is another state that had been discovered in late 1880s, called the liquid crystal phase. This intermediate state of matter was also known as “mesophase”. Liquid crystals (LCs) or mesophases are intermediate state of matter, in between anisotropic solid and isotropic liquid, and they possess long-range orientational order but lost some of the positional order along some directions of space (Ghanem & Al-Hariri, 2013). When a material is melted to a certain temperature before it reaches the isotropic temperature, this material will apparently exhibit a turbid and viscous melt which gives rise to the liquid crystalline phase. At this stage, the molecules will start to lose their positional order but at the same time some of the orientational order is remained. In other words, the molecules in these mesophases, show some degree of orientational order even though the crystal lattice has been destroyed. Thus, they exhibit

both properties of crystal and liquid, lie fluidic in nature like a liquid, giving rise to various interesting properties. At a higher temperature, this mesophase will flow and becomes clear, resulting in the isotropic liquid.

1.2 History of liquid crystals

In year 1888, an Austrian botanist named Friedrich Reinitzer, described his observations of the colored phenomena occurring in melts of cholesteryl acetate and cholesteryl benzoate. He noticed that cholesteryl benzoate compound exhibited two obvious different melting points. In his experiment, Reinitzer observed that a solid sample of cholesteryl benzoate (Figure 1.2) changed into a cloudy liquid at 145.5 °C and as the temperature was further increased to 178.5 °C, the cloudy phase turn into a clear, transparent liquid (Ermakov et al., 2016). This discovery has been acknowledged among the researchers as the first recorded documentation in the history of liquid crystal.

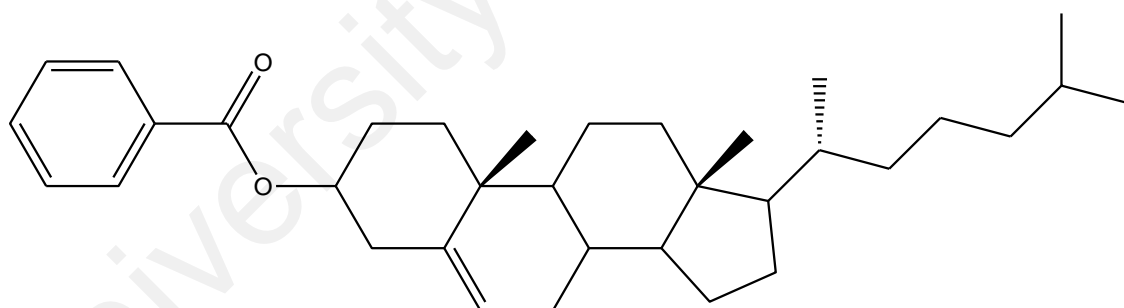


Figure 1.2: Structure of the first liquid crystalline compound, cholesteryl benzoate Redrawn from (Ermakov et al., 2016).

Due to his curiosity, Reinitzer sent some of his samples to Otto Lehman, who was an expert in the crystal optics using his advanced polarizing microscopes, for further investigation. Lehman showed a high interest towards the liquid crystal as it could exist with a softness like anisotropic crystal and could also act nearly like isotropic liquid. To describe this apparent observation, Lehmann used the term “Fliessende Krystalle” which

means flowing or fluid crystal for these states before it changes into liquid crystal later on. In addition, Friedel proposed that it would be preferable to refer the liquid crystalline state as a *mesophase*, which is derived from Greek word, *mesos*, means intermediate, and *phasis*, which can be defined as a state or phase, to stress the intermediate nature of these states of matter (Gray, 1962). Both of these terminologies to describe intermediate phase between solid crystalline and liquid states were still used until today.

After the discovery of the first LC compound (cholestryl benzoate), a vast number of new LC materials has been designed over the last hundred and thirty years. In 1890, Ludwig Gattermann described the synthesis of para-azoxyanisole (PAA), a compound that exhibits mesophases at temperatures between 116 °C and 134 °C. Mauguin (Cristaldi et al., 2009) used this new synthesized compound to study the behavior of LC thin layers confined between plates and observed a birefringent liquid films with a helicoidal structure. In the following years, the physical chemist named Rudolf Schenck reported twenty-four new LC compounds while Daniel Vorlander and his co-workers synthesized hundreds of LC compounds as well as the first thermotropic smectic compound. Besides designing new LC compounds, Friedel, a crystallographer also formulated basic laws concerning the external morphology and internal structure of the crystals. He was the first scientist who clarified that LCs could be divided into three types of molecular organizations, which are smectic, nematic and cholesteric liquid crystals. Between 1920s and 1940s, Carl W. Oseen and Hans Zocher developed mathematical model for the study of liquid crystals and introduced order parameter (Cristaldi et al., 2009).

1.3 Classification of liquid crystals

Liquid crystals are divided into two main classes which are thermotropic liquid crystals and lyotropic liquid crystals. These two types of liquid crystals can be identified through the difference in their self-organization mechanism according to the changes in the environment, either temperature or media.

The most widely used LCs and extensively studied for their linear as well as nonlinear optical properties, are thermotropic liquid crystals. The term “thermotropic” arises as the liquid crystal materials exhibit different textures upon temperature change. Below the melting point temperature, the thermotropic liquid crystals are in the form of crystalline state. A thermotropic phase can be formed by heating the solid or cooling the isotropic material as long as it does not exceed the decomposition temperature. The process is usually reversible by lowering the temperature, though there may be slight temperature differences. Among the thermotropic LCs there are two fundamental classes of substances, which are enantiotropic and monotropic liquid crystals. Materials that are able to form mesophase state by both cooling a liquid and heating a solid are known as enantiotropic liquid crystal. Meanwhile, those that are known as monotropic, can only enter the liquid crystal state either by cooling or heating, but not both methods (Cristaldi et al., 2009). Thermotropic liquid crystal materials are useful in electro-optic displays, temperature and pressure sensors.

On the other hand, materials that exhibit liquid crystal phases by dissolving them in sufficiently high solute concentration of isotropic solvent are called lyotropic liquid crystal. The term “lyo” comes from the Greek word, *liein*, which means “to dissolve”. The most common systems are those formed by water and amphiphilic molecules (individual molecules that contain two distinct regions, a hydrophilic part that interacts strongly with water and a hydrophobic part that is water insoluble) (Collings & Hird,

2017). Lyotropic liquid crystal materials play an important role in living systems and biological studies (Khoo, 2007). However, lyotropic liquid crystals will not be covered in this thesis.

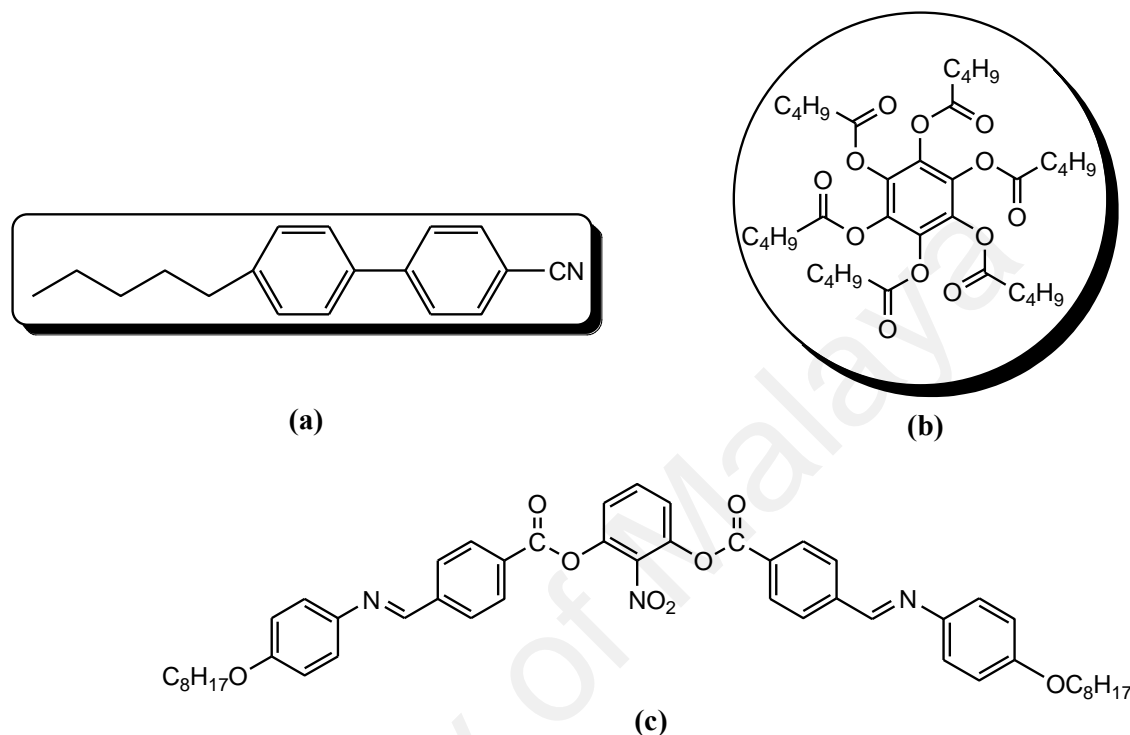


Figure 1.3: Molecular structures of (a) calamitic (b) discotic (c) bent-shaped liquid crystals. Redrawn from (Senyuk, 2011).

Liquid crystalline compounds are commonly classified into three typical well-known categories which are (i) calamitic (rod-shaped), (ii) discotic (disc-shaped) and (iii) bent-shaped (banana-shaped) molecules. Figure 1.3 shows the molecular structure of calamitic, discotic and bent-shaped LCs that have been discovered by previous researchers (Senyuk, 2011). The existence of liquid crystallinity is basically influenced by the ratio of the longitudinal and lateral lengths for calamitic molecules, while the thickness and diameter play a crucial role for discotic molecules (Sarkar & Das, 2014). However, in this section, we will only be discussing the calamitic LCs.

1.4 Calamitic liquid crystals

Calamitic liquid crystal phase is the common liquid crystal that had been studied comprehensively among researchers. Calamitic phase is formed by a combination of rod- or lath- shaped molecules. In the early 1908, Vorlander and his co-workers had synthesized their first mesogenic compound by chance and established some rules to determine the relationship between the mesophase and the elongated molecular structure of their molecules. They concluded that the calamitic LC must possess molecules that are elongated in shape and have molecular length greater than molecular breadth. Besides that, the molecules must have some rigidity in its central region and flexible unit at the end of the molecule to form a rod-like liquid crystalline compound. Elongated molecules have less possibility to collide into each other as the molecules tend to point in the same direction, thus stabilize the formation of mesophase (Collings, 2002).

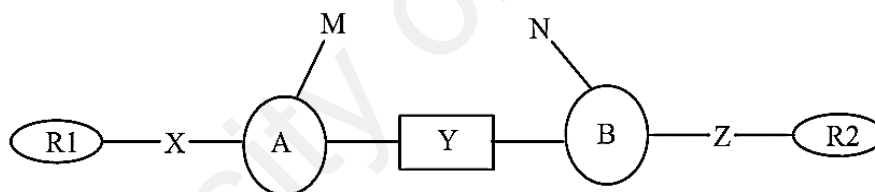


Figure 1.4: General structure template of calamitic liquid crystal. Adopted from (Hudson & Maitlis, 1993).

A schematic basic structure of a rod-like liquid crystal is shown in Figure 1.4 where A-B refer to the mesogenic group, X and Z are the flexible spacers, Y is the linking group, R1 and R2 represent the terminal units, lastly M and N refer to the lateral groups (Hudson & Maitlis, 1993). Generally, calamitic LC must contain a rigid core structure, which is made up from A-B ring system known as mesogen group. Usually, at least two ring systems are required to stabilize the calamitic phase and they are relatively stiff. However, these rules are exceptional to compounds with one ring system and readily forming dimers (Hudson & Maitlis, 1993). The flexible segments that are made up of

alkyl groups, X and Z, known as a spacer chain attached to each end of central benzene rings, will systematically decrease the melting temperature, thus resulting to the detection of mesomorphic properties in the molecules. These core units are connected to one another by a linking group Y. Common examples of linking group are stilbene (-CH=CH-), imine (-N=CH-), azo (-N=N-), acetylene (-C≡C-) and diacetylene (-C≡C-C≡C-) groups. It plays an important role in controlling the rigidity of the molecules (Demus et al., 2011). These type of groups are capable in reducing the freedom of rotation and thus influence the mesomorphic behavior.

R1 and R2, in Figure 1.4, called the terminal units, is another important component in the substances that could influence the liquid crystalline form. According to previous literature, most of the short terminal units and polar group substituents commonly favor the nematic mesophase. In order for molecules to exhibit a smectic mesophase, the molecules must arranged nicely into layers. Symmetrical molecules with two identical cores and two alkyl or alkoxy terminal units usually form a smectic mesophase. Anything that breaks the symmetry or makes it difficult for the molecules to pack tightly into layers will limit the formation of smectic mesophase. Lateral group substituents, M and N, on the core (e.g. halogens and methyl groups) or a central part that is relatively long compared to the length of the molecule will inhibit the possibility of smectic mesophase to form. These two factors will break the symmetry in the substance and makes the molecules difficult to pack tightly into layers (Collings, 2002).

1.5 Basic types of liquid crystals

Friedel had proposed that there are three basic types of liquid crystals known as nematic, smectic and cholesteric. Most of the compounds do not exhibit only one of these types, instead reveal more than one type of LC phase, such as smectic mesophase that are

slightly above the melting point and at higher temperature either the nematic or cholesteric type. These mesophases differ with each other in terms of their orientational order with respect to the long molecular axis.

1.5.1 Nematic mesophase

The word nematic which comes from Greek word, meaning thread, is the simplest texture of the thermotropic liquid crystalline phase and typically found at higher temperature, near to the isotropic liquid phase. As the temperature of a liquid crystalline compounds is increased, the thermal vibrations will also increase to overcome the strong lateral intermolecular attractions. As a result, molecules in the nematic mesophase are no longer maintained their layer arrangement. Additionally, the nematic liquid crystal phase possesses a high degree of long-range orientational order which is nearly the same as liquid and no long-range translational order is found in the arrangement of molecules. Generally, the molecules tend to align their axis along a preferred direction, therefore the rotational symmetry will exist around this direction (Brown, 2012). As consequence, a uniaxial phase will be formed.

Nematic materials are almost fluid-like in the thermotropic phases with a relatively low viscosity and widely used in the display applications. A schlieren texture is the typical mesophase that is usually observed in the nematic mesophase when the molecules are aligned parallel to the glass plates. The dark and light areas of the texture corresponding to different molecular orientations with respect to the axes as defined by the polarizers. The nematic mesophase exhibits a broad X-ray diffraction peak as the molecules are positionally random, very much like liquids (Brown, 2012).

1.5.2 Smectic mesophase

The word smectic comes from the Greek word *smegma*, which means soap-like. All smectic mesophases are characterized by its layered structures with an interlayer spacing d which can be measured by X-ray diffraction. These mesophases are generally more viscous and occur at lower temperature, near to the melting point. As depicted in Figure 1.1, smectic mesophase possesses layers of parallel molecules, in which these layers are free to move over one another and is held by strong cohesive forces between the sides of the molecules rather than forces in between the ends of the molecules. This indicates that the intermolecular lateral attractions must be considerably greater than the terminal attraction to induce smectogenic system. Smectic properties are most likely to form in the long chain members of homologous series as the elongation of an alkyl chain will increase the ratio of the lateral to the terminal attractions between the molecules. Thus, after melting the crystal, the layer of molecular arrangement will remain though the terminal attractions are weakened (Gray, 1962). However, other factors such as the breadth of molecules, polarizability, substituents effect and others, also need to be considered along the formation of smectogenic behavior.

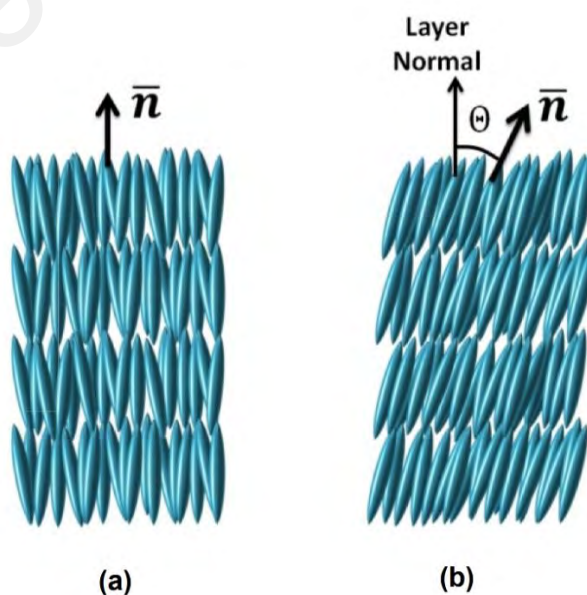


Figure 1.5: Illustration of molecular orientation in (a) SmA and (b) SmC mesophases. Adopted from (Dierking & Al-Zangana, 2017).

There are few different types of smectic structures, but smectic A and smectic C mesophases (Figure 1.6) are the typical phases found in most research. Both of them can be identified through the arrangement of the molecules. In smectic A mesophase, the molecules are arranged parallel to the director in each layer and their interlayer attractions are weak compared with the lateral forces between molecules. As consequences, the layers are able to slide over one another relatively easy and cause the mesophase to have a fluid properties, though it is more viscous compared to nematic mesophase. In contrast, the molecules in smectic C mesophase are inclined or tilted with respect to the normal layer and the smectic layer normal are not collinear (Vertogen & de Jeu, 2012).

1.5.3 Cholesteric mesophase

Cholesteric phase, often called chiral nematic liquid crystals, is similar as nematic LC except that it is composed of optically active molecules and chiral structure. In addition, the molecules in the cholesteric LC undergo a spontaneous twist about an axis normal to the preferred molecular directions (Figure 1.5) forming a helical structure. This can be done easily by rubbing two glass plates in the same direction and then arranging the two plates so that the direction of rubbing on one plate is perpendicular with each other. The liquid crystal in this arrangement will result in the formation of helical structure which is commonly referred to as the pitch and can rotate polarized light through 90° . The spiral arrangement of the molecules in the cholesteric is responsible for its unique optical properties (Brown, 2012).

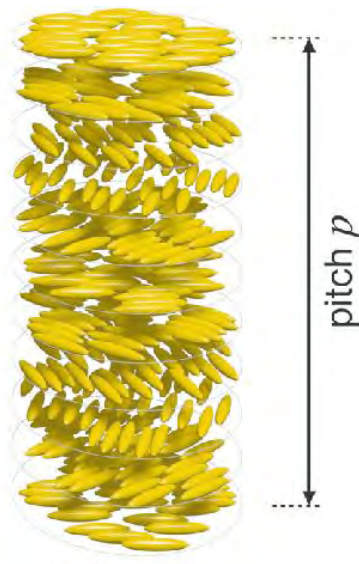


Figure 1.6: Molecular arrangement of chiral nematic mesophase. Adopted from (Dumanli & Savin, 2016).

1.6 Problem statement

The major challenge in device fabrication is to achieve favorable alignment of molecules between sources and drain contacts enabling efficient charge transport through the semiconducting medium (Dutta et al., 2010). Liquid crystalline materials are promising candidates in device fabrication especially in organic electronic applications as the LC phase can induce highly ordered and closely packed structures that lead to high mobilities within the domain boundaries. Thus, the introduction of π -conjugated moieties from rigid core into a liquid crystalline material gives advantages in charge transport properties arising from their self-assembling nature (De Feyter & De Schryver, 2003; Schmidt-Mende et al., 2001).

1.7 Objectives

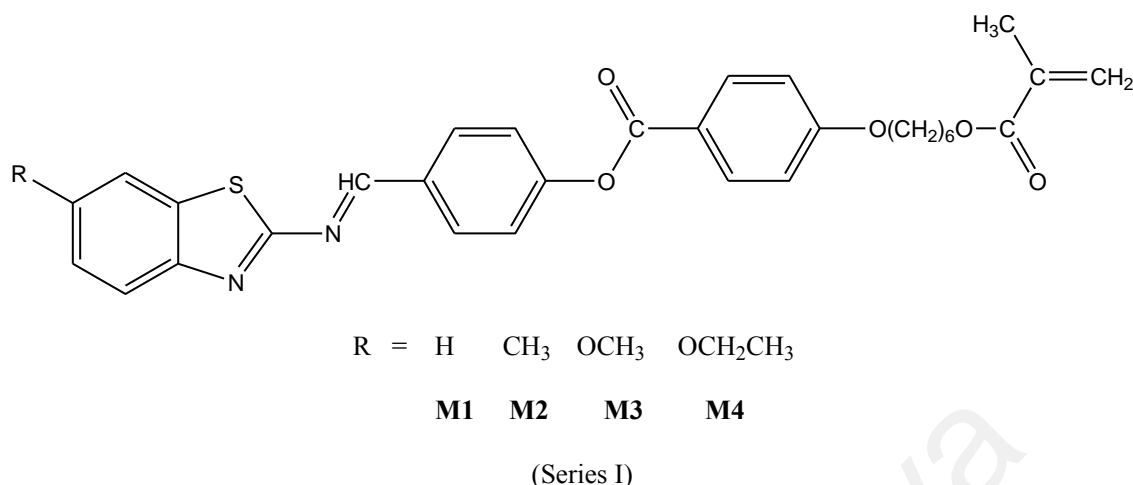


Figure 1.7: Molecular structure of a series of benzothiazole liquid crystalline monomers containing Schiff base-ester group.

Herein, we synthesized a series of Schiff base ester LC monomers incorporated with different electron-donating groups ($-\text{CH}_3$, $-\text{OCH}_3$ and $-\text{OCH}_2\text{CH}_3$), that act as substituents at the sixth position of benzothiazole. The present work is motivated from previous investigation made by Karim et al. (Karim et al., 2015), which they had prepared a series of azo-ester liquid crystalline monomers and polymers containing benzothiazole moiety with various substituents and found that all the compounds exhibited monotropic nematic mesophase except for the unsubstituted compounds. To the best of our knowledge, experimental research on Schiff base ester LC incorporating benzothiazole moiety with methacrylate group at the terminal has not been done yet.

Next, we also evaluated the influence of electron-donating groups ($-\text{H}$, $-\text{CH}_3$, $-\text{OCH}_3$ and $-\text{OCH}_2\text{CH}_3$) at sixth position of benzothiazole mesogenic core in these series in terms of their thermal and liquid crystalline behavior. The substitution at the sixth position on benzothiazole was chosen in this work because substituents at this position is more thermally stable and able to create linearity that can induce mesomorphic behavior to be formed (Ha et al., 2010; Pavluchenko et al., 1976). As these series of liquid

crystalline monomers bear a similar molecular structure as Karim et al. except for the linking group that connects the benzothiazole and benzyl ring, a comparison is made to relate the thermal and mesomorphic behavior with the chemical constitution of molecules. Lastly, the effect of substituents, solvent and temperature on the investigated compounds based on their absorption and emission properties were also investigated.

Thus, to summarize our objectives in this research work, we aim:

- i. To synthesis a series of Schiff base ester LC monomers incorporated with different electron-donating groups (-CH₃, -OCH₃ and -OCH₂CH₃), that act as substituents at the sixth position of benzothiazole.
- ii. To evaluate the influence of electron-donating groups (-H, -CH₃, -OCH₃ and -OCH₂CH₃) at sixth position of benzothiazole mesogenic core in these series in terms of their thermal and mesomorphic behavior.
- iii. To compare the thermal and mesomorphic behavior between liquid crystalline monomers containing Schiff base-ester and liquid crystalline monomers containing azo-ester.
- iv. To study the effect of substituents, solvent and temperature on the synthesized Schiff base-ester liquid crystalline monomers incorporated with benzothiazole based on their absorption and emission properties.

1.8 Thesis outline

Chapter 1 includes the introduction and history of liquid crystals in industry. The problem statement for this project as well as the objectives are also presented.

Chapter 2 presents the literature review for LC compounds synthesized by previous researchers based on few rules. A simplified literature on the effect of solvents and temperatures are also included in this chapter.

Chapter 3 describes the experimental procedures used throughout this work, starting from the material preparations, moving on to the synthesis aspect of the experiments, and finally the characterization methods. Details of the optimum conditions during handling of instruments are included as well in this section.

Chapter 4 discusses the results from the characterization techniques used throughout this work. The molecular structure and purities for all monomers were elucidated using ^1H NMR and ^{13}C NMR spectroscopies. FTIR spectroscopy was used to confirm the presence of functional groups in the synthesized monomers. The solubility behavior of the investigated compounds was observed using common organic solvents with different polarity. Thermal decomposition temperature and weight loss for all monomers were performed using TGA. DSC and POM were used to study the mesomorphic properties of monomers. Relationship between the molecular structure of monomers and their mesomorphic properties were also discussed in this chapter. The last part of Chapter 4 describes the effect of substituents, solvent and temperature on the optical properties of the synthesized monomers.

Finally, Chapter 5 presents concluding remarks of the research output and recommends future works that can be done.

CHAPTER 2: LITERATURE REVIEW

2.1 Liquid crystalline compound bearing heterocyclic moiety

The growing interest in the study of heterocyclic LC compounds has dramatically increased in recent years due to their wide range optical and photochemical behaviors, as well as their interesting fluorescence and photophysical properties. Numerous works have been done for the past few years on synthesizing liquid crystalline materials involving heterocyclic rings such as benzothiazole (Nourmohammadian, 2013; Prajapati & Bonde, 2006), oxazepine (Mohammad et al., 2016) and pyridyl (Lim et al., 2015).

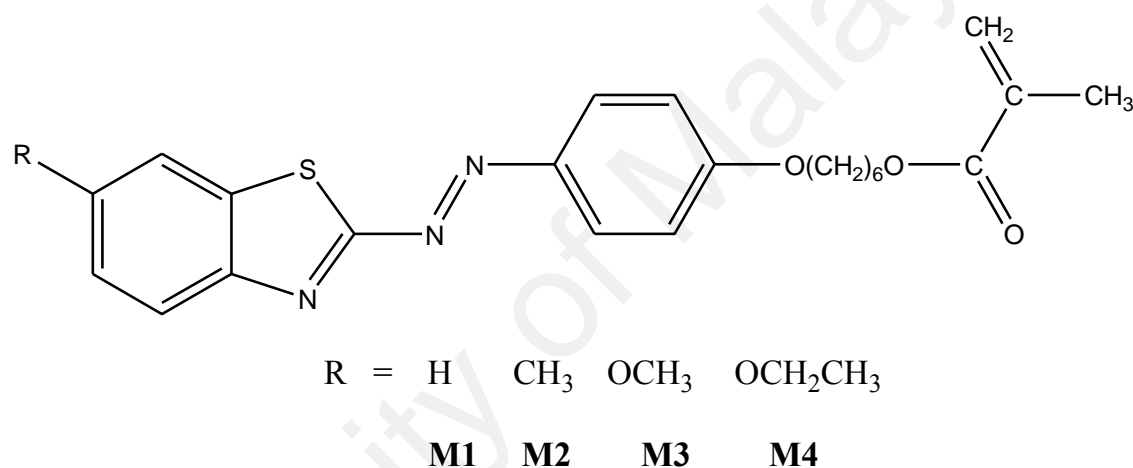


Figure 2.1: A series of azo-benzothiazole compounds (Karim et al., 2013).

Karim et al. (Karim et al., 2013) synthesized a series of azo-benzothiazole liquid crystal monomers and studied the effect of different substituents (-H, -CH₃, -OCH₃, and -OC₂H₅) at sixth position on benzothiazole moiety (Figure 2.1) on mesomorphic, thermal and optical properties. They reported that the unsubstituted LC compound exhibited only a fan-shaped smectic mesophase at 89 °C, while other monomers containing -CH₃, -OCH₃, and -OC₂H₅ groups revealed both smectic and nematic mesophases. Based on the mesomorphic investigations, they concluded that the polarity and strength of the terminal groups affect the formation of liquid crystalline behavior. In addition, in terms of optical

properties, they found that **M3** revealed the highest fluorescence emission due to the largest pushing power of methoxy group.

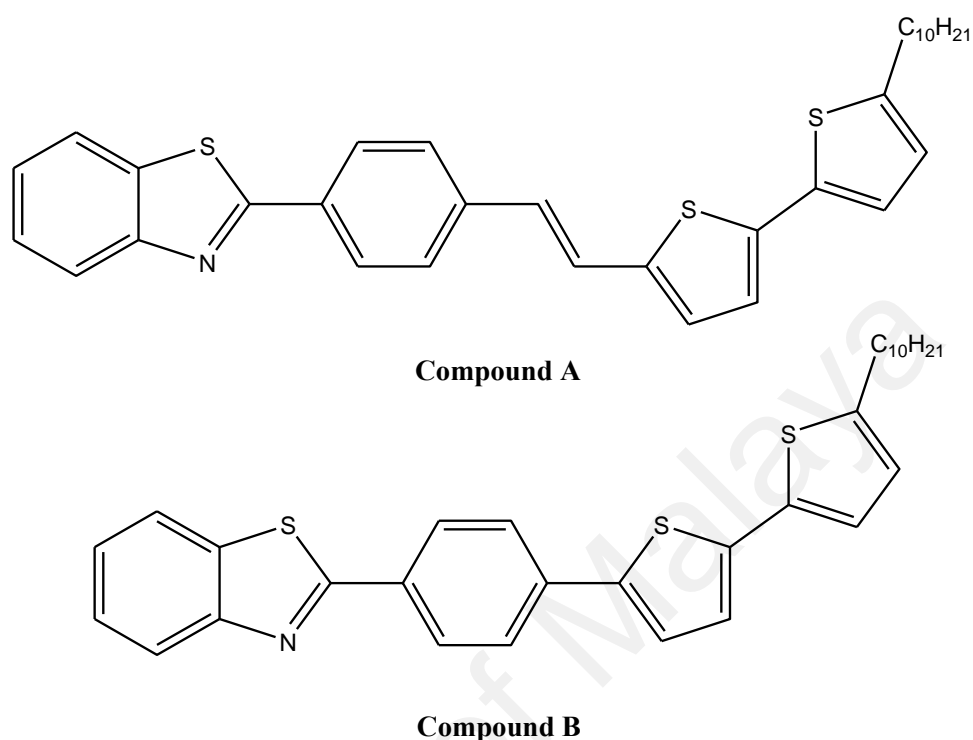


Figure 2.2: Liquid crystalline compounds bearing benzothiazole (Dutta et al., 2010).

Dutta et al. (Dutta et al., 2010) had designed and synthesized two donor-acceptor (D-A) type benzothiazole based molecules (Figure 2.2) showing interesting liquid crystalline and semiconducting properties. They reported that both compounds possessed an excellent thermal stability, with decomposition temperature higher than 300 °C. Compound A, in which benzothiazole group and thiophene group act as acceptor and donor units respectively, are linked through a vinyl bond, started to exhibit a nematic mesophase at 240 °C before it turned into a completely isotropic phase at 260 °C. Meanwhile, an enantiotropic smectic A (SmA) mesophase was observed at 239 °C upon heating and cooling cycles for compound B. Furthermore, they also observed that the emission maxima for both compounds were at longer wavelength than those in solution

indicating a strong interaction between molecules in the solid state, which is essential for good device performances.

Chia and Lin (Chia & Lin, 2013) had prepared and reported the mesomorphic behavior of their synthesized liquid crystalline compounds containing pyridine with different lengths in alkyl chain (Figure 2.3). They observed that all *nO*-PPPyCN homologues, with $n = 2-8$, revealed both enantiotropic nematic and SmA mesophases. As the carbon chain in spacer was increased up to $n = 7$ and $n = 8$, an additional enantiotropic SmC phase was observed. In addition, they also compared the mesomorphic behavior of *nO*-PPPyCN compounds with those of *xO*-PPPCN, *mO*-PPyCN and *iO*-NpPyCN. They found out that *nO*-PPPyCN with low order revealed smectic mesophase, while the other compounds with same order do not possess any smectogenic behavior. This is most probably due to the asymmetrical alignment of pyridyl moiety along the molecular axis which disrupts the mesomorphic lamellar packing. On top of that, the high-aspect-ratio of the linear three-aryl-ring mesogenic core in *nO*-PPPyCN contributes substantially to enhancement of T_{NI} and melting temperature (T_m). Lastly, they also observed that *iO*-NpPyCN favored nematic mesophase as the naphthalene in the mesogenic core provided a linear molecule with one kink which has broadened the structure.

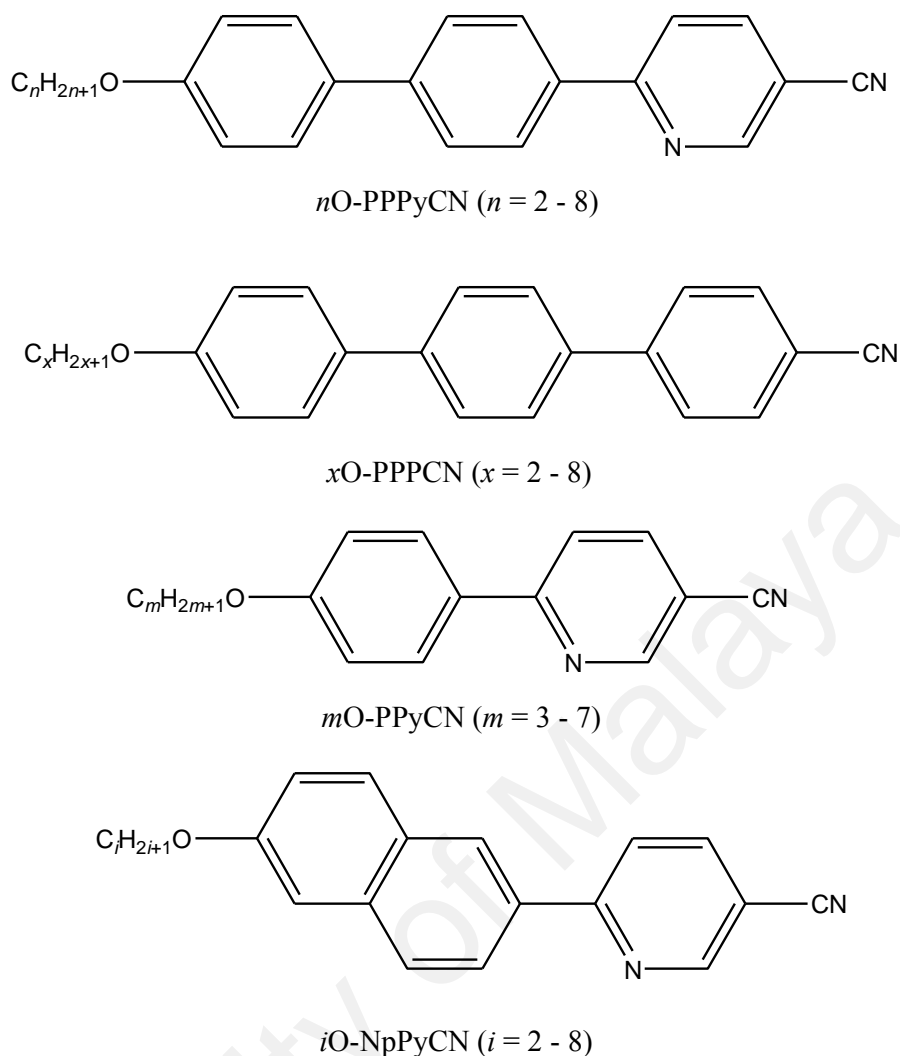


Figure 2.3: Four series of new liquid crystalline compounds (Chia & Lin, 2013).

2.2 Schiff base ester based liquid crystals

Since the discovery of 4-methoxybenzylidene-4'-butylaniline (Kelker & Scheurle, 1969) that exhibited a nematic mesophase at room temperature by Kelker and Scheurle, a vast numbers of new LC compounds containing Schiff base has been designed and synthesized. Schiff base, sub-classes of imine group, is one of the most well-known linking group used in connecting the rigid core groups as it is able to maintain molecular linearity and inducing formation of mesophase. Schiff base has potential to exhibit various interesting properties such as heat stability, catalysis, specific separations, pre-concentration of trace metal ions and semiconductor properties (Gulbas et al., 2013).

Recently, extensive studies have been conducted on Schiff base ester due to their interesting properties for various applications especially in electronic and optoelectronic devices (Ha & Lee, 2014) such as light emitting diodes, solar cells, liquid crystal displays, and sensors.

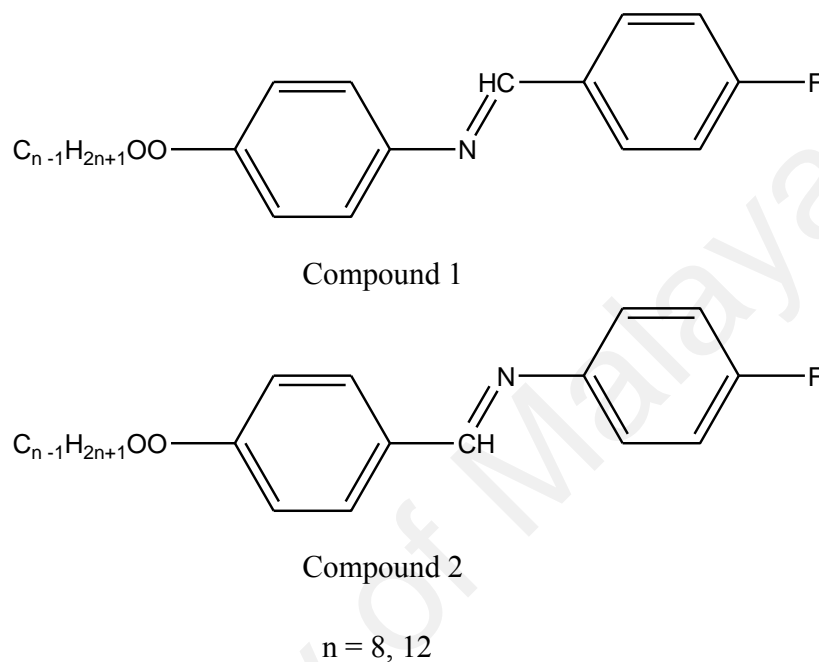
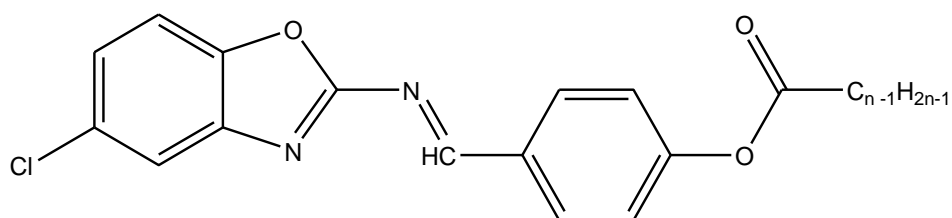


Figure 2.4: Schiff base ester group with fluorinated group (Ha & Lee, 2014).

Ha et al. (Ha & Lee, 2014) prepared two series of calamitic Schiff base ester liquid crystals consisting of a mesogenic core attached with fluorine as terminal group (Figure 2.4). An investigation on the effect of Schiff base orientation and different lengths of alkyl spacer ($n = 8$ and 12) were done to study their mesomorphic properties. They concluded that the former Schiff base from compound 2 exhibited SmA mesophase whereas the reversed orientation of imine linkage in compound 1 had caused depression of mesomorphic property. Furthermore, they also found compound 1 possessed higher melting point compared to compound 2 having the same number of carbons (n) at the alkyl chain due to effect of imine linkage orientation.



$$n = 14, 16, 18$$

Figure 2.5: 5-chloro-2-(4-alkanoyloxybenzylideneamino)benzoxazoles (Ha et al., 2011).

In another work, Ha and co-workers (Ha et al., 2011) described the mesomorphic properties of their synthesized Schiff base ester LC compound made up from heterocyclic benzoxazole (Figure 2.5) as well as the effect of various lengths of alkanoyloxy terminal chains. They observed that all the derivatives exhibited an enantiotropic smectic mesophase and formation of focal-conic fan texture was observed under POM during cooling proved the existence of SmA mesophase. Thus, they concluded that the linking group is one of the factors that influences the target compounds to induce the formation of smectic mesophase as the ester group favors the lamellar packing that potentially generated these mesophase. Moreover, they also reported that the increasing length of the terminal alkanoyloxy chain had led to increase in the melting temperature but reducing the clearing temperatures as well as their mesophase ranges.

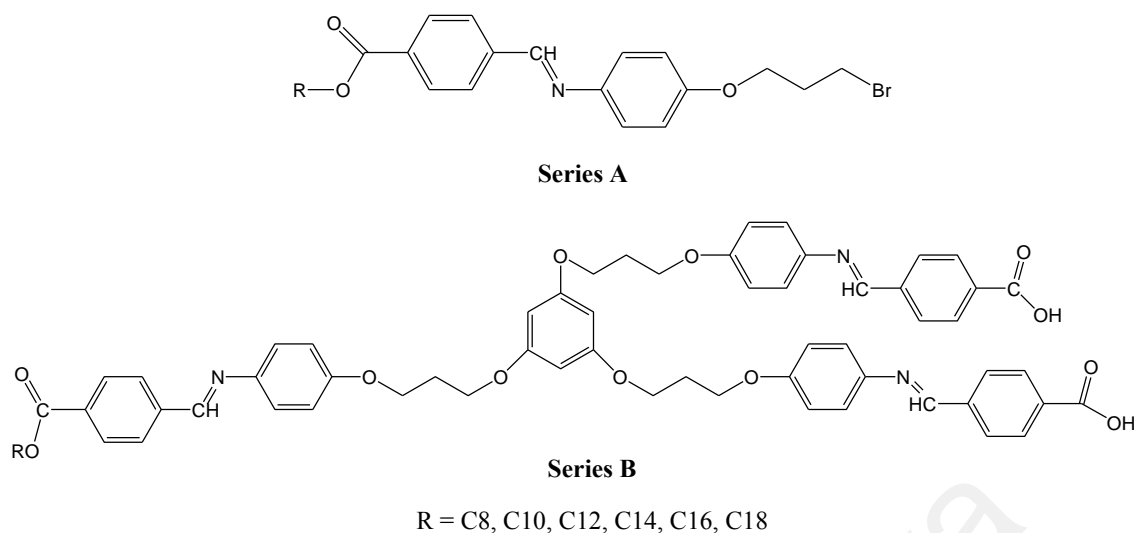


Figure 2.6: Molecular structures of intermediate and final product of trimeric star shaped LC compounds (Ooi et al., 2013).

Ooi and co-workers (Ooi et al., 2013) described the synthesis and mesomorphic properties of a homologous series of Schiff base ester trimeric star-shaped compounds and their calamitic LC intermediates with various even-parity terminal alkyl chain lengths (Figure 2.6). They observed that the star-shaped end products exhibited different mesomorphic properties in comparison to their respective intermediate compounds which proved that molecular architecture plays a vital role on determining liquid crystalline behavior. Intermediate compounds with octyl up to dodecyl carbon chain (Series A) revealed both SmA and SmC mesophases upon cooling were in the form of batonnets which eventually coalesced to form focal conic fan-shaped texture, whereas higher number of alkyl chain membered exhibited solely monotropic SmA mesophase. Meanwhile, the entire series of symmetrical three-armed star-shaped LCs (Series B) exhibited predominantly monotropic SmA and SmC behavior except compound with C8 and C18. In addition, members having medium chain length were found to exhibit larger smectic mesophase range due to the acting forces of molecular induction and polarization from terminal groups in the alkyl chain.

2.3 Schiff base-benzothiazole moiety based compounds

Benzothiazole-type liquid crystals, an important class of heterocyclic compounds, have been extensively studied due to their good hole-transporting properties with a low ionization potential, making them potential hole-transporting materials in organic light-emitting devices (OLEDs) (Ha et al., 2010). Pavluchenko et al. (Pavluchenko et al., 1976) reported on the first mesogenic group comprising benzothiazole and benzoxazole moieties with different central linkages and lateral substituents at different positions to evaluate the effect of structural changes on the mesomorphic properties. Additionally, Belmar (Belmar, 1999) stated in their work that further studies on the fluorescence on their synthesized compounds which are, benzothiazole liquid crystalline with different linking groups and alkyl spacer, could provide interesting possibilities for technological applications.

Although numerous works on Schiff base organic compounds have been done, but information on the liquid crystalline compounds incorporating of heterocyclic Schiff base, specifically benzothiazole core, are still limited. Previous research reported that benzothiazole derivatives can potentially apply in photoconductive materials (Tokunaga et al., 2009; Tokunaga et al., 2009) thin-film, organic field-effect transistors (Dutta et al., 2010) and also exhibit fluorescence properties (Batista et al., 2004). Ha and co-workers have shown interest on designing various compounds with Schiff base incorporating benzothiazole moiety in the mesogenic core that possesses mesomorphism characteristics (Ha et al., 2009; Ha et al., 2012; Ha et al., 2009) .

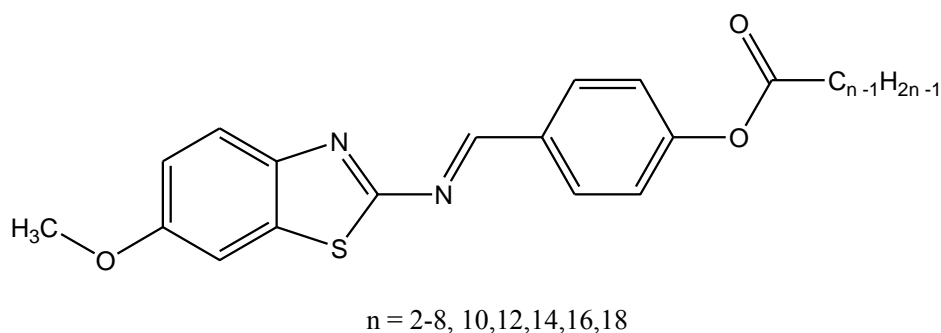


Figure 2.7: 6-methoxy-2-(4-alkanoyloxybenzylideneamino)benzothiazoles liquid crystal compounds (Ha et al., 2010).

In another work, Ha et al. (Ha et al., 2010) had described the synthesis and mesomorphic properties of a homologous series of Schiff base ester liquid crystalline compounds incorporating benzothiazole (Figure 2.7) as mesogenic core, where the length of the alkyl chain was varied ($n = 2-8, 10, 12, 14, 16, 18$). They found out that the short derivatives were non-mesogenic compounds and the mesophases only started to appear beginning from the butanoyloxy derivatives. The nematic mesophase itself was observed from C4 to C8 derivatives and formation of SmC mesophase as well as nematic mesophase were observed as the length of alkanoyloxy chain was increased from C10-C18. On top of that, they reported that the POM results supported the observation as the compound containing C10 alkanoyloxy chain exhibited nematic droplets and coalesced to form the typical schlieren texture with disclination lines upon cooling. They also found out that the XRD pattern revealed a sharp and strong peak at low angle ($1^\circ < 2\theta < 4^\circ$) in a small angle X-ray scattering (SAXS) indicating the presence of a lamellar structure which proves the formation of smectic-layered arrangement of SmC mesophase.

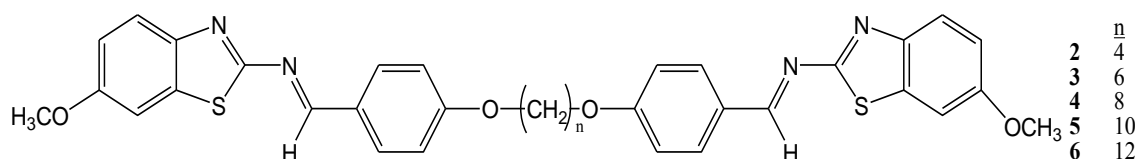


Figure 2.8: Liquid crystalline dimers containing Schiff base benzothiazole moiety (Foo et al., 2015).

Foo and co-workers (Foo et al., 2015) reported the synthesis and mesomorphic properties of a new series of symmetrical dimer molecules (Figure 2.8) in which two mesogens (benzothiazole with Schiff base linkage) are connected by different lengths of alkyl spacer groups of even parity ranging from C4 (C₄H₈) to C12 (C₁₂H₂₄). They observed that all the synthesized compounds were mesogenic, exhibiting nematic mesophase except for the low member of alkyl group, compounds 2 and 3. The appearance of thread-like texture in compound 4 and droplets coalesce with twofold and fourfold brushes in compound 6 from POM confirmed the existence of nematogenic behavior in these LC compounds. Moreover, they also found out that as the length of alkyl spacer increase, the mesophase stability and transition temperatures are decreased due to weakening in their rigidity to fit into the parallel molecular arrangement of a nematic mesophase.

2.4 Structure-mesomorphic properties relationship

Liquid crystalline behavior of calamitic compound is basically dependent on its molecular architecture, in which a minor change in the molecular geometry may bring about substantial changes in its liquid crystalline behavior. A great number of mesomorphic compounds with various molecular structures have been synthesized and interest in such structures corresponding to liquid crystalline properties are constantly growing. The mesomorphic properties are various depending on the type of mesogenic core and linking group, length of spacer (Singh et al., 2014; Singh et al., 2011) as well as the polarizability and position of substituents attached (Yeap et al., 2009; Yeap et al., 2011) that control the length and breadth of molecular structure of synthesized compounds.

2.4.1 Effect of mesogenic core in mesomorphic behavior

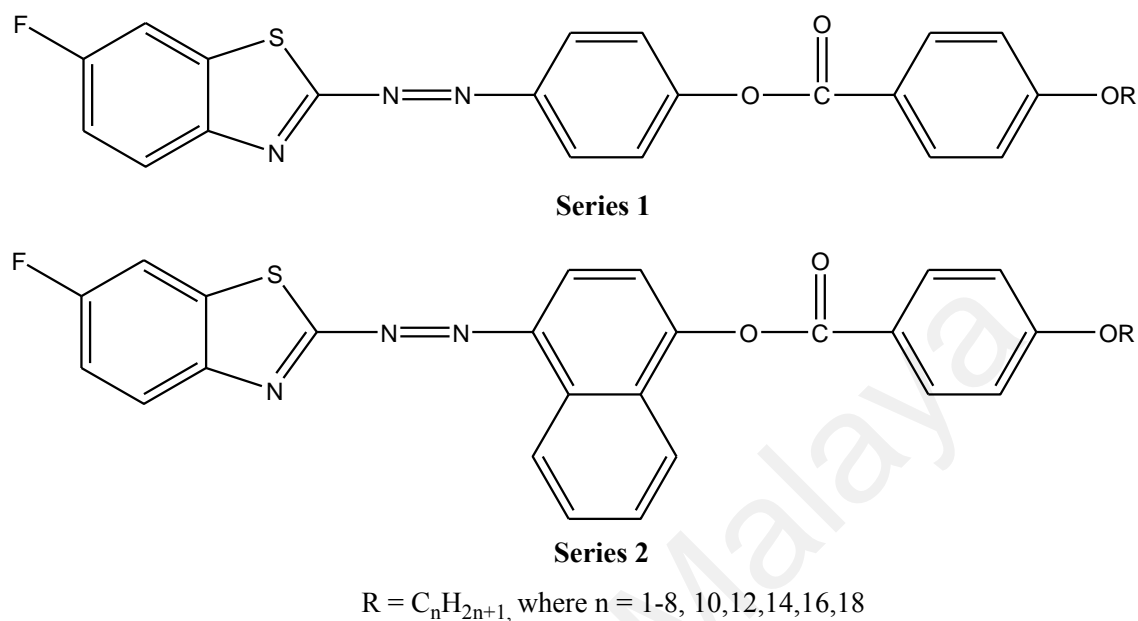


Figure 2.9: 2-[4-(4-*n*-alkoxybenzoyloxy) phenylazo]-6-fluorobenzothiazoles (Series 1) and 2-[4-(4-*n*-alkoxybenzoyloxy) naphtha-1-ylazo]-6-fluorobenzothiazoles (Series 2) (Thaker et al., 2013).

Thaker et al. (Thaker et al., 2013) had synthesized and investigated the effect of different mesogenic core on the mesomorphic behavior (Figure 2.9). They observed that compounds in series 1 exhibited nematic mesophase along with SmC and SmA mesophases, whereas series 2 were purely nematogenic. Besides that, compounds in series 1 showed greater mesophase thermal stability and mesomorphic ranges than compounds in series 2. This is attributed to the introduction of naphthalene analogue as mesogenic group that favored the formation of the nematic mesophase due to increase in breadth of molecules leading to low length to breadth ratio. In addition, the presence of a naphthalene group also weakens the lateral attraction between the molecules. Both of these factors tend to eliminate the smectogenic tendencies as well as decreasing the mesophase range.

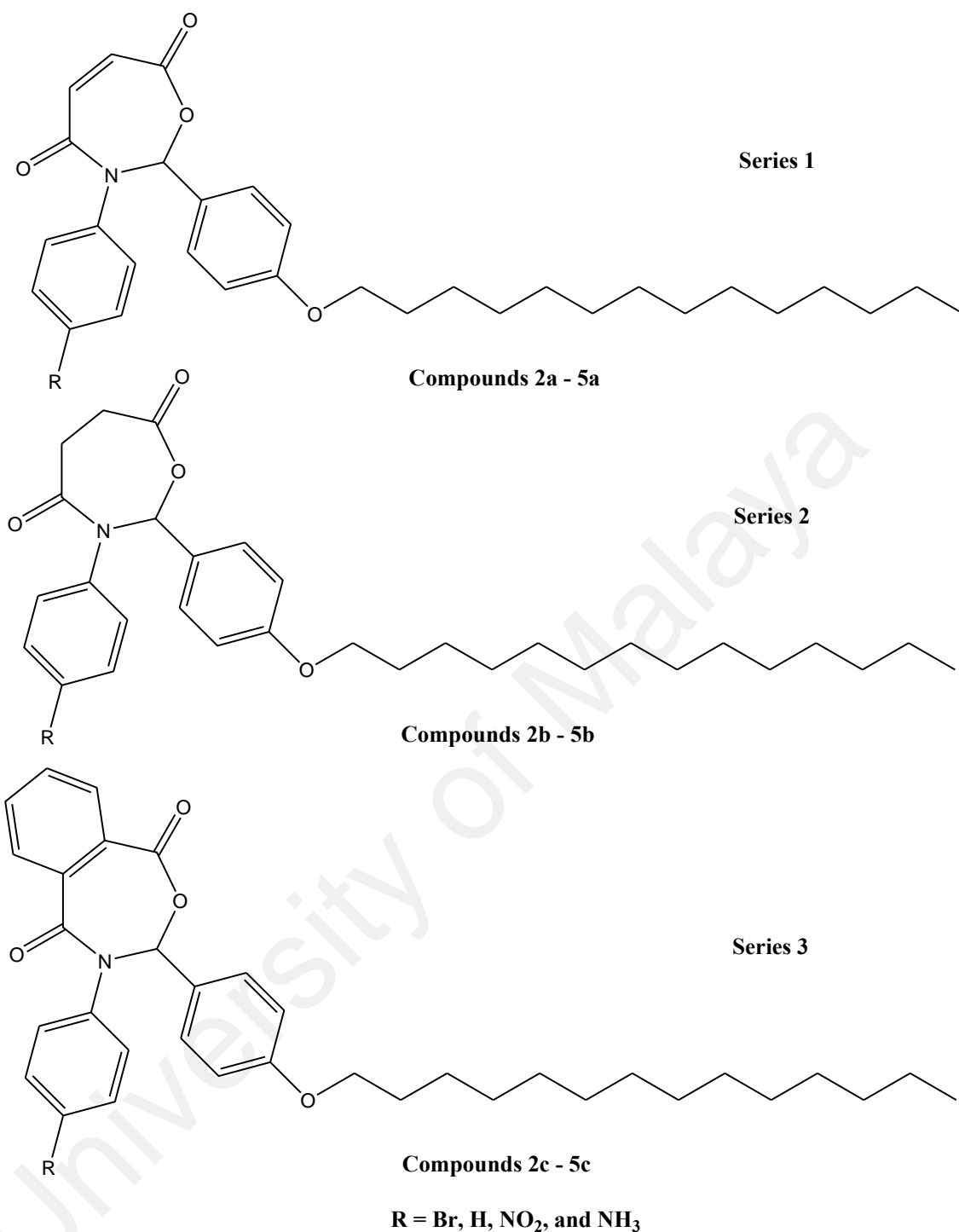


Figure 2.10: Liquid crystalline compounds containing different mesogenic groups (Yeap et al., 2010).

In another work, Yeap and co-workers (Yeap et al., 2010) had reported the synthesis and mesomorphic properties of new compounds from different mesogenic cores, 3-substituted-phenyl-2-(4-(tetradecyloxy)phenyl)-2,3-dihydro-1,3-oxazepine-4-one (Series 2a-5a), 7-diones,3-substituted-phenyl-2-(4-(tetradecyloxy)phenyl)-1,3-

oxazepane-4, 7-diones (Series 2b-5b) and 4-substituted-phenyl-3-(4-(tetradecyloxy)phenyl)-3, 4-dihydro-benzo[e][1,3]-oxazepine-1,5-diones (Series 2c-5c) (Figure 2.10). They also studied the effect of various substituents attached to the cores for each of the compounds in terms of liquid crystalline behavior. They observed that only series containing 1,3-oxazepine-1,5-diones, compounds 2c-5c, exhibited nematic mesophase. On the contrary, compounds incorporated oxazepine and oxapane cores were reported to be non-mesogenic. The formation of nematic mesophase was supported with a present of schlieren texture observed under the POM for compounds in Series 3. This result showed that the mesomorphic behavior are formed with the influence of suitable mesogenic cores attached into the compounds.

2.4.2 Effect of linking group on mesomorphic behavior

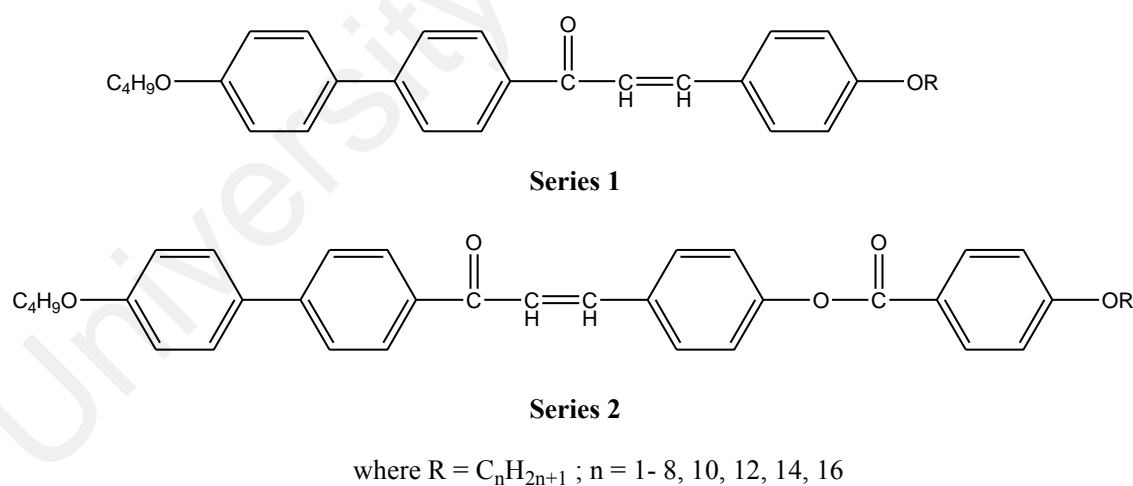


Figure 2.11: Two series of liquid crystalline compounds with chalcone as central linkage (Thaker & Kanojiya, 2011).

In another work, Thaker and his co-workers (Thaker & Kanojiya, 2011) also prepared two series of liquid crystalline compounds, 1-(4'-butyloxybiphenyl-4-yl)-3-(4-

alkoxyphenyl) prop-2-en-1-one (Series 1) and 4-[3-(4'-butoxybiphenyl-4-yl)-3-oxoprop-1-en-1-yl] phenyl 4-alkoxybenzoate (Series 2), with different central linkage (Figure 2.11). Series 1 contains only chalcone as a central linkage, while series 2 has chalcone and ester as linkage with additional benzene ring. They observed that compounds in series 1 with chalcone linker were less conducive to mesomorphism as lower member up to medium member ($n = 1-6$) did not exhibit any LC phases. In contrast, all compounds containing chalcone and ester linkages in series 2 exhibited either SmC, nematic mesophases or both depending on the length of alkoxy group in the terminal segment. The different behavior on both series proved that compounds with the presence of chalcone (-CH=CH-) linkage are less favorable in inducing mesomorphism compared to -CH=N- and -COO- linkages due to its non-linearity and angle strain arising from the keto group.

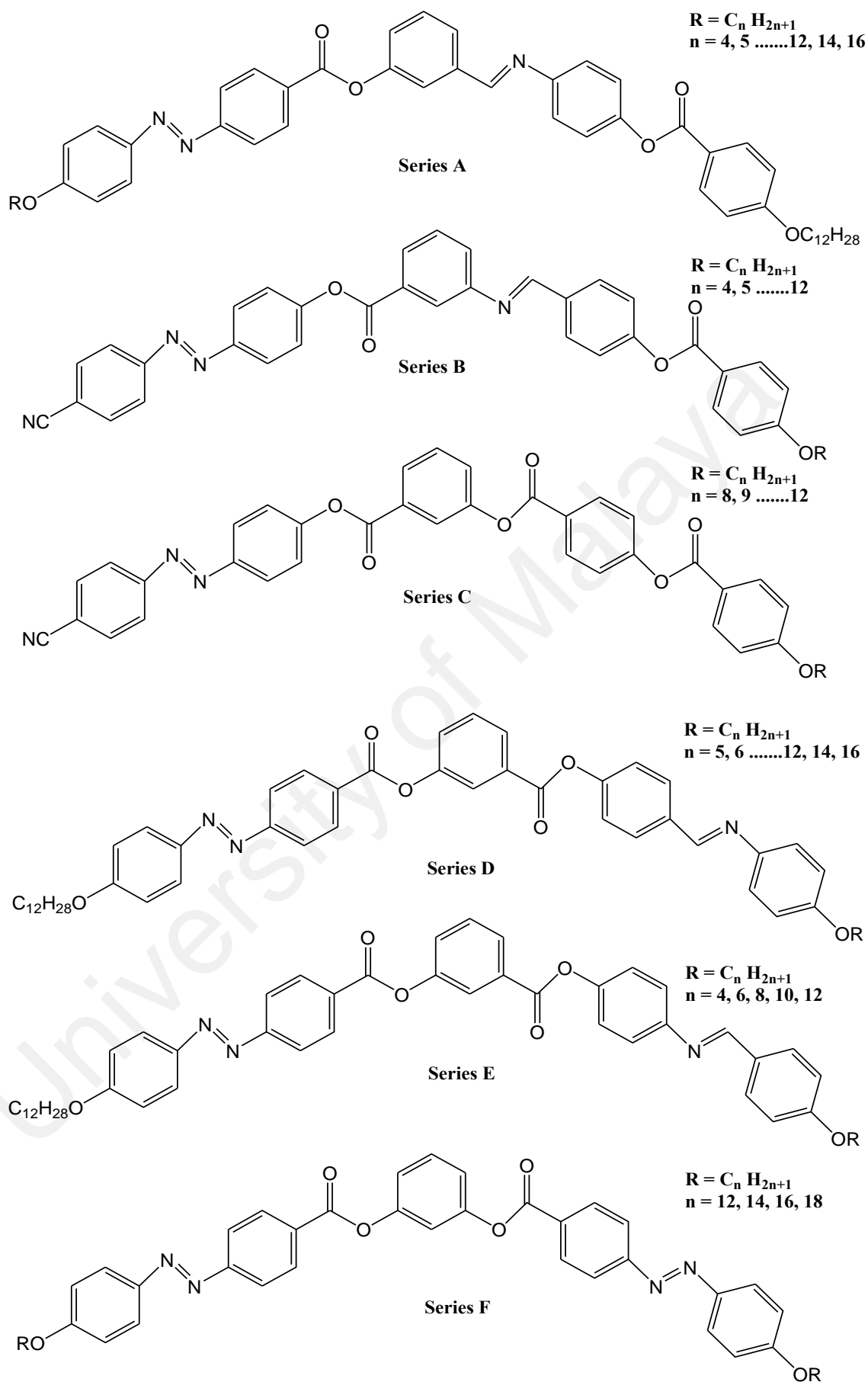
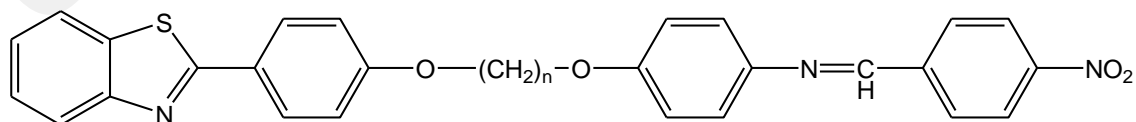


Figure 2.12: Azo substituted bent-core compounds (Nagaveni et al., 2012).

In order to investigate the structure-property relationship, Nagaveni et al. (Nagaveni et al., 2012) had synthesized 6 new series of azo substituted bent-core compounds (Figure 2.12), by changing the different linking groups as well as their linking directions in the molecule and studied the effect of these variations on their liquid crystalline properties. The first five series of compounds, series A-E, are made of unsymmetrical molecules with a fixed substitution at one end of the molecules, whereas series F consists of symmetrical molecules. They observed the liquid crystalline and thermal properties were different when the type or position of linking group was varied. As an example, higher homologous in series B, compounds with azomethine group near to central aromatic ring, exhibited an enantiotropic $Sm_{AD}P_A$ mesophase. In contrast, almost all compounds in series D, as azomethine linkage has been moved away from the central, are found to revealed monotropic B_2 mesophase in nature throughout the series. In series C, compounds with ester group as linker instead of azomethine linkage, exhibited a similar liquid crystalline mesophase as compounds in series B, which is $Sm_{AD}P_A$ mesophase. However, they possessed monotropic mesophase which was attributed to unstable behavior in the molecules.

2.4.3 Effect of length of flexible spacer on mesomorphic behavior



where $n = 1-6, 8, 10, 12$

Figure 2.13: A series of non-symmetric liquid crystal dimers (Seou et al., 2014).

Seou et al. (Seou et al., 2014) had investigated the mesomorphic properties of a series non-symmetric LC dimers N-(4-(n-(4-(benzothiazol-2-yl) phenoxy)alkoxy)-4-nitrobenzylideneimine) containing benzothiazole and benzylideneaniline as the mesogenic core units by varying the length of carbon number in the spacer chain (Figure 2.13). The synthesized compounds with a low even number of alkyl spacers ($n = 2$) exhibited nematic mesophase only while compounds with a medium to a higher even number of alkyl spacers showed polymorphism (smectic and nematic mesophases). In contrast, odd members with shorter alkyl spacers ($n = 1$ and 3) were non-LC, but longer alkyl spacer dimer ($n = 5$) was able to exhibit a single nematic mesophase. Thus, different molecular structures for all synthesized compounds revealed that the formation of mesomorphic behavior and transition temperature were greatly influenced by the number of alkyl spacer in the terminal group.

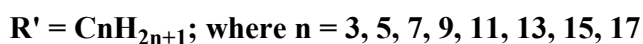
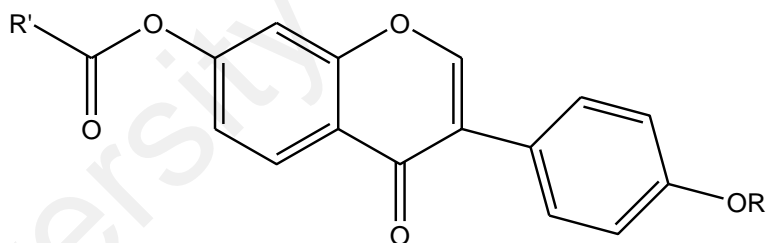


Figure 2.14: Series of calamitic isoflavone ester with different length of alkanoyloxy chain (Yam & Yeap, 2011).

Yam and Yeap (Yam & Yeap, 2011) synthesized and characterized a new series of calamitic isoflavone ester, 7-alkanoyloxy-3-[40-(3-methylbutyloxyphenyl)]-4H-1-benzopyran-4-ones (Figure 2.14), with various alkanoyloxy chain lengths in odd-parity. They found that compounds with short alkoxy chain, $n = 3$ and 5 , exhibited an

enantiotropic nematic mesophase as confirmed by the formation of marble nematic texture in the POM. Meanwhile, derivatives with carbon atoms in the odd-parity terminal chain revealed smectogenic behavior and was supported with formation of batonnets coalesced with broken fan-shaped texture. They also performed powder X-ray diffraction (PXR) measurement on compound with seven carbon chain and found out that the layer spacing of this compound was 0.8-1.1 Å, shorter than its effective molecular length, 1 (28.5 Å). This observation in the layer spacing indicated the formation of tilted SmC mesophase instead of SmA mesophase. Moreover, they also concluded that the clearing temperature was increased with increasing the length of alkyloxy chains in odd-parity.

2.4.4 Effect of terminal substituents on mesomorphic behavior

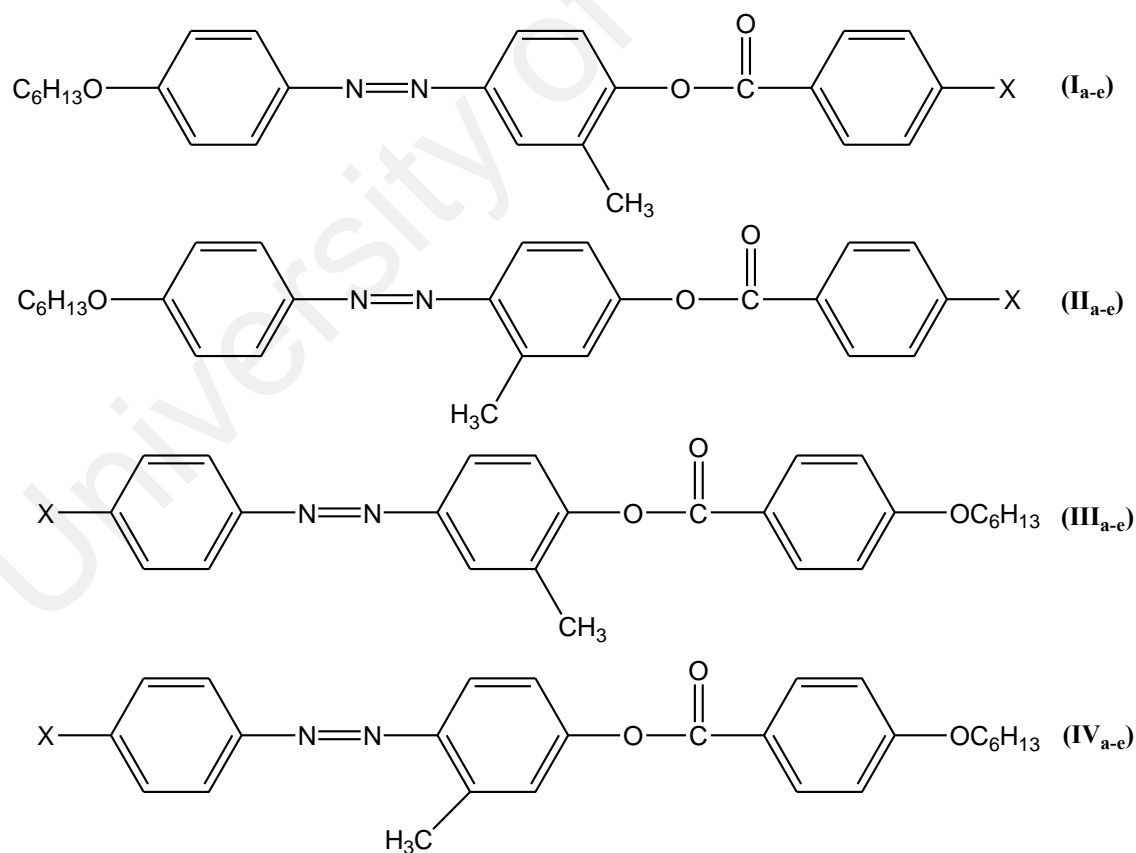


Figure 2.15: Azo ester based liquid crystalline compounds (Naoum et al., 2011).

Naoum and co-workers (Naoum et al., 2011) had prepared and investigated the mesomorphic properties of four series of liquid crystalline compounds incorporated with different polarizability of substituents attached at terminal end (Figure 2.15). They observed that all the investigated compounds to be monomorphic exhibiting the enantiotropic nematic mesophase. They found out that the linear strong electron-withdrawing, CN group, possessed the most stable mesomorphic range among all the series. Besides on that, they also studied the effect of exchange of the two wing substituents ($C_6H_{13}O$ and X) on the mesophase behavior on the resulting isomers. They observed that isomers with substituents near to azo group (series III and IV) had a better nematic stability with respect to the effect of the terminal polar substituent X attached except for compounds containing halogen group. They also found out that the bulky methyl group was associated with lower value of entropy change of nematic-isotropic range due to increase in the biaxiality of the mesogenic group, which resulted in the flexible terminal alkoxy chain being less anchored at its end.

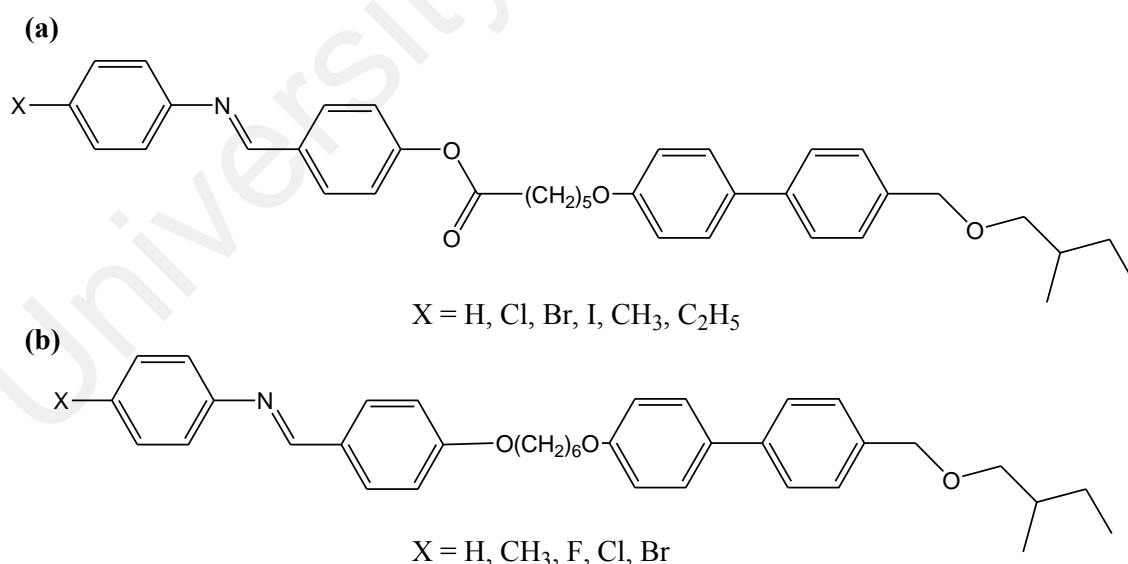


Figure 2.16: a) Liquid crystalline compounds containing imine and ester linker b) a series of LC compounds with imine group (Yeap et al., 2015).

In another work, Yeap et al. (Yeap et al., 2015) prepared and studied the effect of different terminal substituents attached on a new series of non-symmetric dimers containing ester and ether groups in the flexible spacer, (R,S)-(benzylidene-4'-substituted-aniline)-2''-methylbutyl-4''''-(4''''-phenoxy)benzoateoxy)hexanoates (Figure 2.16a). They reported that dimers containing halogen group at terminal exhibited monotropic SmA mesophase and enantiotropic nematic mesophase, while other compounds revealed only enantiotropic nematic mesophase (except dimer with ethyl group). The mesomorphic properties was further confirmed by POM; the smectic mesophase revealed a focal conic fan texture coalescence with homeotropic alignment, while nematic mesophase showed a schlieren texture with point singularity and flashed when subjected to mechanical stress. On top of that, they also investigated the effect of linking group on the synthesized compounds and compared them with previous reported compounds, 1-(4-benzylidene-substituted-aniline-4'-oxy)-6-(2-methylbutyl-4'-(4'-phenyl)benzoate-oxy) hexanes (Figure 2.16b), in terms on mesomorphic and thermal properties. They concluded that the size of substituents and van der Waals volume affected the nematic-isotropic transition temperature as both of the series showed similar trend in the thermal transition.

2.5 Effect of environment on liquid crystal compounds

2.5.1 Influence of solvents on liquid crystalline compounds

Solvatochromic shift refers to a strong dependence of absorption and emission of the solvated molecules on the polarity of the solvent medium and is caused by differential solvation of the ground and first excited state of the light-absorbing molecule. Molecules with significant solvatochromic shift property can be in principle used in sensors and molecular electronics (Zhou, 2014). A hypsochromic (or blue) shift of the band is called

negative solvatochromism while bathochromic (or red) shift is termed positive solvatochromism, with respect to increase in solvent polarity. Negative solvatochromism occurs when the ground state molecule is better stabilized by solvation than the molecule in the excited state upon ascending of solvent polarity. In contrast, a better stabilization of the molecule in the first excited state relative to that in the ground state with increasing solvent polarity will lead to positive solvatochromism (Heger, 2006).

Preparation on LC layer are often difficult because the absorption may be very high and extremely thin layers may be needed. Thus, modification induced by a solvent is introduced as it can play a significant role in the photophysics of the excited states (Ghoneim & Suppan, 1997). In fact, the electro-optic switching properties of the solutions are, to some extent, better than those of 'pure' LC compound (Boussoualem et al., 2010; Lorenz & Kitzerow, 2011). Although numerous studies on the effect of solvent on organic compounds have been reported but similar experimental works on liquid crystal compounds are still limited.

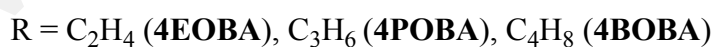
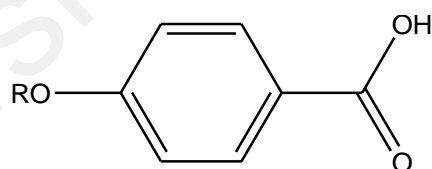


Figure 2.17: A series of 4-alkoxybenzoic acid liquid crystalline derivatives (Sıdır et al., 2015).

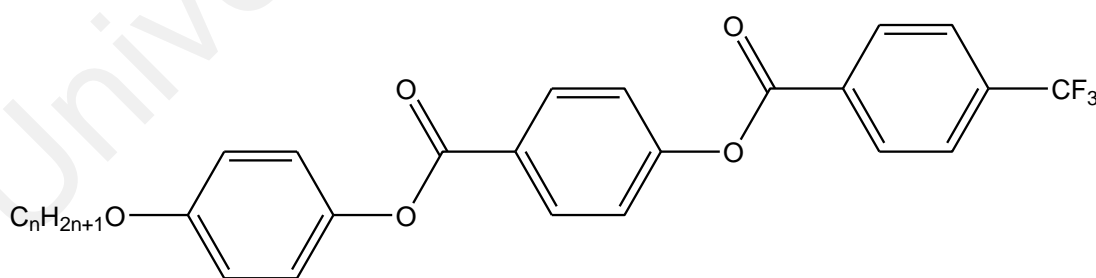
Sıdır and co-workers (Sıdır et al., 2015) had investigated the solvatochromic behavior on a series of 4-alkoxybenzoic acid liquid crystalline derivatives (Figure 2.17). UV spectra showed that 4POBA and 4BOBA compounds shifted to a longer wavelength compared to 4EOBA which indicated that the elongation of alkyl chain leads to red shift in absorbance resulting in stronger charge transfer. Besides on that, they also used two

multiparametric methods, Kamlet-Taft solvent scale and Catalan solvent scale to determine the solute-solvent interactions. The equations expression for both models are described below:

$$\text{Kamlet-Taft model: } \nu_{(\max)} = C_0 + C_1.f(n) + C_2.f(\epsilon) + C_3.\beta + C_4.\alpha \quad \text{Eq. (1.1)}$$

$$\text{Catalan model: } \nu_{(\max)} = C_5 + C_6.SPP + C_7.SA + C_8.SB \quad \text{Eq. (1.2)}$$

where, $\nu_{(\max)}$ is defined as the maximum absorption band depending on solvent polarity change. In Eq. (1.1), dielectric function is characterized as $f(\epsilon) = (\epsilon-1) / (\epsilon+2)$, refractive index function as $f(n) = (n^2-1) / (n^2+2)$ and Kamlet-Taft parameters as β and α . In Eq. (1.2), polarity/polarizability is described as SPP, acidity of solvent as SA and basicity of solvent as SB, respectively. They reported that both Kamlet-Taft and Catalan methods confirmed that absorption and fluorescence emission maxima band revealed positive solvatochromism, which is dominantly controlled by hydrogen bond donor ability. In addition, this positive solvatochromic behavior indicates the ground state is less stabilized compared to excited state which corresponds to stronger effect of dispersion-induction interaction.



$n = 1$ FLUORO1; and $n = 3$ FLUORO2

Figure 2.18: Liquid crystalline compound with different fluoro substituents (Praveen & Ojha, 2012).

Praveen and Ojha (Praveen & Ojha, 2012) studied the effect of substituents and solvents on their investigated liquid crystalline compounds containing fluoro as substituents in terms of optical properties (Figure 2.18). They reported that both of the compounds exhibited two strong absorptions, which corresponds to HOMO \rightarrow LUMO transition, and has been assigned as $\pi \rightarrow \pi^*$ transition in the molecule. However, compound FLUORO2 revealed a higher absorption wavelength in UV range compared to FLUORO1 molecule, which is beneficial for several electro-optic applications. With respect to solvent effect, a small red-shift was observed in comparable with pure molecules, which suggested an increased contribution of lone pairs of the electronegative atoms to the delocalized π electronic system. They also observed that compound FLUORO1 exhibited higher UV stability in water, whereas, FLUORO2 molecules revealed higher UV stability in benzene with minimum transition energy.

2.5.2 Influence of temperature on liquid crystal compounds

Besides solvent effect, investigations on the effect of temperature or we called it as thermochromism have received significant attention among the researchers as it crucial in sensing applications such as biosensor, drug delivery, logic gates and optical sensing (Pietsch et al., 2010). Various parameters such as absorbance, fluorescence, dielectric constant, transmittance and relaxation mode are used to study the relationship between the temperature and optical behavior of materials.

Chandran et al. (Chandran et al., 2014) studied the behavior of low frequency dielectric relaxation mode on their investigated ferroelectric liquid crystal (FLC) materials with respect to changes in the temperature. The relaxation frequency (ν_R) of the low frequency mode as well as the Goldstone mode (GM) was observed to shift toward

higher frequency upon increasing temperature. GM was referred as the phase fluctuations in the azimuthal orientation.

Using a similar work, Misra and co-workers (Misra et al., 2015) reported the optical studies on some series of ferroelectric liquid crystal (FLC) materials doped with different concentrations and temperatures of fluorescent dye. The fluorescent dye used for doping was poly (3,3',4,4'-benzophenonetetracarboxylicdianhydride-alt-3,6-diaminoacridine hemisulfate) with various concentrations such as 1%, 3% and 5% into the pure FLC. They found out that the value of relative permittivity increased with an increase in temperature until it reached their maximum point before decreasing continuously. The interaction between FLC and fluorescent dye molecules supported the dipole moment of system and hence strengthened the helix which caused the relative permittivity to increase.

CHAPTER 3: EXPERIMENTAL

3.1 Materials and reagents

The chemicals used to synthesize the monomers were: 2-aminobenzothiazole (Aldrich, Germany, 97%), 2-amino-6-methylbenzothiazole (Aldrich, Japan, 98%), 2-amino-6-methoxybenzothiazole (Aldrich, Germany, 98%), 2-amino-6-ethoxybenzothiazole (Aldrich, Switzerland, technical grade), *p*-hydroxybenzaldehyde (Merck, 98%), *p*-hydroxy benzoic acid (Sigma-Aldrich, 98%), hydrochloric acid (R&M Chemicals, 95%), anhydrous sodium sulphate (R&M Chemicals, 99.5%), potassium hydroxide (R&M Chemicals), potassium iodide (R & M Chemicals, UK, 99.9%), 6-chlorohexanol (Merck, 98%), methacrylic acid (Sigma Aldrich, 99%), dimethyl sulfoxide-D₆, (DMSO-D₆) (Merck, Germany, 99.8%), hydroquinone (Merck, Germany, 99.5%), *p*-toluenesulfonic acid (Merck, 95%), *N,N'*-dicyclohexylcarbodiimide (DCC) (Merck, 98%), and *p*-dimethylaminopyridine (DMAP) (Merck, 95%). All chemicals were used without further treatment.

All the used solvents such as ethanol, methanol, *N,N*-dimethylformamide, dichloromethane, diethyl ether, *n*-hexane, isopropanol, tetrahydrofuran, chloroform, chlorobenzene and toluene were of reagent grade and purchased from Merck, Friendemann Schmidt Chemicals and J. T. Baker.

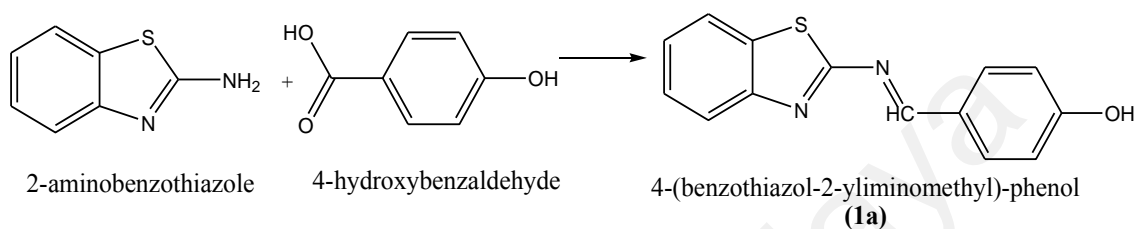
3.2 Synthesis of liquid crystal monomers

In this work, a series of similar structures of Schiff base ester liquid crystal monomers incorporating benzothiazole ring with variations in the strength of electron-donating groups (-H, -CH₃, -OCH₃, -OCH₂CH₃) as substituent were synthesized. The procedure, synthetic route and chemical structure identification of all synthesized compounds and monomers are described in this section. The structural characterization

of compounds was determined by ^1H NMR, ^{13}C NMR and FTIR spectroscopic techniques.

3.2.1 Synthesis of monomer M1.

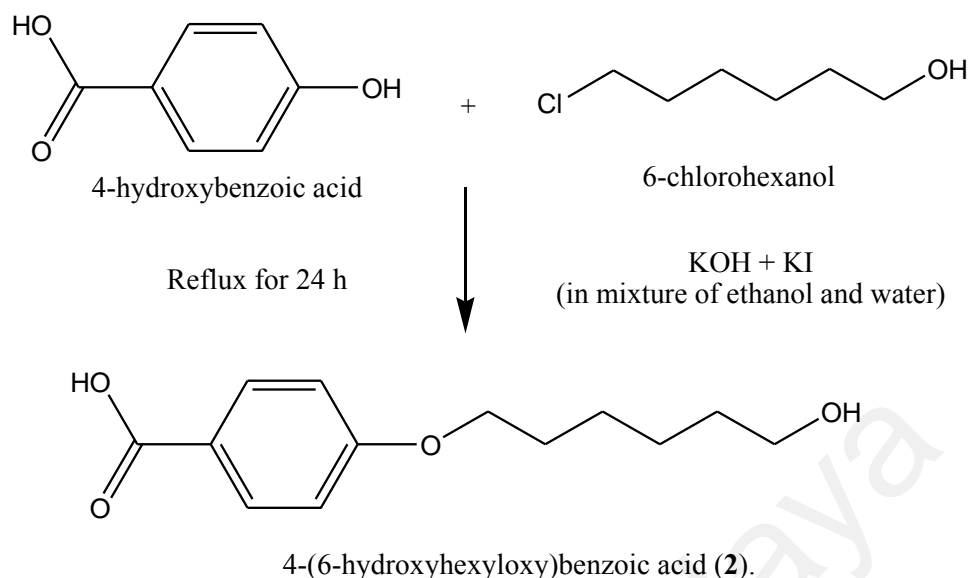
4-(benzothiazol-2-yliminomethyl)-phenol (**1a**)



Scheme 3.1: Synthesis of 4-(benzothiazol-2-yliminomethyl)-phenol (1a**).**

2-aminobenzothiazole (1.5 g, 10 mmol) and 4-hydroxybenzaldehyde (1.2 g, 10 mmol) were dissolved in ethanol and then refluxed with stirring for 4 h. The colored residue was recrystallized several times using ethanol to obtain **1a**. Yellow solid, yield: 71%, ^1H NMR (400 MHz, $\text{DMSO-}d_6$) δ (ppm): 9.74 (s, 1H, -OH), 8.99 (s, 1H, -N=CH-, Schiff base group), 7.99-7.98 (d, 1H, benzo-H), 7.92-7.91 (d, 2H, Ar-H), 7.86-7.85 (d, 1H, benzo-H), 7.47-7.44 (t, 1H, benzo-H), 7.37-7.34 (t, 1H, benzo-H), 6.92-6.90 (d, 2H, Ar-H), ^{13}C NMR (100 MHz, $\text{DMSO-}d_6$) δ (ppm): 172.5 (benzo-C-N=CH-), 167.0 (Ar-C-OH), 163.4 (-N=CH-, Schiff base group), 152. (benzo-C-N), 134.4 (benzo-C-N), 133.3 (Ar-C-CH=N-), 133.0, 127.0, 126.4, 125.4, 122.8, 116.7 (Ar-C), FTIR (cm^{-1}): 3370 (-OH), 3000 (C-H, aromatic), 2905, 2807, 2677, 2604, 1900 (C=N, aromatic), 1603 (-N=CH-, Schiff base group), 1517 (C-C, aromatic), 1295 (C-O), 1238, 1157, 1136 (benzothiazole), 862, 831, 798, 683, 642 (C-S-C).

4-(6-hydroxyhexyloxy)benzoic acid (**2**).

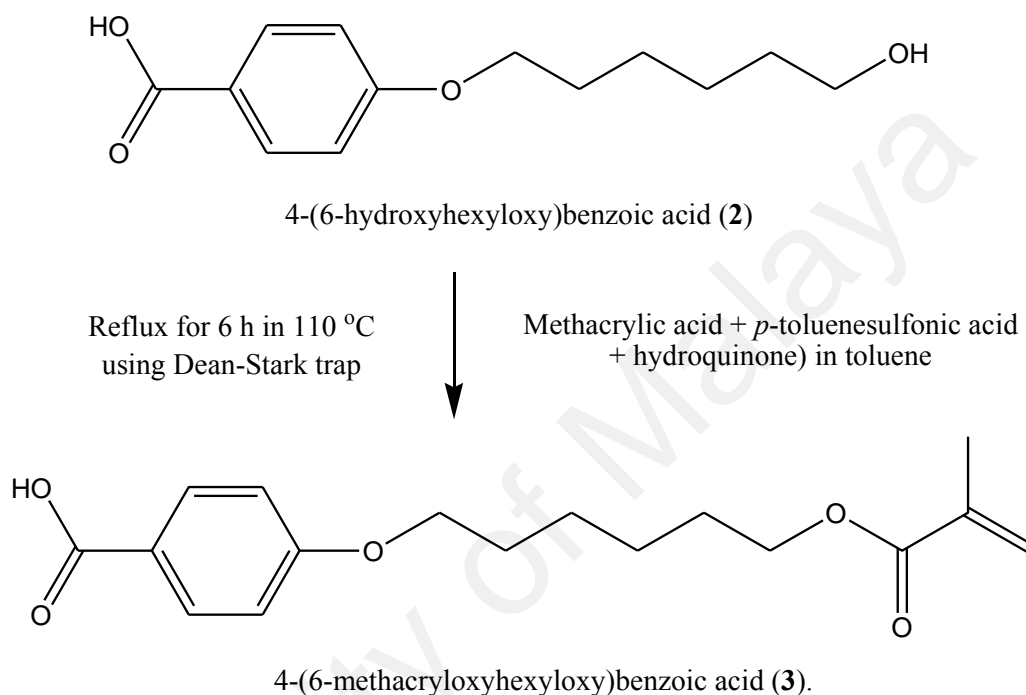


Scheme 3.2: Synthesis of 4-(6-hydroxyhexyloxy)benzoic acid (2**).**

In a reaction flask, 4-hydroxybenzoic acid (10.0 g, 70 mmol), potassium hydroxide (11.0 g, 190 mmol), potassium iodide (trace amount) were dissolved in a mixture of (1.5:1) of ethanol and water respectively until it dissolved. At room temperature, 6-chlorohexanol (9.0 g, 70 mmol) was added into the mixture and was refluxed at 80 °C while stirring for 24 h. After completion of the reaction, the mixture was cooled to room temperature and the solvent was removed under reduced pressure. The solid residue obtained was then dissolved into (100 mL) water. The solution was extracted with diethyl ether (3x30 mL) using separating funnel to remove impurities in the end-product. The aqueous phase was then acidified with concentrated hydrochloric acid until reached pH 2. The obtained white product was then filtered off, washed with water and recrystallized from ethanol to obtain solid **2**. White solid, yield: 55%, ¹H NMR (400 MHz, DMSO-*d*₆) δ (ppm): 12.6 (s, 1H, -COOH), 7.82-7.84 (d, 2H, Ar-H), 6.94-6.96 (d, 2H, Ar-H), 4.35 (1H, -OH), 3.96-3.99 (t, 2H, -CH₂OPh), 1.64-1.71 (m, 2H, -OCH₂-), 1.25-1.41-1 (m, 8H, -CH₂). ¹³C NMR (100 MHz, DMSO-*d*₆) δ (ppm): 167.6 (-COOH), 162.8, 131.9, 123.3, 114.7 (Ar-C), 68.3 (-OCH₂-), 61.6(-CH₂OH), 33.0, 29.1,

25.9, 25.8 (aliphatic-C), **FTIR** (cm^{-1}): 3373 (-OH), 2950, 2855, 2522 (-C-H, aliphatic), 1666 (-C=O), 1604, 1411 (C=C, aromatic), 1576 (C-C, aromatic), 1283, 1255 (C-O).

4-(6-methacryloxyhexyloxy)benzoic acid (3)

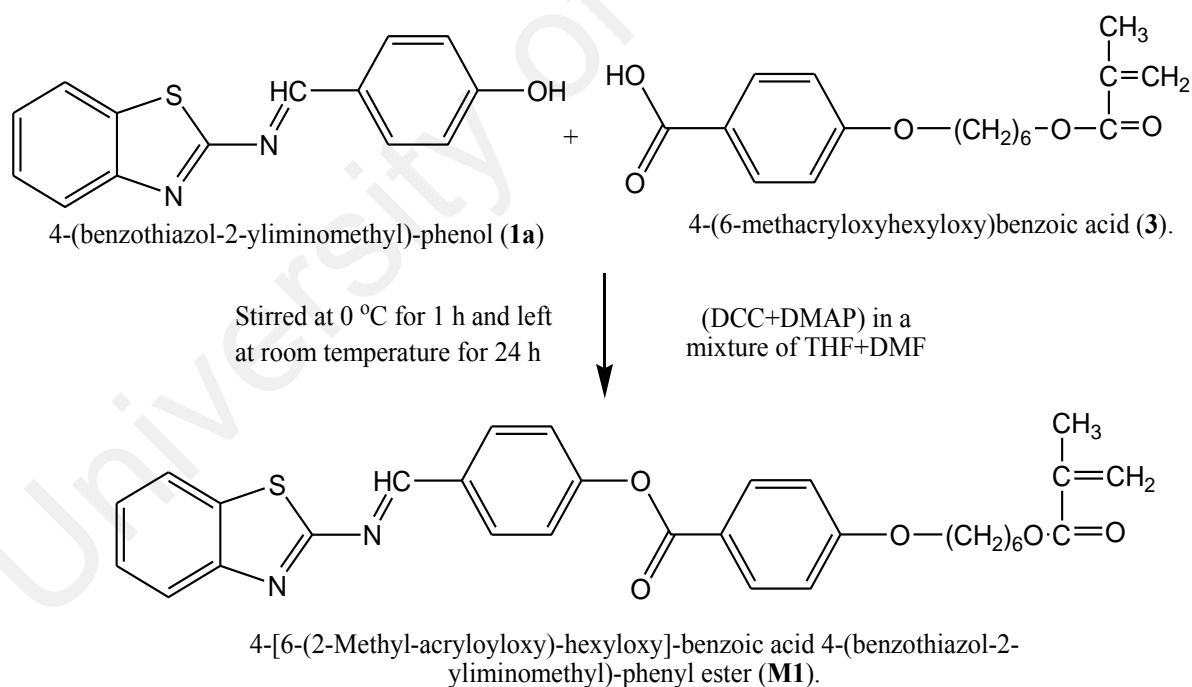


Scheme 3.3: Synthesis of 4-(6-methacryloxyhexyloxy)benzoic acid (3).

Compound **2** (2.4 g, 10 mmol), methacrylic acid (3.4 mL, 40 mmol), *p*-toluene sulfonic acid (0.7 g, 0.004 mmol) and hydroquinone (0.2g, 2.0 mmol) were added into a 250 mL two neck round bottom flask containing 60 mL toluene. The resultant mixture was refluxed at 110 °C for 6 h using Dean-Stark trap to remove produced water from the reaction vessel. The obtained clear solution was diluted with diethyl ether and the resultant mixture was extracted several times with warm water. The organic layer was separated, dried over anhydrous sodium sulphate and then solvent was removed under reduced pressure. The obtained dull-white solid was recrystallized from isopropanol-water mixture (2:1) to get solid **3**. Dull-white solid, yield: 80%, ¹H NMR (400 MHz,

DMSO-*d*₆) δ (ppm): 12.6 (1H, -COOH), 7.81-7.86 (d, 2H, Ar- H), 6.94-6.96 (d, 2H, Ar- H), 5.96, 5.61 (s, 1H, CH₂=C(CH₃)-), 3.97-4.01 (m, 4H, -OCH₂-), 1.82 (s, 3H, CH₂=C(CH₃)-), 1.65-1.72 (m, 2H, -OCH₂CH₂-), 1.56-1.61 (m, 2H, -CH₂), 1.34-1.44 (m, 4H, -(CH₂)₂-). ¹³C NMR (100 MHz, DMSO-*d*₆) δ (ppm): 167.6 (Ar-COOH), 167.1 (-OC=O), 136.5 (-C(CH₃)=CH₂), 126.1 (-C(CH₃)=CH₂), 162.8, 131.9, 123.3, 114.7 (Ar-C), 68.3 (-OCH₂-), 64.8 (-CH₂O-), 28.9, 28.5, 25.9, 25.6, 18.5 (aliphatic-C + -CH₃), FTIR (cm⁻¹): 2569, 2942 (-C-H, aliphatic), 1710, 1682 (-C=O), 1636 (C=C, aliphatic), 1609 (C=C, aromatic), 1515 (C-C, aromatic), 1295, 1252 (C-O).

4-[6-(2-Methyl-acryloyloxy)-hexyloxy]-benzoic acid 4-(benzothiazol-2-yliminomethyl) phenyl ester (M1).



Scheme 3.4: Synthesis of 4-[6-(2-Methyl-acryloyloxy)-hexyloxy]-benzoic acid 4-(benzothiazol-2-yliminomethyl)-phenyl ester (M1).

In a mixture of THF and DMF (1:1), compound **1a** (1.30 g, 5 mmol) and compound **3** (1.53 g, 5 mmol) were dissolved in a 250 mL Erlenmeyer flask. p-

Dimethylaminopyridine (DMAP) (0.06 g, 0.5 mmol) and N,N'-dicyclohexylcarbodiimide (DCC) (1.03 g, 5 mmol) were dissolved in 80 mL dichloromethane and then poured into the reaction flask. The resulting mixture was cooled in an ice bath with stirring for 1 h. After that, the reaction mixture was stirred for another 24 h at room temperature for completion of the reaction. The solvent was removed under reduced pressure to obtain concentrated yellow mixture. Ethanol and n-hexane mixture (1:1) were added to the concentrated mixture and was kept in a refrigerator for 24 h to crystallize. The product was re-crystallized with a mixture of methanol and ethanol to increase purity of the compound. The resulting yellowish crystals were separated by simple filtration and dried in a vacuum oven at 45 °C. Light yellow solid, yield: 30%, **¹H NMR** (400 MHz, DMSO-*d*₆) δ (ppm): 9.21 (s, 1H, -N=CH-, Schiff base group), 8.17-8.16 (d, 2H, Ar-H), 8.07-8.04 (m, 3H, benzo-H + Ar-H), 7.93-7.91 (d, 1H, benzo-H), 7.51-7.47 (m, 3H, benzo-H + Ar-H), 7.46-7.44 (t, 1H, benzo-H), 7.42-7.39 (t, 1H, Ar-H), 5.98 (s, 1H, =CH₂), 5.63 (s, 1H, =CH₂), 4.08-4.05 (m, 4H, -OCH₂-), 1.84 (s, 3H, -CH₃), 1.74-1.71 (m, 2H, -CH₂-), 1.63-1.60 (m, 2H, -CH₂-), 1.46-1.37 (m, 4H, -CH₂-CH₂-), **¹³C NMR** (100 MHz, DMSO-*d*₆) δ(ppm): 167.1 (-O-CO-), 166.9 (benzo-C-N=CH-), 164.3 (-N=CH-, Schiff base group), 164.0 (Ar-O-CO-Ar), 155.9 (Ar-C-O-), 153.3 (Ar-C-O-CO-), 136.5 (benzo-C-N), 134.4 (benzo-C-S), 132.7 (-C(CH₃)=CH₂), 131.6 (Ar-C-CH=N-), 131.4, 131.3, 126.1, 123.5, 121.4, 121.3, 120.8, 118.2, 115.3 (Ar-C), 126.0 (-C(CH₃)=CH₂), 68.5 (-OCH₂-), 64.8 (-CH₂-O-), 28.9, 28.5, 25.7, 25.6, 18.5 (aliphatic-C + -CH₃), **FTIR** (cm⁻¹): 3063 (C-H, aromatic), 2928, 2853 (C-H, aliphatic), 1721 (C=O), 1617 (C=C), 1601 (-N=CH-, Schiff base group), 1578 (C=C, aromatic), 1302, 1260 (C-O), 1229, 1199, 1162, 1125, 1102, 1053 (benzothiazole), 984, 939, 842, 812, 751, 693, 683, 648, 671 (C-S-C), Anal. Calcd. for C₃₁H₃₀N₂O₅S (in percentage by weight, %): C, 68.61; H, 5.57; N, 5.16; found: C, 68.10; H, 5.90; N, 5.26.

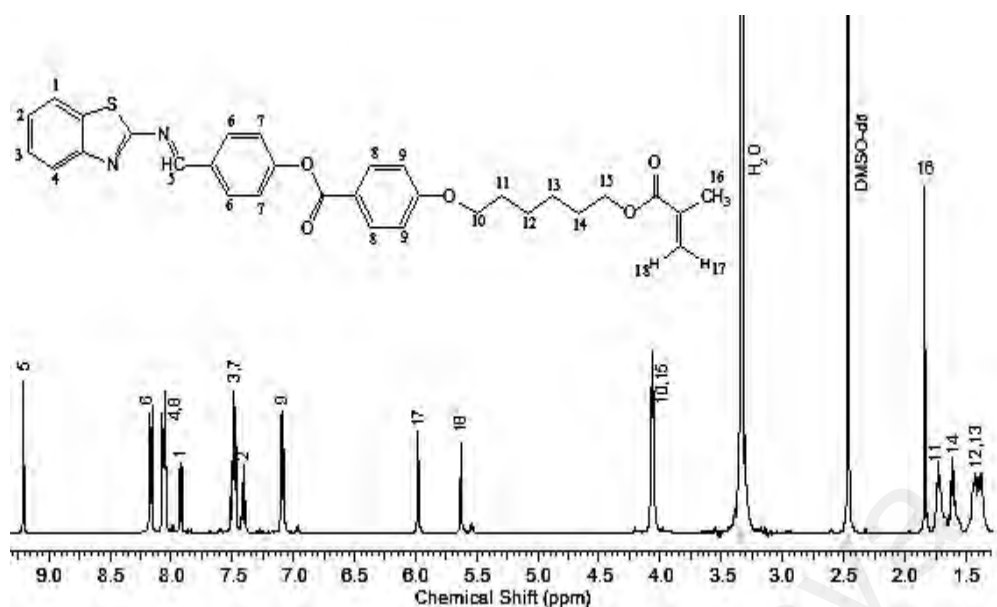


Figure 3.1: ^1H NMR spectra of M1.

3.2.2 Synthesis of monomer M2

4-[(6-Methyl-benzothiazol-2-ylimino)-methyl]-phenol (**1b**)

The synthesis of compound **1b** was similar to that described for compound **1a**. Yellow solid, yield: 87%. ^1H NMR (400 MHz, DMSO- d_6) δ (ppm): 9.75 (s, 1H, -OH), 8.96 (s, 1H, -N=CH-, Schiff base group), 7.91-7.89 (d, 2H, benzo-H), 7.77 (s, 1H, benzo-H), 7.74-7.72 (d, 1H, benzo-H), 7.27-7.26 (d, 1H, benzo-H), 6.91-6.90 (d, 2H, Ar-H), 2.39 (s, 3H, -CH₃), ^{13}C NMR (100 MHz, DMSO- d_6) δ (ppm): 171.5 (benzo-C-N=CH-), 166.6 (Ar-C-OH), 163.3 (-N=CH-, Schiff base group), 149.9 (benzo-C-N), 135.2 (benzo-C-S), 134.5 (Ar-C-CH=N-), 133.1, 132.7, 128.4, 126.4, 122.3, 116.7 (Ar-C), 21.6 (benzothiazole-CH₃), FTIR (cm^{-1}): 3397 (-OH), 3030 (C-H, aromatic), 2917, 2813, 2683, 2609, 1894 (C=N, aromatic), 1699 (-N=CH-, Schiff base group), 1572 (C=C, aromatic), 1296 (C-O), 1239, 1160, 1129 (benzothiazole), 912, 831, 807, 690, 638 (C-S-C).

4-[6-(2-Methyl-acryloyloxy)-hexyloxy]-benzoic acid 4-[(6-methyl-benzothiazol-2-ylimino)-methyl]-phenyl ester (**M2**)

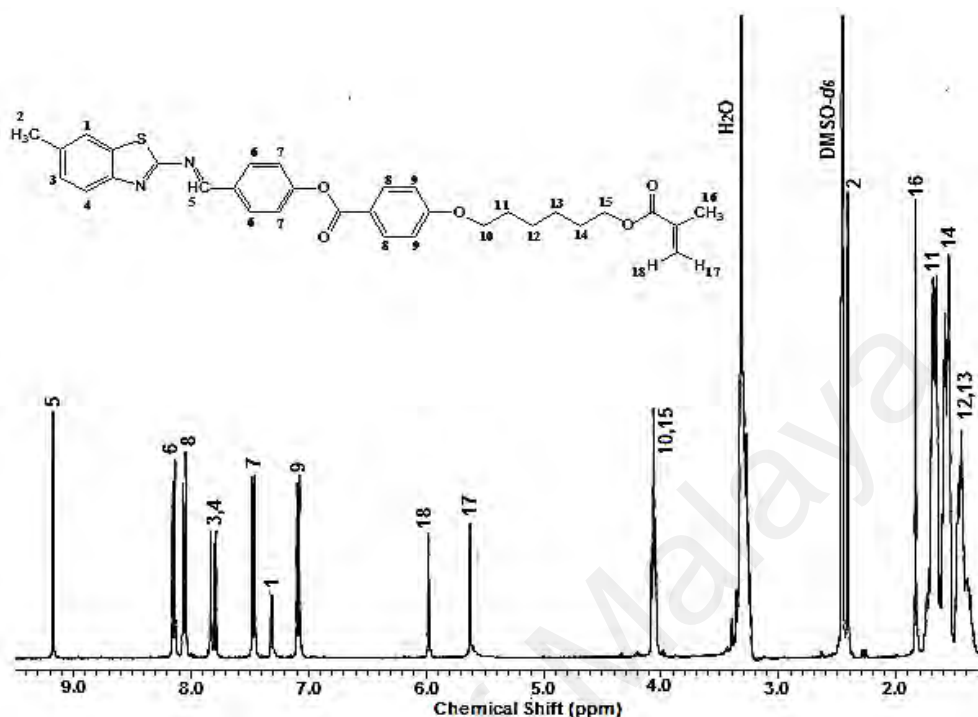


Figure 3.2: ^1H NMR spectra of **M2**.

Compound **1b** (1.35 g, 5 mmol) and compound **3** (1.53 g, 5 mmol) were dissolved in THF and DMF (1:1) mixture. The rest of the succeeding steps were identical to that described for the synthesis of monomer **M1**. Yellow solid, yield: 31%. ^1H NMR (400 MHz, $\text{DMSO-}d_6$) δ (ppm): 9.17 (s, 1H, $-\text{N}=\text{CH}-$, Schiff base group), 8.16-8.14 (d, 2H, Ar-H), 8.07-8.05 (d, 2H, Ar-H), 7.83-7.84 (t, 2H, benzo-H), 7.48-7.46 (d, 2H, Ar-H), 7.32-7.30 (d, 1H, benzo-H), 7.10-7.08 (d, 2H, Ar-H), 5.98 (s, 1H, $=\text{CH}_2$), 5.63 (s, 1H, $=\text{CH}_2$), 4.08-4.04 (m, 4H, $-\text{OCH}_2-$), 2.41 (s, 3H, benzo- CH_3), 1.84 (s, 3H, $-\text{CH}_3$), 1.70-1.66 (m, 2H, $-\text{CH}_2-$), 1.61-1.55 (m, 2H, $-\text{CH}_2-$), 1.47-1.44 (m, 4H, $-\text{CH}_2-\text{CH}_2-$), ^{13}C NMR (100 MHz, $\text{DMSO-}d_6$) δ (ppm): 170.7 ($-\text{O}-\text{CO}-$), 167.1 (benzo- $\text{C}-\text{N}=\text{CH}-$), 166.5 ($-\text{N}=\text{CH}-$, Schiff base group), 164.4 (Ar- $\text{O}-\text{CO}-\text{Ar}$), 163.9 (Ar- $\text{C}-\text{O}-$), 157.1 (Ar- $\text{C}-\text{O}-\text{CO}-$), 155.1 (benzo- $\text{C}-\text{N}$), 149.9 (benzo- $\text{C}-\text{S}$), 136.5 ($-\text{C}(\text{CH}_3)=\text{CH}_2$), 135.6 (benzo- $\text{C}-\text{CH}_3$), 134.7 (Ar- $\text{C}-\text{CH}=\text{N}$), 132.7, 132.0, 128.6, 123.5, 122.8, 122.5, 120.9, 115.3 (Ar-C),

126.1 (-C(CH₃)=CH₂), 68.5 (-OCH₂-), 64.8 (-CH₂-O-), 28.9, 28.5, 25.8, 25.7, 21.6, 18.5 (aliphatic-C + -CH₃), **FTIR** (cm⁻¹): 3055 (C-H, aromatic), 2929, 2850 (C-H, aliphatic), 1723, 1713 (C=O), 1611 (C=C), 1600 (-N=CH-, Schiff base group), 1576 (C=C, aromatic), 1302, 1266 (C-O), 1211, 1203, 1167, 1105, 1061 (benzothiazole), 980, 932, 841, 807, 757, 684, 669, 650, 517 (C-S-C), Anal. Calcd. for C₃₂H₃₂N₂O₅S (in percentage by weight, %): C, 69.40; H, 5.79; N, 5.03; found: C, 69.32; H, 5.90; N, 5.26.

3.2.3 Synthesis of monomer M3

4-[(6-Methoxy-benzothiazol-2-ylimino)-methyl]-phenol (1c).

The synthesis of compound **1c** was similar to that described for compound **1a**. Yellow solid, yield: 79%. **¹H NMR** (400 MHz, DMSO-*d*₆) δ (ppm): 9.74 (s, 1H, -OH), 8.91 (s, -N=CH-, Schiff base group), 7.89-7.87 (d, 1H, benzo-H), 7.75-7.73 (d, 2H, Ar-H), 7.57 (s, 1H, benzo-H), 7.05-7.03 (d, 1H, benzo-H), 6.90-6.88 (d, 2H, Ar-H), 3.79 (s, 3H, -OCH₃), **¹³C NMR** (100 MHz, DMSO-*d*₆) δ (ppm): 170.0 (benzo-C-N=CH-), 165.9 (Ar-C-OH), 163.2 (-N=CH-, Schiff base group), 157.6 (benzo-C-N), 146.1 (benzo-C-S), 135.6 (Ar-C-CH=N-), 133.1, 126.9, 123.5, 116.7, 116.0, 105.6 (Ar-C), 56.2 (-O-CH₃), **FTIR** (cm⁻¹): 3382 (-OH), 3085 (C-H, aromatic), 2942, 2835, 2685, 2613, 1907 (C=N, aromatic), 1642 (-N=CH-, Schiff base group), 1576, 1573, 1406 (C=C, aromatic), 1271 (C-O), 1241, 11654, 1110 (benzothiazole), 1018, 812, 692, 602 (C-S-C).

4-[6-(2-Methyl-acryloyloxy)-hexyloxy]-benzoic acid 4-[(6-methoxy-benzothiazol-2-ylimino)-methyl]-phenyl ester (**M3**)

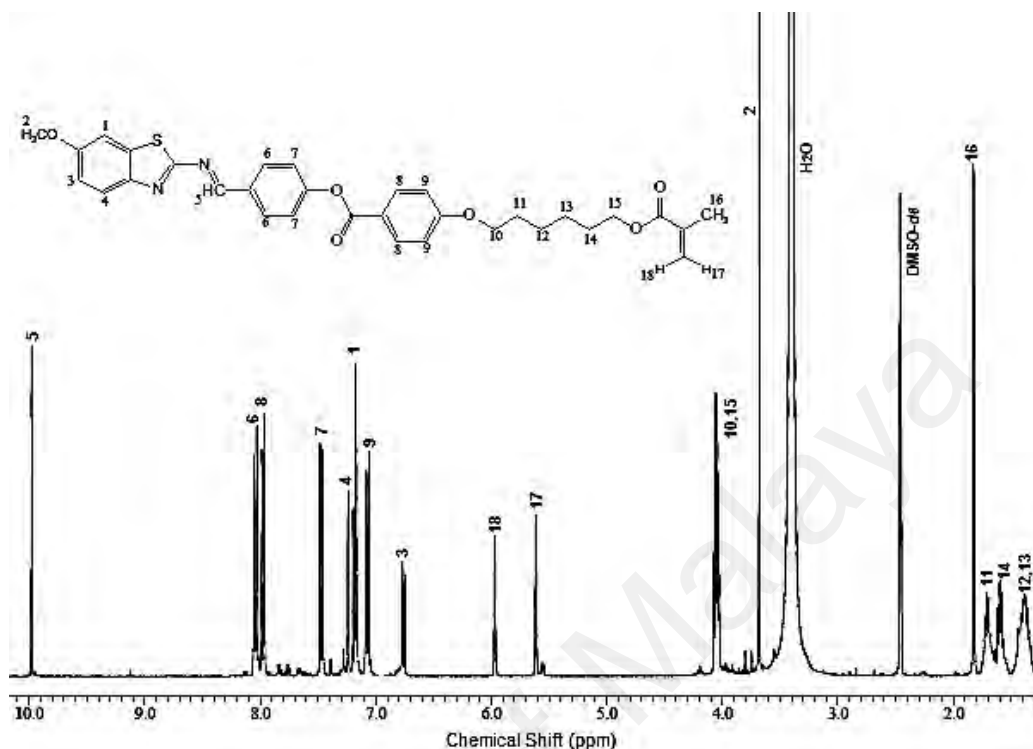


Figure 3.3: ^1H NMR spectra of **M3**.

Compound **1c** (1.43 g, 5 mmol) and compound **3** (1.53 g, 5 mmol) were dissolved in THF:DMF (1:1) mixture. The rest of the succeeding steps were identical to that described for the synthesis of monomer **M1**. Bright yellow solid, yield: 33%. ^1H NMR (400 MHz, DMSO- d_6) δ (ppm): 9.98 (s, 1H, -N=CH-, imine group), 8.05-8.03 (d, 2H, Ar-H), 7.98-7.96 (d, 2H, Ar-H), 7.48-7.46 (d, 2H, Ar-H), 7.24 (d, 1H, benzo-H), 7.17 (s, 1H, benzo-H), 7.08-7.06 (d, 2H, Ar-H), 6.77-6.74 (d, 1H, benzo-H), 5.97 (s, 1H, =CH₂), 5.61 (s, 1H, =CH₂), 4.07-4.03 (m, 4H, (-OCH₂-)), 3.68 (s, 3H, -OCH₃), 1.83 (s, 3H, -CH₃), 1.71-1.69 (m, 2H, -CH₂-), 1.60-1.58 (m, 2H, -CH₂-), 1.41-1.37 (m, 4H, -CH₂-), ^{13}C NMR (100 MHz, DMSO- d_6) δ (ppm): 169.2 (-O-CO-), 167.1 (benzo-C-N=CH-), 165.3 (-N=CH-, imine group), 164.3 (Ar-O-CO-Ar), 163.9 (Ar-C-O-), 157.9 (CH₃O-C-benzo), 157.2 (benzo-C-N), 155.8 (benzo-C-S), 147.3 (-C(CH₃)=CH₂), 136.5 (Ar-C-CH=N-), 134.3, 132.7, 131.9, 123.9, 123.4, 120.8, 116.8, 115.3, 106.0 (Ar-C), 126.1 (-

C(CH₃)=CH₂), 68.5 (-OCH₂-), 64.8 (-CH₂-O-), 56.3 (-OCH₃) 33.9, 28.9, 28.5, 25.6, 18.5 (aliphatic-C), **FTIR** (cm⁻¹): 3063 (C-H, aromatic), 2928, 2855 (C-H, aliphatic), 1723, 1709 (C=O), 1618 (C=C), 1602 (-N=CH-, imine group), 1580 (C=C, aromatic), 1312, 1298 (C-O), 1257, 1230, 1203, 1168, 1064 (benzothiazole), 938, 889, 847, 807, 755, 723, 682, 655 (C-S-C), Anal. Calcd. for C₃₂H₃₂N₂O₆S (in percentage by weight, %): C, 67.11; H, 5.63; N, 4.89; found: C, 67.13; H, 5.59; N, 4.84.

3.2.4 Synthesis of monomer **M4**

*4-[(6-Ethoxy-benzothiazol-2-ylimino)-methyl]-phenol (**1d**).*

The synthesis of compound **1d** was similar to that described for compound **1a**. Light yellow solid, yield: 88%. **¹H NMR** (400 MHz, DMSO-*d*₆) δ (ppm): 9.75 (s, 1H, -OH), 8.92 (-N=CH-, Schiff base group), 7.90-7.88 (d, 1H, benzo-H), 7.74-7.72 (d, 2H, Ar-H), 7.86 (s, 1H, benzo-H), 7.10-7.08 (d, 1H, benzo-H), 6.91-6.89 (d, 2H, Ar-H), 4.06-4.04 (q, 2H, -OCH₂-), 1.33-1.32 (t, 3H, -CH₃), **¹³C NMR** (100 MHz, DMSO-*d*₆) δ (ppm): 170.0 (benzo-C-N=CH-), 165.5 (Ar-C-OH), 163.8 (-N=CH-, Schiff base group), 154.0 (benzo-C-N), 147.3 (benzo-C-S), 132.7 (Ar-C-CH=N-), 133.0, 128.9, 118.6, 116.4, 113.9, 106.7 (Ar-C), 64.0 (-O-CH₂CH₃), 15.3 (-O-CH₂CH₃), **FTIR** (cm⁻¹): 3416 (-OH), 3067 (C-H, aromatic), 2921, 2839, 2693, 2599, 1907 (C=N, aromatic), 1662 (-N=CH-, Schiff base group), 1571 (C=C, aromatic), 1264 (C-O), 1214, 1155, 1110 (benzothiazole), 941, 830, 789, 686, 636 (C-S-C).

4-[6-(2-Methyl-acryloyloxy)-hexyloxy]-benzoic acid 4-[(6-ethoxy-benzothiazol-2-ylimino)-methyl]-phenyl ester (**M4**)

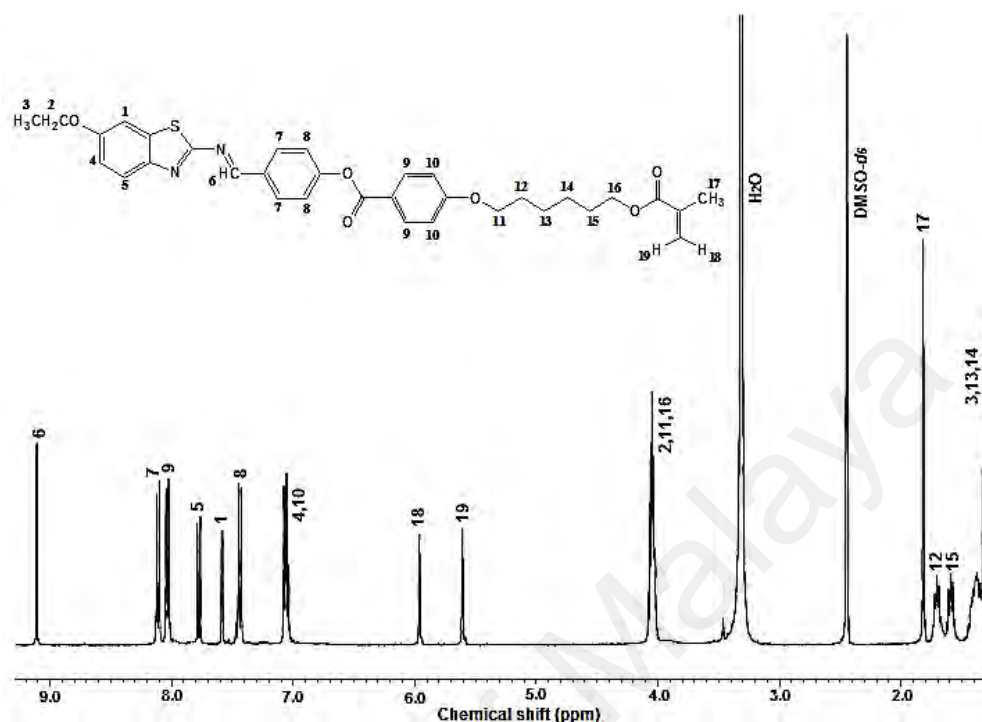


Figure 3.4: ^1H NMR spectra of **M4**.

Compound **1d** (1.31 g, 5 mmol) and compound **3** (1.53 g, 5 mmol) were dissolved in THF:DMF (1:1) mixture. The rest of the succeeding steps were identical to that described for the synthesis of monomer **M1**. Light yellow solid, yield: 30%. ^1H NMR (400 MHz, DMSO- d_6) δ (ppm): 9.13 (s, 1H, -N=CH-, Schiff base group), 8.14-8.12 (d, 2H, Ar-H), 8.06-8.04 (d, 2H, Ar-H), 7.80-7.78 (d, 1H, benzo-H), 7.61 (s, 1H, benzo-H), 7.46-7.45 (d, 2H, Ar-H), 7.09-7.06 (m, 3H, benzo-H + Ar-H), 5.98 (s, 1H, =CH₂), 5.63 (s, 1H, =CH₂), 4.08-4.05 (m, 6H, -OCH₂-), 1.84 (s, 3H, -CH₃), 1.73-1.70 (m, 2H, -CH₂-), 1.62-1.59 (m, 2H, -CH₂-), 1.42-1.31 (m, 7H, -CH₃ and -CH₂-), ^{13}C NMR (100 MHz, DMSO- d_6) δ (ppm): 169.2 (-O-CO-), 167.1 (benzo-C-N=CH-), 165.7 (-N=CH-, Schiff base group), 164.4 (Ar-O-CO-Ar), 163.9 (Ar-C-O-), 157.1 ($^3\text{HC}_2\text{HCO-C-benzo}$), 155.0 (benzo-C-N), 146.0 (benzo-C-S), 136.5 (-C(CH₃)=CH₂), 136.0 (Ar-C-CH=N-), 132.7, 131.9, 131.6, 123.9, 123.4, 120.9, 116.7, 115.3, 106.2 (Ar-C), 126.1 (-C(CH₃)=CH₂), 68.5

(-OCH₂-), 64.5 (-CH₂-O-), 64.3 (-OCH₂CH₃), 28.9 (-OCH₂CH₃), 28.5, 25.7, 25.6, 18.5, 15.2 (aliphatic-C), **FTIR** (cm⁻¹): 3072 (C-H, aromatic), 2930, 2850 (C-H, aliphatic), 1726,1700 (C=O), 1614 (C=C), 1602 (-N=CH-, Schiff base group), 1565 (C=C, aromatic), 1315, 1309 (C-O), 1254, 1231, 1208, 1158, 1107, 1068 (benzothiazole), 943, 867, 844,815, 755, 732, 686, 667 (C-S-C), Anal. Calcd. for C₃₃H₃₄N₂O₆S (in percentage by weight, %): C, 67.56; H, 5.84; N, 4.77; found: C, 67.47; H, 6.15; N, 4.89.

3.3 Characterization methods and instrumentations

The synthesized monomers were characterized by using various instrumental techniques as described in this section to identify the structure as well as the properties of these monomers.

3.3.1 Nuclear Magnetic Resonance Spectroscopy (NMR)

NMR spectroscopy is a versatile and non-destructive technique for exploring the structure of compound. ¹H NMR and ¹³C NMR measurements, two types of NMR instrumentations that are commonly used, were performed with JEOL ECA 400 MHz spectrometer. All compounds with weight 10.0 mg and 20.0 mg for ¹H NMR and ¹³C NMR analyses respectively were dissolved in an appropriate deuterated solvent in NMR tube with depth 4.5 cm. The chemical shifts were referenced against TMS as 0 ppm and the deuterated dimethyl sulfoxide (DMSO-D₆) peaks showed a typical peak at δ value of 2.50 ppm for ¹H NMR and 39.51 ppm for ¹³C NMR.

3.3.2 Fourier Transform Infrared Spectroscopy (FTIR)

Infrared spectroscopy is a universal and important tool to determine the functional groups present in the compound. FTIR spectra were recorded with a Spotlight 400 PerkinElmer spectrometer using attenuated total reflectance (ATR) method with 4 scans and a resolution of 4 cm^{-1} at room temperature. The wavelength was recorded from region 650 to 4500 cm^{-1} . A minimum amount of samples were placed over the ATR crystal and maximum pressure was applied using the slip-clutch mechanism. As this analysis does not related with concentration and a qualitative measurement, the transmittance (%T) was chosen over the absorbance as the y-axis (Smith, 2011), while the x-axis represent the wavenumber in the spectra.

3.3.3 CHN Analysis

Carbon, hydrogen and nitrogen elemental content was obtained using a Perkin Elmer CHNS 2400 Series II Elemental Analyzer. The CHN mode is based on the classical Pregl-Dumas method where samples are combusted in a pure oxygen environment, with the resultant combustion gases measured in an automated fashion. It is ideal for the rapid determination of carbon, hydrogen, and nitrogen content in organic and other types of materials (inorganic, fiber, oil, and etc.). The combustion oven temperature was above $925\text{ }^{\circ}\text{C}$ while the reduction oven had a temperature over $640\text{ }^{\circ}\text{C}$. The instrument was purged using a mixture of pure oxygen and helium gas. The calibration standard was acetanilide.

3.3.4 Differential Scanning Calorimetry (DSC)

Thermal transition temperature and corresponding enthalpy changes of the synthesized monomers were investigated using Perkin Elmer Pyris 6 DSC instrument. During DSC measurement, the samples were heated up from $30\text{ }^{\circ}\text{C}$ to $220\text{ }^{\circ}\text{C}$ at a rate 10

$^{\circ}\text{C min}^{-1}$ and annealed for 1 min. Next, the samples were cooled back to room temperature with slower rate, and hold for another 1 min before second heating cycle to erase any previous thermal history. The monomers were weighed about 5 to 8 mg in a standard sample aluminium pan. All of the data collected were analyzed using Pyris v9.1.0.0203 software.

3.3.5 Polarized Optical Microscopy (POM)

The LC behavior of the synthesized monomers was determined by using polarized optical microscopy instrument. The thermotropic liquid crystalline monomers were heated on the top of Mettler Toledo FP82HT hot stage and viewed with an Olympus BX51 microscope fitted with polarizing filters. There are two polarizers in POM instrument and they are designed to be oriented at right angle to each other, which is termed as cross polar. In addition, the liquid crystalline texture image was captured using Olympus camera that is connected to the microscope. A small amount of the sample was placed on a glass slide and covered with a cover slip. Each sample was heated up until it reached isotropic temperature and then cooled back to room temperature at the rate of $1^{\circ}\text{C min}^{-1}$ for better images. These steps were repeatedly done during heating and cooling cycles as long as it does not reach its decomposition temperature.

3.3.6 Thermogravimetric Analysis (TGA)

Thermogravimetric analysis (TGA) measures loss of mass sample as a function of temperature during decomposition. TGA detects changes in the mass of a sample, evaluates stepwise changes in mass as well as the temperature for each step in the mass changes. Thermal data were obtained using a Perkin Elmer Pyris TGA 4000 instrument. Thermogravimetric analysis were done under N_2 atmosphere with heating rate of 20°C

min⁻¹ from 50 °C to 900 °C. Each sample weighs about 5 mg for all the experiment and all data were processed using the instrument's built in Pyris v9.1.0.0203 software.

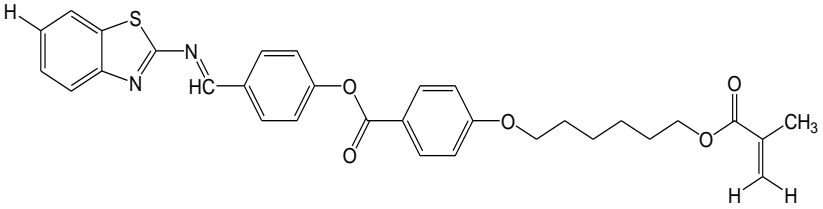
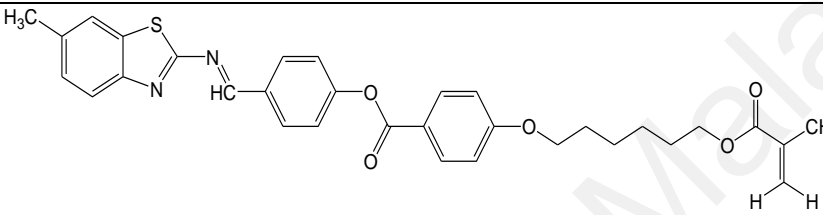
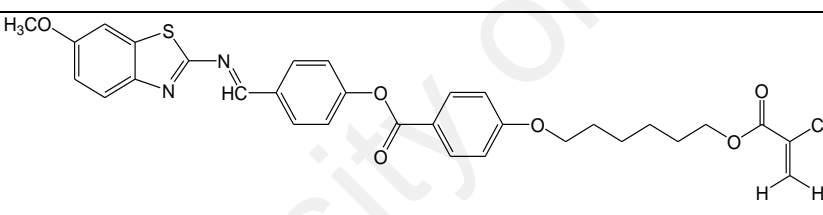
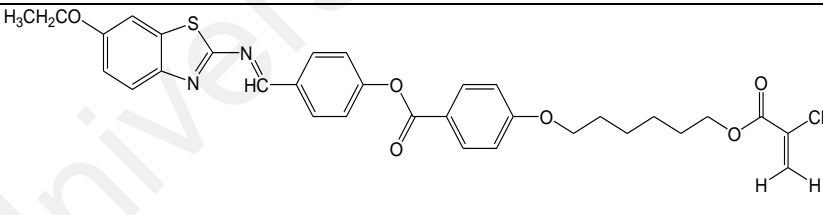
3.3.7 UV-Visible (UV-Vis) and Photoluminescence Spectrometry

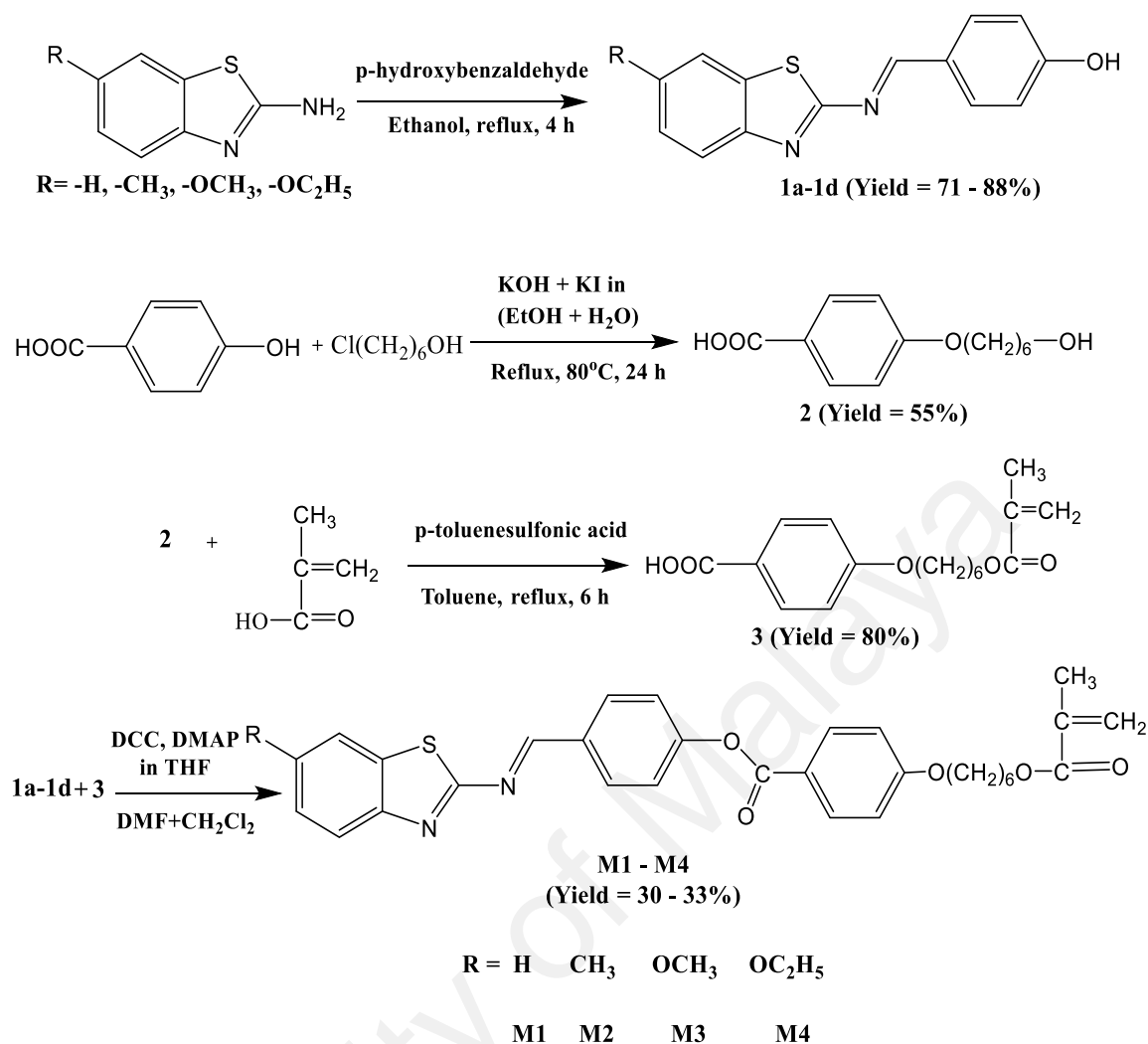
UV-Vis absorption spectra were recorded with a Cary 60 UV-Vis spectrophotometer to study the optical properties of synthesized materials. The prepared monomers were prepared in various polarity of solvents such as dichloromethane (DCM), *N,N*-dimethylformamide (DMF), tetrahydrofuran (THF), chloroform (CHCl₃) and chlorobenzene with concentration of 5x10⁻⁵ M. The polarity of solvents are arranged in an ascending order as follow i.e chlorobenzene, THF, CHCl₃, DCM and DMF (Murov et al., 2017). The solution was placed into 4 sided clear quartz cuvette and the sample was measured from 200 nm to 800 nm with medium scan rate. Meanwhile, the photoluminescence emission spectra were obtained by using Photon Technology International EL-1000 spectrofluorometer equipped with temperature adapter. The sample was heated up from 20 °C to 50 °C with an interval of 5 °C and was measured from 200 nm to 600 nm to study the effect of temperature on the synthesized LC compounds.

CHAPTER 4: RESULTS AND DISCUSSION

4.1 LC monomers and mechanism

Table 4.1: Molecular structure and yield of synthesized LC monomers.

Molecular structure	Monomer	Yield (%)
	M1	30
	M2	31
	M3	33
	M4	30



Scheme 4.1: Synthetic route of LC monomers, M1 - M4.

The molecular structures of LC monomers that have been successfully synthesized are shown in Table 4.1. **M1 - M4** have a similar structure except for the strength of electron-donating groups (-CH_3 , -OCH_3 , $\text{-OCH}_2\text{CH}_3$) at the sixth position of benzothiazole. Benzothiazole group has been chosen to be part of mesogenic core in all monomers due to its unique property in the optical and mesomorphic behaviors. The substituents are located at the sixth position on benzothiazole as this will create a more linearity that can induce mesomorphic behavior to be formed at this position (Ha et al., 2010). Additionally, Pavluchenko and co-workers reported that the substitution at sixth position are more thermally stable as compared to that of the fifth position on the benzothiazole ring (Pavluchenko et al., 1976). Meanwhile, the existence of six-membered

methyl group $(-\text{CH}_2)_6-$ that act as flexible unit plays a crucial role on inducing the liquid crystalline phase and reducing the melting point of the synthesized compounds for application purpose. The ester and Schiff base act as the linking group that connect the flexible chain and the mesogenic rigid core to form liquid crystalline monomers. In this experiment, all the monomers are prepared in the same pathway route involving (i) Schiff base formation, (ii) Williamson etherification, (iii) esterification through condensation and (iv) Steglich esterification. The synthetic route of monomers **M1 - M4** is illustrated in Scheme 4.1.

4.1.1 Schiff base formation

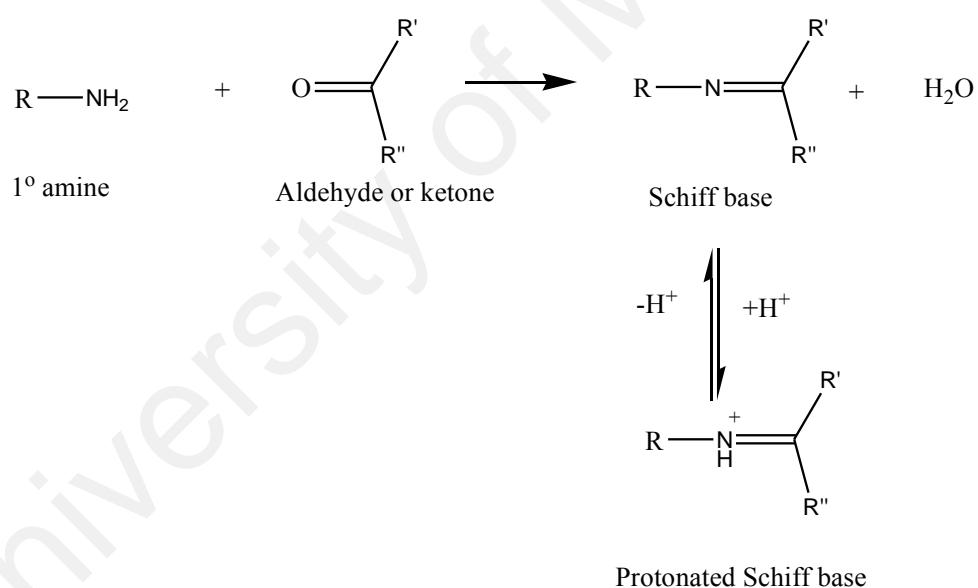


Figure 4.1: Mechanism of Schiff base reaction. Redrawn from (Islam et al., 2018).

Schiff base is usually formed by condensation of an aldehyde or ketone with a primary amine as shown in Figure 4.1., under acid/base catalysis or upon heating condition. The Schiff base reaction undergoes two types of reactions, which are nucleophilic addition followed by elimination. The nitrogen atom from amine acts as nucleophile and attacks the electrophilic carbonyl atom from aldehyde or ketone to give

an unstable tetrahedral carbonyl compound called carbinolamine. Later, the unstable carbinolamine undergoes either acid catalyzed dehydration or through base catalyzed to eliminate water and eventually forms the Schiff base (imine) group. Dehydration of carbinolamine is typically dependable on the rate-determining step of Schiff base formation as the reaction synthesis requires a mild acidic pH (Cordes & Jencks, 1963).

4.1.2 Williamson etherification reaction

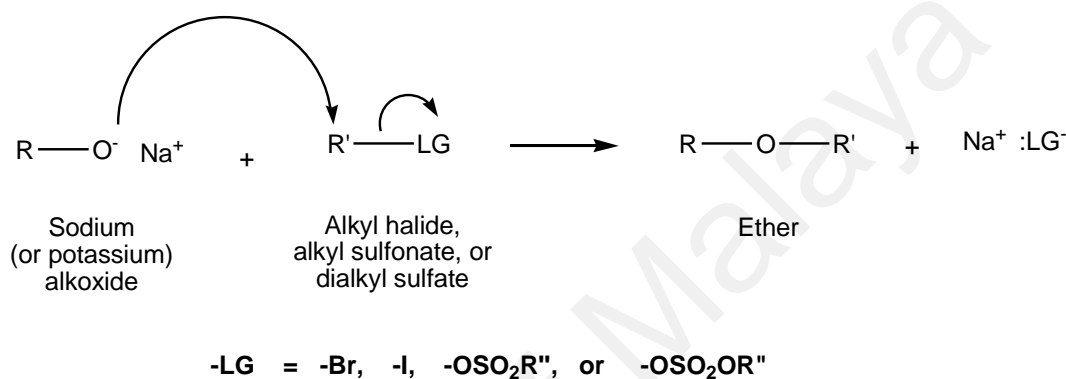


Figure 4.2: Reaction mechanism of Williamson etherification. Redrawn from (Solomons & Fryhle, 2000).

Williamson synthesis of ether, which was introduced by Alexander Williamson in year 1850, is one of the nucleophilic substitution reaction that plays an important route to produce unsymmetrical ether. Mechanistically, the formation of ether through Williamson etherification is depicted in Figure 4.2. This reaction involved S_N2 reaction of an alkoxide ion from deprotonated alcohol with substrates, forming ether group. Typical substrates are 1° and 2° alkyl halides, alkyl sulfonates or alkyl sulphates. The substrates must have a characteristic of a good leaving group and unhindered (Williamson, 1852). In this reaction, the sodium or potassium salt of an alcohol will react with an alkyl halide to produce an ether. However, this alternative does not support reaction using 3° alkyl halide because S_N2 reactions does not occur with this reactant. Therefore, selection on the best combination of alcohol and alkyl halide as reactant should be taken into account in the Williamson synthesis (Fuhrmann & Talbiersky, 2005). This

method is preferable as it avoids the formation of mixtures during the synthesis of unsymmetrical ethers.

4.1.3 Steglich esterification reaction

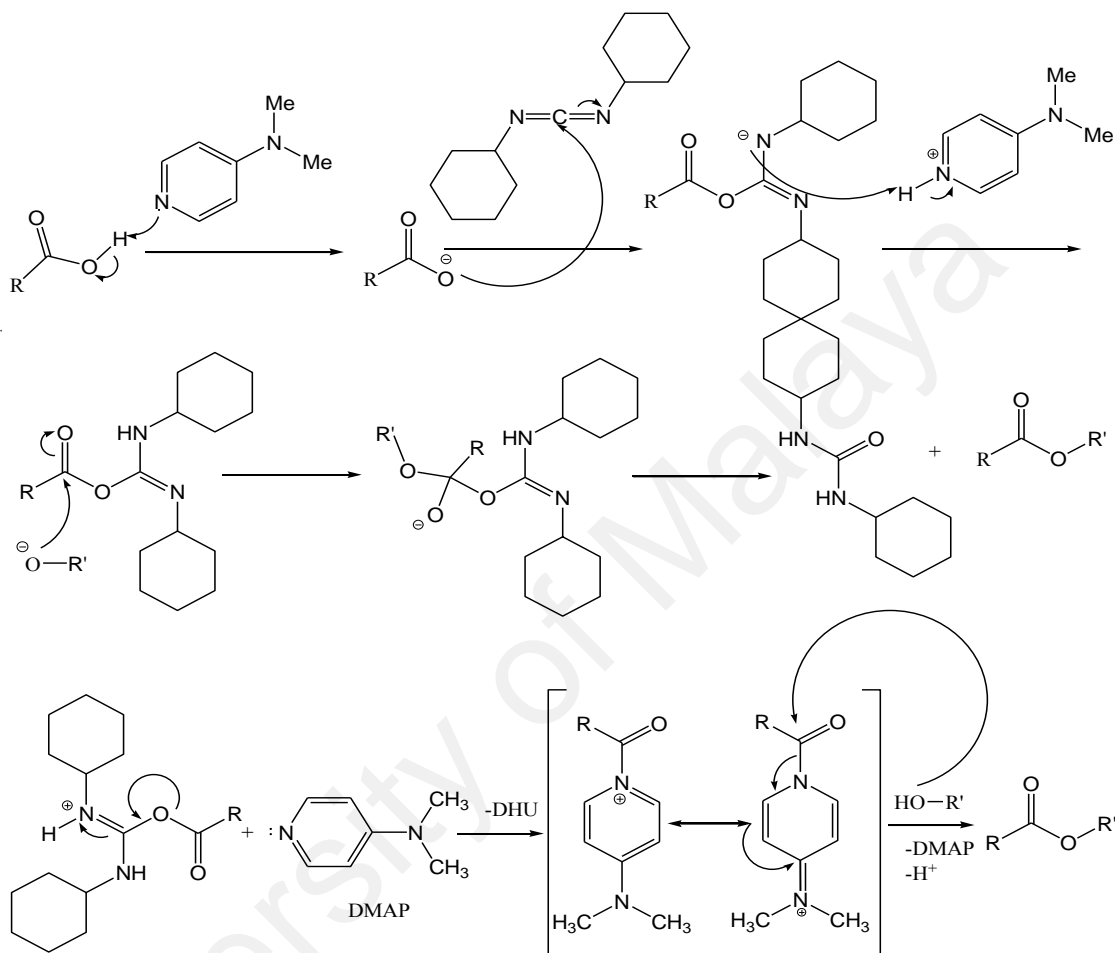


Figure 4.3: Early stage of Steglich esterification reaction. Adopted from (Yan et al., 2012).

Figure 4.3 represents the mechanistic reaction between dicyclohexylcarbodiimide (DCC) and carboxylic compound for Steglich esterification reaction. DCC that acts as coupling reagent will react with carboxylic acid and converts to an *O*-acylisourea intermediate. Later, this activated carboxylic acid can now either react with another equivalent of the carboxylate to form the symmetric anhydride, with alcohol to form the final-product ester and the by-product dicyclohexylurea (DHU), which is easily removed by conventional techniques involving precipitation and chromatography (Boden & Keck,

1985) or undergo intramolecular rearrangement to form the undesirable by-product, *N*-acylurea.

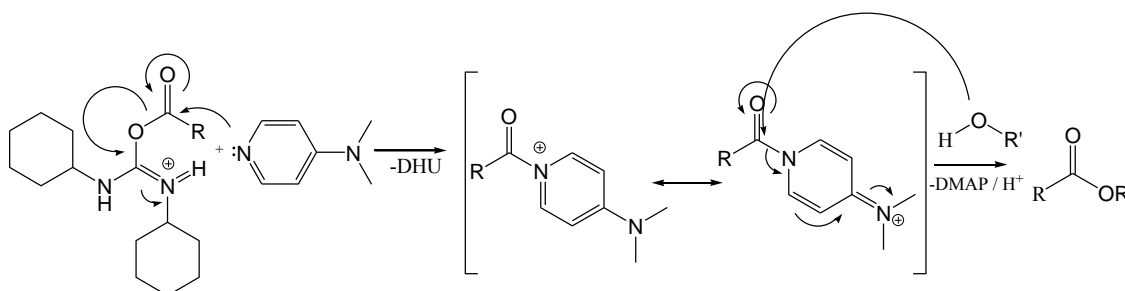


Figure 4.4: Role of DMAP in Steglich esterification reaction. Adopted from (Tsakos et al., 2015).

However, alcohols are generally poor nucleophiles, and hence the degree of *N*-acylurea formation is greater in carbodiimide-mediated esterification reactions. Thus, additional of DMAP, that acts as a stronger nucleophile than the alcohol, in catalytic amounts, can compensate for this tendency by rapid reaction between DMAP and the *O*-acylisourea to form an acyl pyridinium species that are incapable to form the intramolecular by-product. Instead, this intermediate can react rapidly with the alcohol to form the ester (Tsakos et al., 2015). The function of DMAP in the Steglich esterification reaction is shown mechanistically in Figure 4.4.

4.2 Structural determination

The chemical structure of the synthesized monomers **M1** - **M4** was confirmed by 1H NMR, ^{13}C NMR and FTIR spectroscopic techniques. The chemical shifts and peak integrations of all protons in the monomers are in excellent agreement with their expected molecular structure. The characteristic FTIR vibrational frequencies, 1H NMR and ^{13}C NMR chemical shifts of monomers **M1** - **M4** have been described in experimental

section. Signals from ^1H NMR and ^{13}C NMR spectroscopy techniques are used to assign chemical shifts for protons and carbon atoms and shown in Table 4.2. and Table 4.3, respectively. Meanwhile, FTIR vibrational frequencies are vital on determining various types of functional groups of investigated monomers are summarized in Table 4.4. In this section, the spectral properties of monomer **M1** will be discussed as an example.

4.2.1. ^1H NMR spectra

Figure 4.5 depicts the ^1H NMR spectrum for monomer **M1** with its molecular structure. Signals for deuterated DMSO and water in ^1H NMR spectrum are fixed located at δ 2.50 ppm and δ 3.30 ppm respectively. The most de-shielded signal at chemical shift of δ 9.21 ppm represents the proton on imine group (5). Anisotropic field of π electrons in the double bond as well as the electron withdrawing effect from nitrogen atom are the reasons for this proton to be shifted to the most downfield (Salleh et al., 2013). In addition, this signal appears as singlet because there are no neighbouring protons.

The signals between δ 7.39-8.17 ppm are assigned to proton on benzothiazole and benzyl rings (1,2,3,4,6,7,8,9). This ring system belongs to the group of annulenes with $4n+2$ π -electrons ($n=0,1,2,\dots$) which follow the Huckel rule. Thus, they possess aromatic character. The protons on aromatic system are de-shielded due to the π electrons circulating in the entire aromatic rings. When an external magnetic field is applied on the sample, a diamagnetic ring current is induced resulting in the secondary field known as anisotropic field. As a result, protons in the molecular plane and outside the ring are de-shielded (Field et al., 2012).

Two singlet peaks at δ 5.98 ppm (17) and δ 5.63 ppm (18) are attributed to the vinylic protons of methacrylate backbone. These vinylic protons appearing at a

moderately high chemical shift are obviously due to sp^2 hybridized effect in olefin group that produces anisotropic field near to the vinylic protons (Günther, 2013). Meanwhile, quartet signals at δ 4.05 - 4.08 ppm represent the protons on the carbon that is attached to the single-bonded oxygen ($-OCH_2-$) (10 and 15). Protons on α carbon located next to oxygen atom are shifted downfield in the spectrum due to the large electronegativity of the oxygen atom (Pavia et al., 2008). The signal at δ 1.84 ppm is ascribed to the protons of methyl group ($-CH_3$) in the methylene unit (16). This intense peak singlet signal is mainly because of the absence of adjacent protons. The multiplet signals that resonate in the range of δ 1.37 - 1.74 ppm (11 - 14) are attributed to the methylene protons of the flexible chain attached to the rigid phenyl rings.

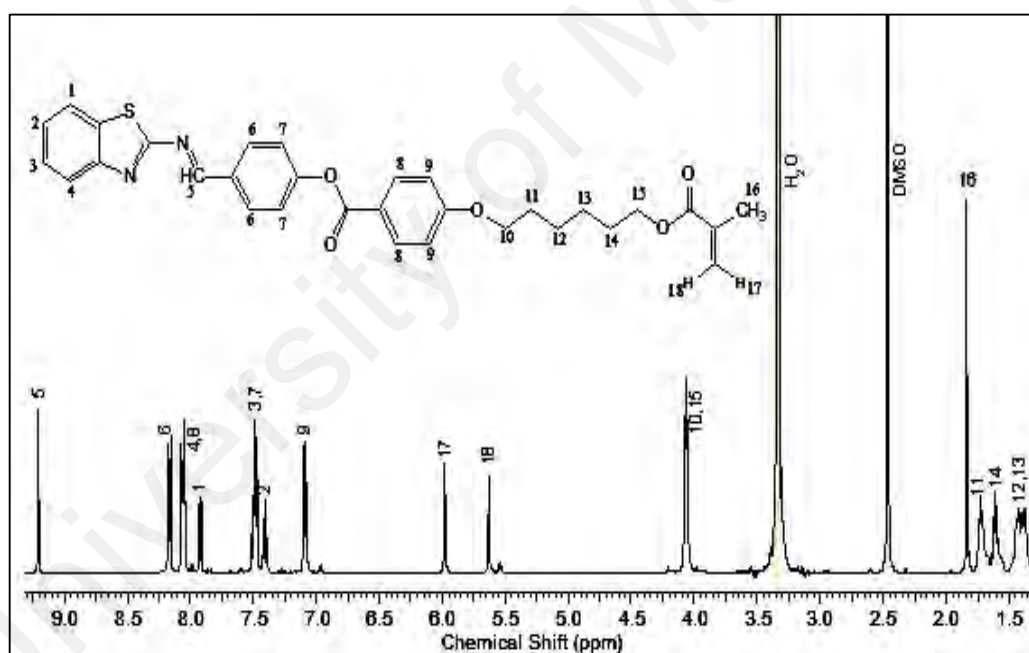


Figure 4.5: ^1H NMR spectra of **M1**.

Likewise monomer **M1**, the rest of monomers, **M2** - **M4**, show similar ^1H NMR spectral properties as described for monomer **M1** as they bear structural similarities except for the substituents attached on the sixth position of benzothiazole moiety. An extra singlet peak appeared at δ 2.41 ppm in ^1H NMR spectra for **M2** indicating the methyl

group (-CH₃) substituted in the benzothiazole core. On the contrary, an intense signal at δ 3.68 ppm in **M3** spectra represents the terminal methoxy group attached to the benzothiazole ring. Methoxy group is an electron donating group and the electronegative oxygen atom in the methoxy group increases the shielding of the hydrogens causing them to move upfield (Abraham et al., 1988). Meanwhile, two new signals at δ 1.42 - 1.31 ppm and δ 4.08 - 4.05 ppm along with -CH₂- group are attributed to -CH₃ unit and -OCH₂- unit from ethoxy group in spectra of monomer **M4**, respectively.

Table 4.2: ¹H NMR chemical shifts of different types of protons present in M1 - M4.

Type of Proton	Chemical shifts, δ (ppm)
H-C=N	9.21 - 9.98
Schiff base-Ar-H	8.03 - 8.16
Benzo-H (4 th position)	7.24 - 7.93
Benzo-H (5 th position)	6.74 - 7.51
Benzo-H (6 th position)	7.44 - 7.46
Benzo-H (7 th position)	7.17 - 7.93
Ar-H	7.04 - 7.42
=CH ₂ , vinyl group	5.61 - 5.98
-OCH ₂ -	4.03 - 4.08
-CH ₃ , methacrylate group	1.83 - 1.84
-CH ₂ -, hexyl group	1.37 - 1.73
-CH ₃ , methyl group	2.41
-OCH ₃ , methoxy group	3.68
-OCH ₂ CH ₃ , ethoxy group	4.05 - 4.08 (-OCH ₂ -), 1.31 - 1.42 (-CH ₃)

4.2.2. ^{13}C NMR spectra

^{13}C NMR spectrum of monomer **M1** is illustrated in Figure 4.6. The signals at the most de-shielded region between δ 167.1 - 131.6 ppm are assigned as the quaternary carbon atom with no proton attached on them (C_{24} , C_7 , C_8 , C_{13} , C_{17} , C_{12} , C_6 , C_1 , C_{25} and C_9). These peaks are shifted to higher chemical shift mainly due to sp^2 hybridization anisotropy. The signals at δ 167.1 ppm and δ 164.3 ppm are assigned as carbon of carbonyl group, $-\text{OC}=\text{O}$, C_{24} , and imine group, C_8 , respectively. These carbons have the largest chemical shift due to sp^2 hybridization effect of the double bond as well as the insertion of electronegative oxygen atom and nitrogen atom that have caused them to de-shield further (Pavia et al., 2008).

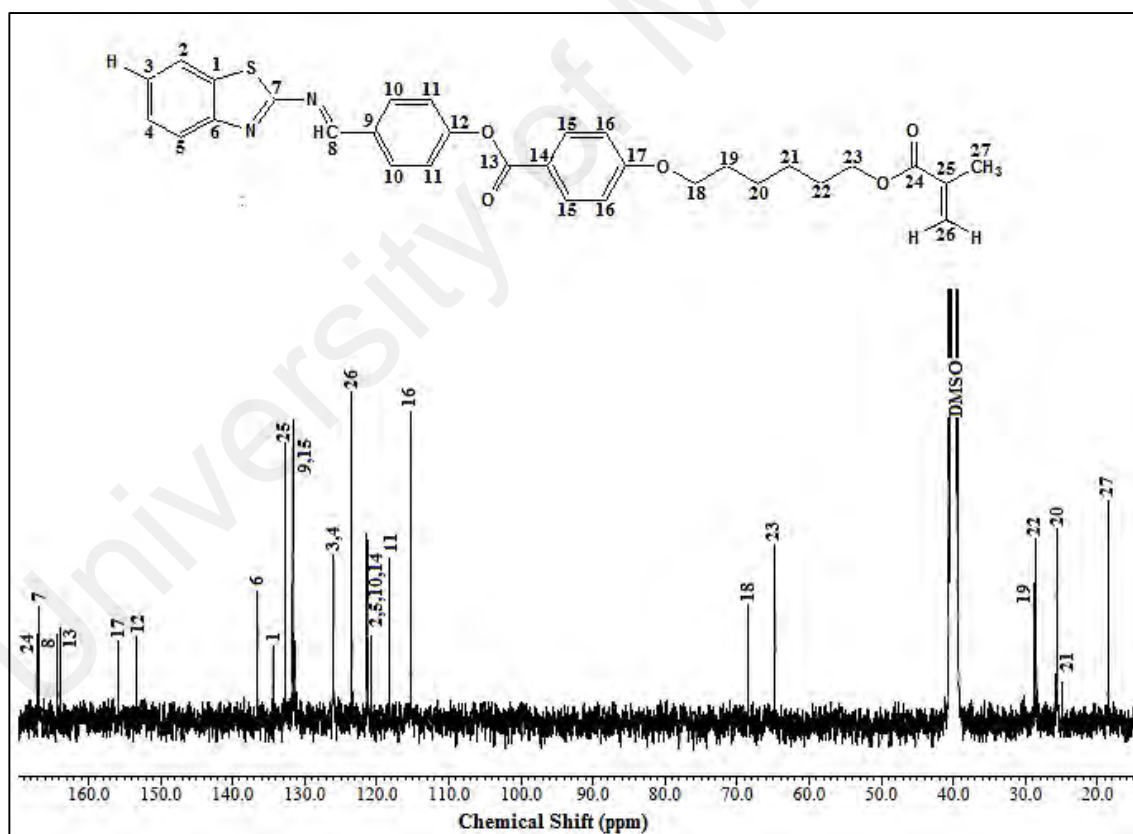


Figure 4.6: ^{13}C NMR spectra of M1.

The signals for aromatic rings basically one in a moderately high field region at δ 131.4 to 115.3 ppm. At δ 68.5 ppm and δ 64.8 ppm, the two signals appeared are assigned to C_{18} and C_{23} , both carbons on the flexible alkyl chain attached to an electronegative

oxygen atom and aromatic rings (-OCH₂-) respectively. Signal for carbon C₁₈ is slightly de-shielded than C₂₃ as this carbon is near to aromatic rings that possess anisotropic effect. The signals around δ 28.9 ppm until δ 18.5 ppm are attributed to methylene group (-CH₂-) in the long alkyl chain as well as the methyl group (-CH₃).

Table 4.3: ¹³C NMR chemical shifts of various types of carbons present in M1 - M4.

Type of Carbons	Chemical shifts, δ (ppm)
-O- <u>C</u> O-	169.2 - 167.1
benzo- <u>C</u> -N=CH-	167.1 - 166.6
-N= <u>C</u> H-, Schiff base group	165.8 - 163.3
Ar-O- <u>C</u> O-Ar	164.4 - 164.0
Ar- <u>C</u> -O-	155.9
Ar- <u>C</u> -O-CO-	155.3
benzo- <u>C</u> -N-	136.5
benzo- <u>C</u> -S	134.4
- <u>C</u> (CH ₃)=CH ₂	132.7
Ar- <u>C</u> -CH=N-	131.6
Ar- <u>C</u>	131.4 - 115.3
-C(CH ₃)= <u>C</u> H ₂	126.0
-O <u>C</u> H ₂ -	68.5
- <u>C</u> H ₂ -O-	64.8
Aliphatic- <u>C</u> + - <u>C</u> H ₃	28.9 - 18.5
- <u>C</u> H ₃ (substituent)	25.0
-O <u>C</u> H ₃ (substituent)	56.2
-OCH ₂ CH ₃ (substituent)	64.3 (-O <u>C</u> H ₂ -), 28.9 (-CH ₃)

A similar ^{13}C NMR spectral properties are observed in the rest of monomers **M2** - **M4** as they possess similar molecular structure except for the different substituents attached at the sixth position on benzothiazole moiety (see Table 4.3). An extra signal at δ 25.8 ppm for monomer **M2** is assigned to methyl group ($-\text{CH}_3$) attached on sixth position of benzothiazole mesogen group. In contrast, a signal at δ 56.3 ppm in **M3** spectra represents the terminal methoxy group ($-\text{OCH}_3$) attached on the benzothiazole ring. As for monomer **M4**, two signals at δ 64.3 ppm and δ 28.9 ppm along with methylene group from the long alkyl chain indicate the presence of $-\text{CH}_3$ unit and $-\text{OCH}_2-$ unit from ethoxy group in ^{13}C NMR spectra of monomer **M4**, respectively.

4.2.3. FTIR spectra

FTIR spectrum of monomer **M1** is shown in Figure 4.7. Monomer **M1** exhibits various vibrational modes indicating the stretching and bending of different functional groups in the molecule. A very weak band observed near 3063 cm^{-1} is attributed to aromatic unsaturated $=\text{C}-\text{H}$ stretching vibration. Two vibrational bands around 2928 cm^{-1} and 2853 cm^{-1} represent the asymmetric and symmetric stretching of methylene group ($-\text{CH}_2-$) of aliphatic alkyl chain. An intense absorption band that at 1721 cm^{-1} corresponds to ($\text{C}=\text{O}$) stretching vibration of ester group located in the terminal group. The strong absorption band at 1615 cm^{-1} reflects the alkene group ($\text{C}=\text{C}$) in the terminal methacrylate functional group. The $\text{C}=\text{N}$ stretching vibration from Schiff base group exhibits a medium intense absorption band around 1601 cm^{-1} . The band at 1578 cm^{-1} is ascribed to $\text{C}=\text{C}$ stretching from aromatic rings in the structure. The $\text{C}-\text{O}$ link in the methacrylate group appears as stretching near 1302 cm^{-1} and 1260 cm^{-1} . The strong absorption bands in the region $1229-1053\text{ cm}^{-1}$ are attributed to the overall structure of benzothiazole ring in mesogenic moiety. The stretching vibration bands of $\text{C}-\text{S}-\text{C}$ group of benzothiazole are

observed at 984-671 cm^{-1} . Generally, a similar spectral behaviors are also observed for other LC monomers (**M2** - **M4**) with slight variations in intensity and shifting of the bands.

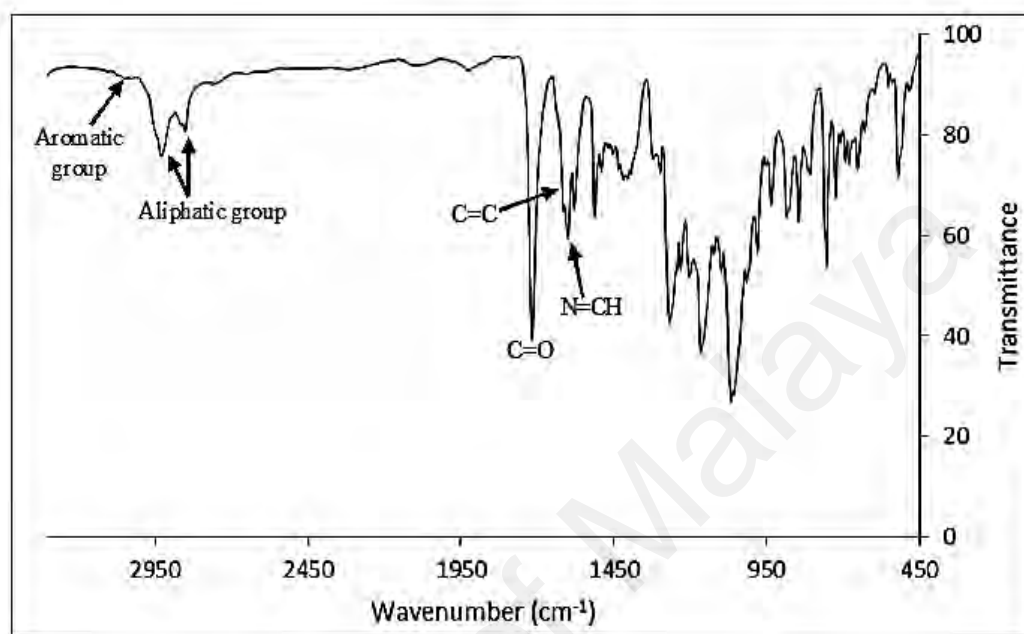


Figure 4.7: FTIR spectra for M1.

Table 4.4: General FTIR absorption spectra for M1 - M4.

Wavenumber (cm^{-1})	Functional groups
3055 – 3072	C-H, aromatic
2930 – 2850	CH_2 , aliphatic
1726 – 1700	C=O
1618 – 1565	C=C
1602 – 1600	HC=N, schiff base
1578 – 1565	C=C, aromatic
1315 – 1260	C-O
1257 – 1053	Benzothiazole
984 – 517	C-S-C

4.3 Solubility behavior

The solubility tests for all LC monomers were done by dissolving a small amount of solid (approximately 3 - 5 mg) in 2 mL of few polar and non-polar solvents at room temperature. The monomers show an excellent solubility in some typical organic solvents, such as chlorobenzene, tetrahydrofuran (THF), chloroform (CHCl₃), N,N-dimethylformamide (DMF) and dichloromethane (DCM). The introduction of bent structure in the aromatic ring and the presence of aliphatic segments in the backbone that provide flexibility to the system had proven to give a positive effect on the solubility of the synthesized monomers (Hussein et al., 2012). Vasanthi and Ravikumar (Vasanthi & Ravikumar, 2007) reported that their investigated compounds, poly(phenylthiourea azomethine ester)s, are soluble in aprotic polar solvents due to the insertion of flexible bonds between main chain aromatic rings as well as the structural irregularities in the compounds .

4.4 Thermal properties of M1 – M4

The TG and DTG curves for monomers **M1** - **M4** are depicted in Figure 4.8 and Figure 4.9 respectively and their thermal results are summarized in Table 4.5.

Based on Table 4.5, compounds **M1** - **M3** show an average thermal stability corresponding to their 5% weight loss (T_d 5%) indicating the thermal decomposition temperatures being below 280 °C. Balaji and Murugavel (Balaji & Murugavel, 2012) reported that the presence of ether linkage in the spacer units would provide flexibility to the methylene chain of the monomer and bring down the thermal stability. On the contrary, thermal decomposition temperature corresponding to 5% (T_d 5%) weight loss of monomer **M4** was above 280 °C which proves that compound **M4** is thermally stable (Karim et al., 2013; Salleh et al., 2013) compared to other monomers. The greater thermal

stability of monomer **M4** may be due to the stronger molecular interaction in the solid state and thus requires high temperature to break the bond (Medvidović-Kosanović et al., 2015).

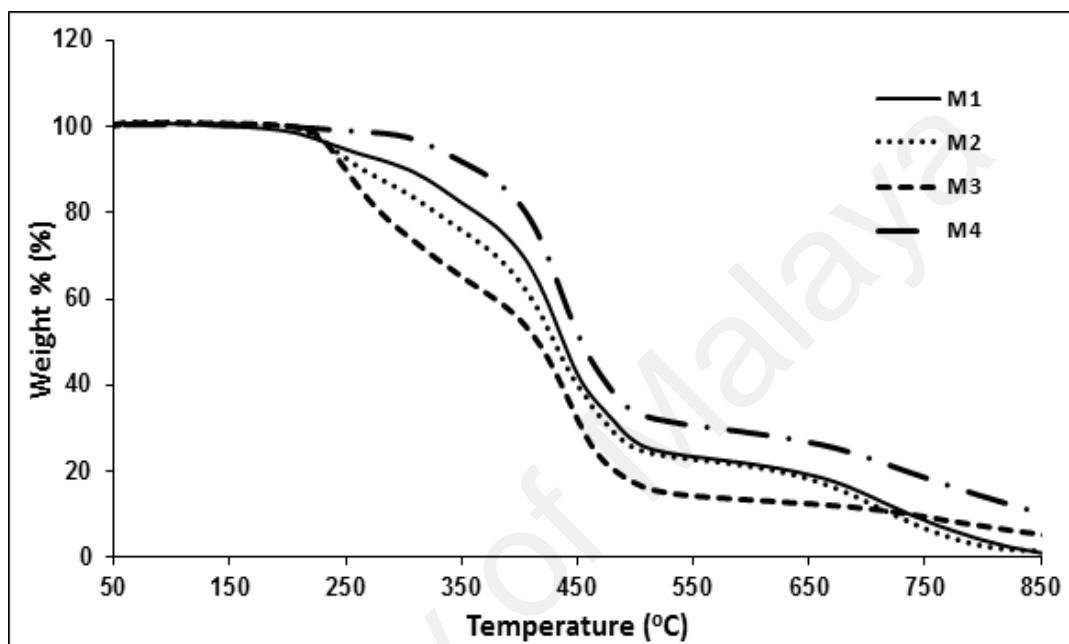


Figure 4.8: TG traces of M1 - M4.

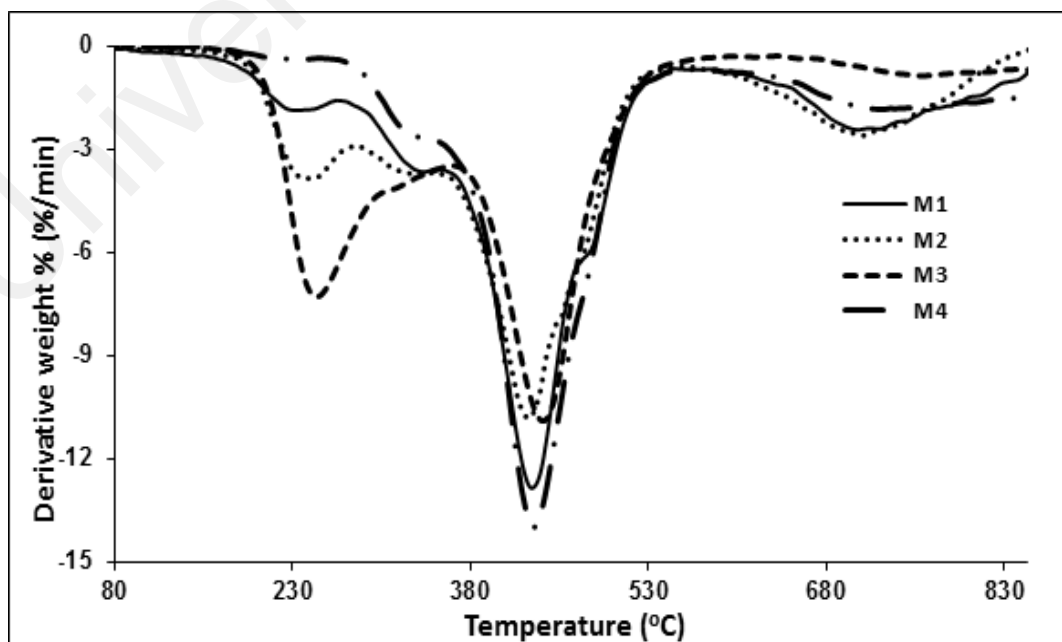


Figure 4.9: DTG curves of LC monomers.

Four-staged of decomposition are observed for all monomers (except **M4**). The first-stage is started around 182 – 363 °C with a mass loss of 6.6 - 24.3% attributed to the thermal decomposition of Schiff base group and the substituents simultaneously. This is followed by second decomposition stage ranging from 273 – 351 °C with a mass loss of 8.2 - 14.1% (calcd. 15.5%) for **M1 - M3** which is due to the thermal cleavage of aliphatic hexyl group in the spacer part of the compounds. A similar observation was also reported by Xiang (Xiang, 2012), who observed the decomposition temperature of aliphatic chain in his studied materials started to occur around 230 °C.

Table 4.5: Thermal analysis data for M1 - M4

Monomer		M1	M2	M3	M4
T _d 5% (°C)		249	238	236	331
1 st decomposition	Temperature (°C)	182-272	191-275	195-297	212-363
	Wt. loss (%)	6.6	11.7	24.3	9.5
2 nd decomposition	Temperature (°C)	273-338	276-351	298-396	364-567
	Wt. loss (%)	8.2	12.7	14.1	60.0
3 rd decomposition	Temperature (°C)	339-556	352-555	370-551	568-831
	Wt. loss (%)	61.4	53	47.4	18.3
4 th decomposition	Temperature (°C)	556-870	556-869	552-818	-
	Wt. loss (%)	21.5	21.1	7.7	-
Char Yield (%) at 850°C		1.3	1.5	5.4	10.5

Meanwhile, the third decomposition stage at 339 – 567 °C with the highest weight loss of 61.4%, 53.0%, 47.4% and 60.0% (calcd. 53.3%) for monomers **M1 – M4** respectively, show a sharp differential peak in DTG curves. This decomposition stage corresponds to the degradation of benzene and benzothiazole rings in the monomers. The presence of π and σ bonds in aromatic ring provide conjugation system across the entire molecules as these structures contain overlapping *p*-orbitals and consequently will

delocalized the electrons in the structure. As a result, the conjugated rings become more stable and required high temperature to break the bond (Vančik, 2014).

Lastly, decomposition transition from 552 – 870 °C with a mass loss of 7.7 - 18.3% (calcd. 23%) for compounds **M1** - **M4** is attributed to the thermal cleavage of carbonyl group or the scission of other C-O bonds in the structure and the methacrylate group form CO₂ and H₂O (Kaya et al., 2008; Liu et al., 2008) Reddy and his co-workers (Reddy et al., 2014) also suggested that their investigated compounds containing lengthy core with ester connecting units favor high thermal stability. Besides possessing strong chemical bond, the ester linkage is stabilized due to occurrence of the charge-separated resonance, where more energy is needed for bond rupture (Critchley et al., 2013).

4.5 Mesomorphic behavior of M1 – M4

The mesomorphic behavior of monomers **M1** - **M4** were studied using differential scanning calorimetry (DSC) and polarizing optical microscope (POM). Phase transitions and associated enthalpy changes (ΔH) of all synthesized monomers are summarized in Table 4.6. The mesophase textures from POM observations are in good agreement with corresponding DSC thermograms. The effect of terminal group substituents and the effect of linking group on the mesomorphic behavior of the monomers will be discussed below.

4.5.1 Effect of thermal substituents on mesogenic unit

The thermal transition temperatures (T_g) and mesomorphic behaviors of all the synthesized monomers are studied by DSC and POM. The DSC traces of **M1** – **M4** are illustrated in Figure 4.10 and the results of the thermal properties including enthalpy changes (ΔH) are summarized in Table 4.6. **M1** exhibits significant mesophase peaks

during cooling and heating cycles. On the contrary, there were no distinct exothermic peaks identified for monomers **M2** - **M4** during cooling scan due to the partial decomposition of the monomers. This phenomena was also encountered in azine-type liquid crystals (Wei et al., 2008). Thus, we will only consider the first heating DSC data of monomers **M2** - **M4** for further discussion.

Table 4.6: Mesophase length, phase transitions, and enthalpy changes for M1 - M4 upon heating and cooling scans.

Monomers	Phase transition temperature (°C) ^{a,b} (enthalpy changes, J g ⁻¹)		Mesophase length for heating (°C)	
	Heating		N	S
M1	Cr1 77.7 (0.5) Cr2 84.4 (-0.6) S 121.5 (0.3) N 147.0 (0.3) I	I 115.3 (-0.4) N 77.8 (-1.0) S	25.5	37.1
M2	Cr1 87.9 (0.3) Cr2 95.8 (3.9) N 187.2 (-0.01) I	-	91.4	-
M3	Cr 92.9 (35.3) N 184.1 (0.3) I	-	91.1	-
M4	Cr1 110.6 (12.0) Cr2 117.5 (- 0.9) N 202.5 (2.5) I	-	85.0	-

^a Transition temperatures (°C) and enthalpies (in parentheses, J g⁻¹) were measure by DSC (at a heating and cooling rate of 10°C min⁻¹)

^b Note: Cr = crystal; S = smectic phase; N = nematic phase; I = isotropic phase

Figure 4.10(a) shows the DSC thermograms of heating and cooling cycles for monomer **M1** at a heating rate of 10 °C/min. Compound **M1** exhibits two exothermic peaks on cooling process: (i) isotropic to nematic transition at 115.3 °C and (ii) nematic to smectic phase at 77.8 °C. No crystallization peak up to room temperature was observed. Hamryszak et al. (Hamryszak et al., 2012) also reported similar observations, in which no cold “crystallization” peak was observed on the symmetrical azobenzeneimine during cooling scan in the DSC thermogram. In contrast, **M1** shows three thermal transition

peaks during the second heating scan: (i) a crystal to smectic at 84.4 °C, (ii) smectic to nematic at 121.5 °C and (iii) nematic to isotropic at 147.0 °C.

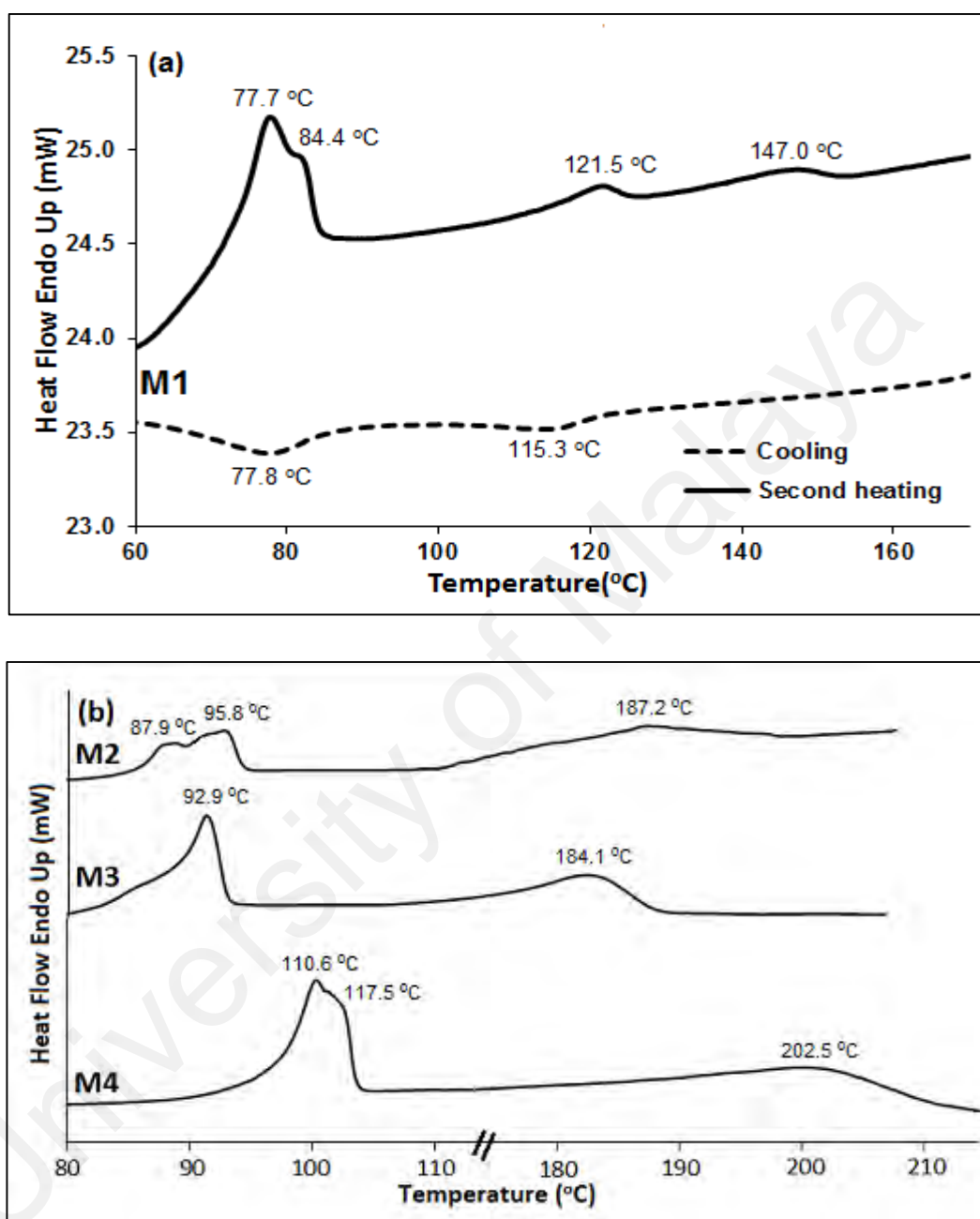


Figure 4.10: DSC thermograms of (a) M1 (b) M2 - M4.

On the other hand, monomers **M2 - M4** revealed two thermal transitions at lower and higher temperatures during heating, indicating that the transitions are from anisotropic crystal phase to nematic mesophase and nematic mesophase to isotropic

phase, respectively (Figure 4.10(b)). Monomer **M2** exhibits (i) a crystal to nematic phase transition at 95.8 °C and change from (ii) nematic phase to isotropic phase at 187.2 °C. Similarly, monomer **M3** exhibits (i) a crystal to nematic transition at 92.9 °C and (ii) nematic to isotropic transition at 184.1 °C. Likewise, monomer **M4** shows two thermal transitions: (i) crystal solid to nematic phase at 117.5 °C and (ii) nematic to isotropic phase at 202.5 °C.

According to Table 4.6 and Figure 4.10, we observe that monomers **M1**, **M2** and **M4** exhibit two non-separable crystalline peaks in the DSC thermograms during the second heating. This could be due to the partial solidification of the materials on keeping at room temperature. Therefore, the first peak at a lower temperature was assigned to a solid to solid transition and the second peak at a higher temperature was attributed for melting transition (Kumar & Pal, 2005).

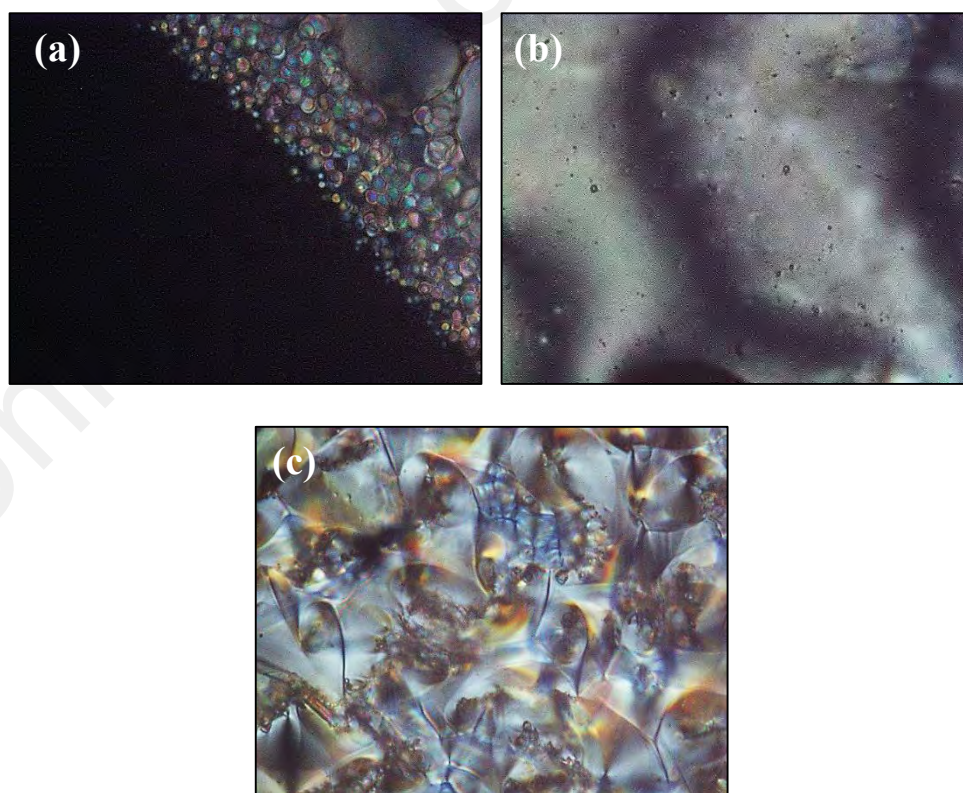


Figure 4.11: Optical photomicrographs (magnification $\times 50$) of M1 observed under POM upon cooling cycle: (a) nematic droplets texture at 120.7 °C (b) marble texture of nematic phase at 113.7 °C and (c) smectic phase showing broken fan-shaped texture at 74.2 °C.

The identification of mesophases was made by comparing the detected textures with those reported in the literatures (Findeisen-Tandel et al., 2012; Ghosh et al., 2014; Muniprasad et al., 2012; Parra et al., 2003; Qaddoura & Belfield, 2009; Sackmann & Demus, 1966). The optical photomicrographs of monomer **M1** were recorded during cooling scan whereas POM images of **M2** – **M4** were taken during heating as these monomers did not show any mesophase texture during cooling scan due to the partial decomposition of the monomers. Monomer **M1** exhibited droplets texture of nematic phase at 120.7 °C (Figure 4.11(a)) upon cooling from isotropic liquid and upon further cooling the nematic droplets coalesced, forming a marble domains of nematic phase at 113.7 °C (Figure 4.11(b)). The marbled texture in the nematic-smectic transition commonly begins to appear like a mixed aligned smectic phase, but then converts to a nematic-like texture (Kumar, 2001). Upon further cooling, a broken fan-shaped texture of smectic phase, a typical texture found in smectic C (SmC) phase (Demus et al., 1971), appeared at 74.2 °C (Figure 4.11(c)).

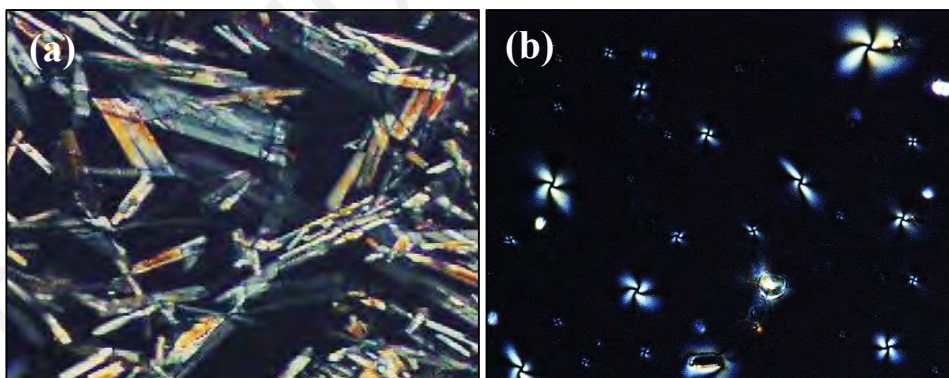


Figure 4.12: The optical textures (magnification $\times 50$) of **M2 observed under POM. (a) crystalline texture at room temperature and (b) schlieren texture of nematic phase at 108.4 °C.**

Figure 4.12 shows the POM of monomer **M2** textures obtained at different temperatures. The crystalline phase of monomer **M2** appeared when the monomer was

cooled to room temperature (Figure 4.12(a)). In contrast, monomer **M2** displayed a schlieren texture of nematic phase upon heating to 108.4 °C (Figure 4.12(b)), which exhibited characteristics sets of four-dark brushes. The dark nematic line defects are attributed to disclinations to indicate discontinuities in the inclination of the molecules (Sakthivel & Kannan, 2005). The texture observed is mainly due to the thread perpendicular to the layer.

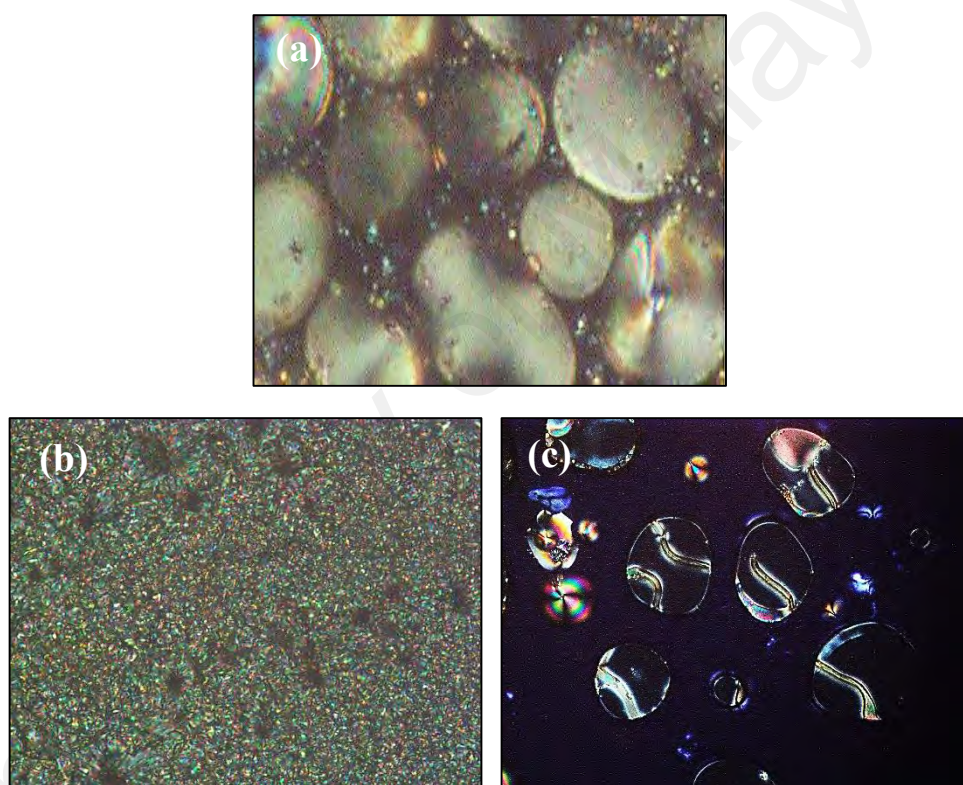


Figure 4.13: The optical textures (magnification $\times 50$) of **M3 observed under POM. (a) large nematic droplets at 113.2 °C, (b) fine grain texture of nematic phase at 103.3°C and (c) nematic droplets with thread-like texture at 109.1 °C.**

Figure 4.13 shows the POM of monomer **M3** textures obtained at different temperatures. The large nematic droplets started to appear when the monomer was cooled to 113.2 °C from the isotropic phase as shown in Figure 4.13(a). As the monomer was

heated slowly at a rate of 1°C/min from its crystal phase, a fine grain texture characteristic of nematic texture was observed at 103.3 °C (Figure 4.13(b)). The fine grains seen are believed to correspond to regions of uniform orientation correlation within nematic structures bounded by disclinations (Demus et al., 2011). Upon further heating, monomer **M3** exhibited nematic droplets with thread-like texture on heating from the anisotropic crystal phase at 109.1 °C (Figure 4.13(c)). The formation of large nematic domains occurred due to the growth of large monodomains, which could possibly be ascribed to the significant segmental mobility and the mesogens taking maximum unidirectional alignment in the melt condition (Balaji & Murugavel, 2012).

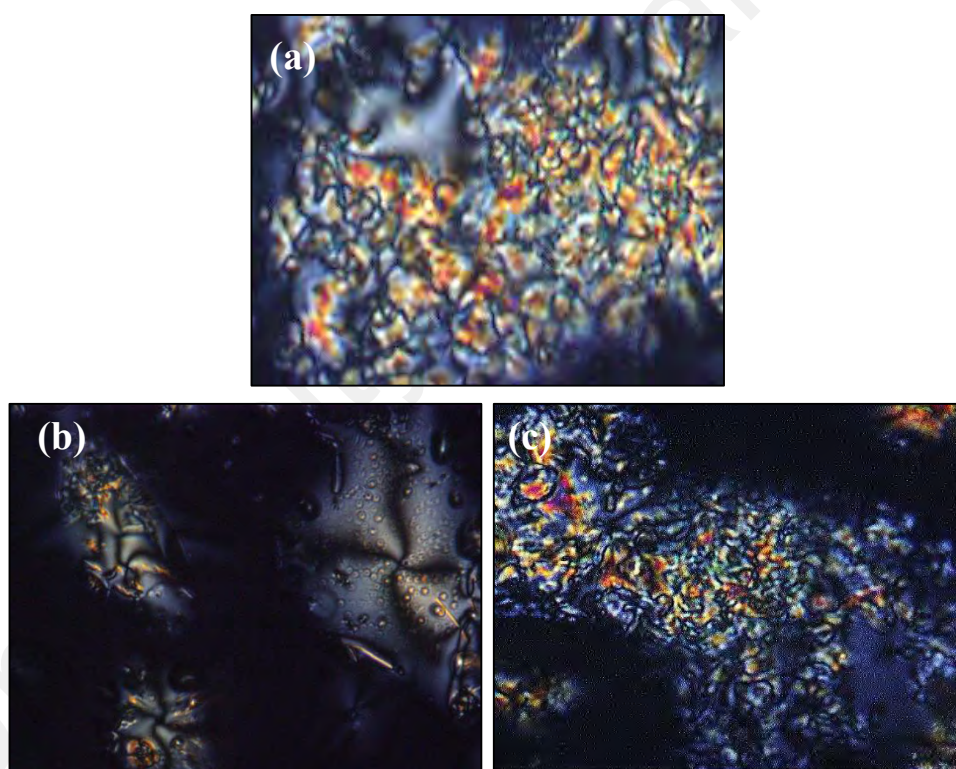


Figure 4.14: The optical textures (magnification $\times 50$) of M4 observed under POM. (a) schlieren texture of nematic phase at 118.9 °C, (b) schlieren texture with four-dark brushes of nematic phase at 114.9 °C and (c) schlieren texture of nematic phase at 119.8 °C.

Figure 4.14 shows the POM of monomer **M4** textures obtained at different temperatures. Upon cooling from isotropic melt, schlieren texture of nematic mesophase appeared at 118.9 °C (Figure 4.14(a)). On the contrary, the schlieren texture with sets of

four-dark brushes of nematic phase was first to appear when the monomer was heated to 114.9 °C from its crystalline phase as shown in Figure 4.14(b). Upon further heating, a similar observation as cooling cycle, the schlieren nematic texture displayed when the monomer was heated to 119.8 °C as depicted in Figure 4.14(c).

Based on the DSC and POM results, the molecular length-to-width ratio and the nature of the terminal groups might facilitate the molecular arrangement and the formation of the mesophases for these compounds. Monomer **M1** exhibited both nematic and smectic phases whereas **M2 – M4** showed only nematic phase as supported in Figure 4.10. This observation may be due to the decrease in the ratio of terminal attractions to lateral attractions that leads to the formation of layered smectic phase in **M1**. The presence of both smectic and nematic phases in monomer **M1** can be explained in terms of the ratio of terminal attractions to lateral attractions. In this case, the calculated molecular length (l) of **M1** is smaller compared to the molecular length of substituted monomers (**M2 – M4**) while the breadth of the molecules are constant (Figure 4.15) causing the ratio of terminal attractions and lateral attractions to decrease. Under such condition, the layered smectic texture is maintained, giving rise to a smectic phase. As the temperature is further increased, the layered structure breaks down due to increased thermal vibrations. The molecules slowly possess a more fluid nature, but retain the orientational order, which gives rise to the formation of nematic texture to the molecules (Selvarasu & Kannan, 2016).

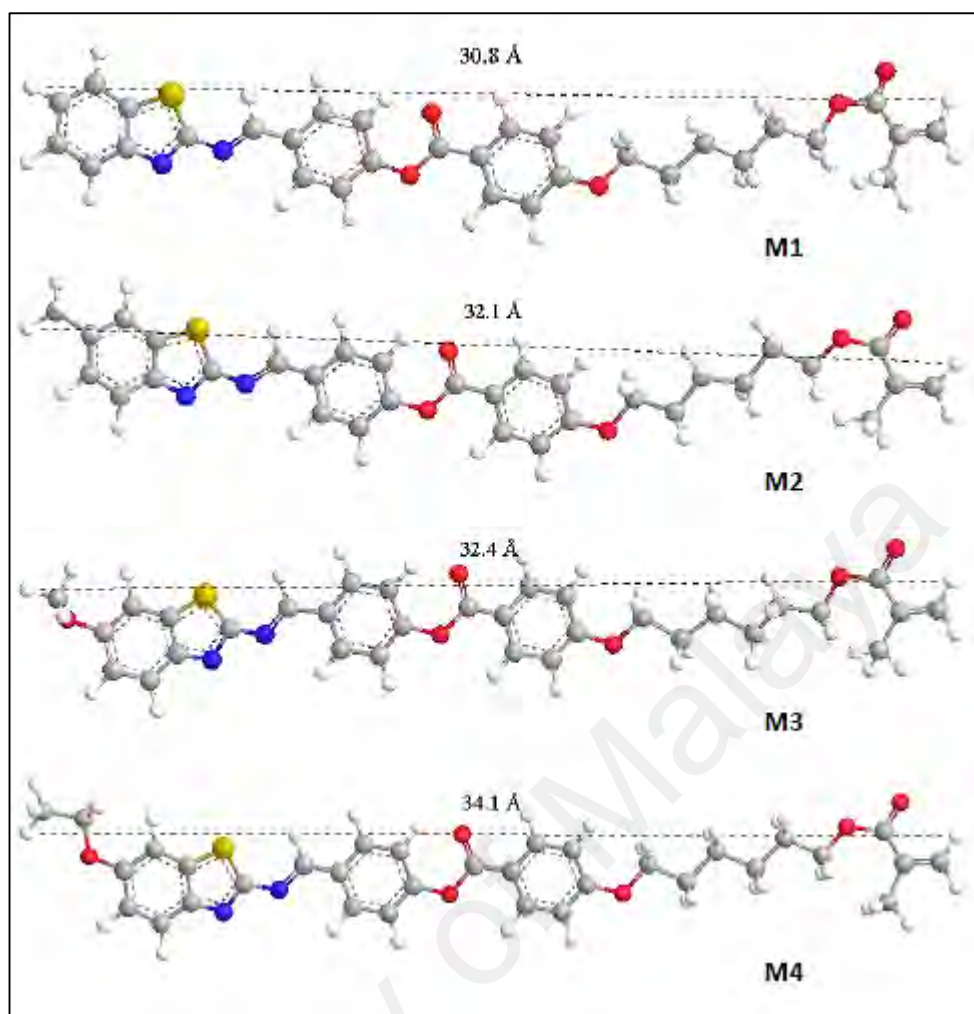


Figure 4.15: Molecular structures and molecular lengths of monomers M1 – M4. The molecular lengths of the studied compounds were calculated from the most extended conformation with optimized energy level by simple molecular modelling (MM2 energy parameters derived from ChemBio3D Ultra 11.0 software).

Replacement of hydrogen atom by the methyl, methoxy and ethoxy groups at the sixth position on the benzothiazole ring in **M2 – M4** plays a vital role in the polarization or electron distribution in electron-deficient benzothiazole moiety which could facilitate the formation of nematic phase (Karim et al., 2013). Besides that, formation of nematic mesophase in **M3** and **M4** is likely attributed to the weak dipole moment and dynamic nature of the freely rotating electron-donating groups (Han et al., 2009).

As apparent in Table 4.6 and Figure 4.10, **M4** with ethoxy group as terminal substituent exhibits the highest N-I transition temperature compared to other monomers. This could be explained that in $-\text{OCH}_2\text{CH}_3$ group, the lone pair of electrons of oxygen is shielded by an insulator-like ethyl group. The repulsive forces involving the oxygen lone pairs are thereby substantially reduced and allow a close approach of the neighboring molecules, increasing bonding forces. This leads to an increase in the N-I transition temperature (Thaker et al., 2010). Additionally, the reduced nematic phase stability of monomers **M3** (91.1 °C) and **M4** (85.0 °C) may be attributed to the fact that the oxygen being in conjugation with the heteroaromatic core extends the length of the rigid core as well as enhances the polarizability anisotropy (Collings & Hird, 2017).

4.5.2 Structural-mesomorphic relationship

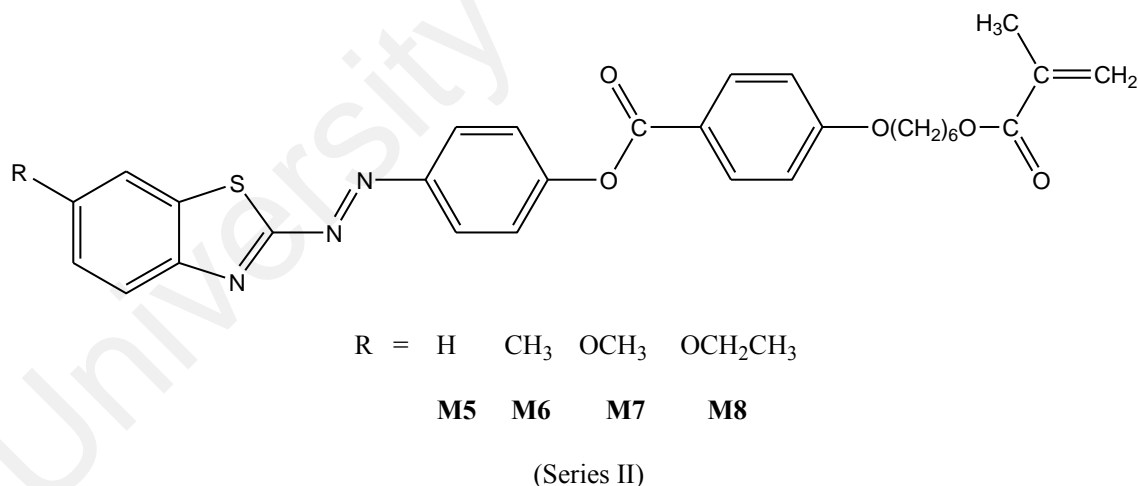


Figure 4.16: A series of azo-ester based liquid crystalline monomers (Karim et al., 2013).

In order to study the influence of different linking groups on the thermal and LC behaviors, a comparison is made between the properties of the present Schiff base-ester monomers with those of our earlier reported azo-ester LC monomers (Karim et al., 2013).

The molecular structure of azo-ester based liquid crystalline monomers as shown in Figure 4.16.

Table 4.7: Comparison on thermal, mesomorphic and optical properties M1 - M4 and M5 – M8.

Monomers		Thermal properties	Mesomorphic properties			Optical properties	
		T _d 5% (°C)	Phase transition temperature (°C) (enthalpy changes, J g ⁻¹)	Mesophase length for heating (°C)		λ _{abs} (nm)	λ _{em} (nm)
				N	S		
Series I	M1	249	Cr1 77.7 (0.5) Cr2 84.4 (-0.6) S 121.5 (0.3) N 147.0 (0.3) I	25.5	37.1	349	404
	M2	238	Cr1 87.9 (0.3) Cr2 95.8 (3.9) N 187.2 (-0.01) I	91.4	-	357	441
	M3	236	Cr 92.9 (35.3) N 184.1 (0.3) I	91.1	-	368	416, 446
	M4	331	Cr1 110.6 (12.0) Cr2 117.5 (-0.9) N 202.5 (2.5) I	85	-	373	419, 452
Series II	M5	316	Cr 104.8 (46.1) SmC 143.3(0.5) N 197.2 (0.6) I	53.4	38.5	N/A ^a	N/A ^a
	M6	318	Cr 106.6(36.5) N 229.6 (0.7) I	123	-	N/A ^a	N/A ^a
	M7	318	Cr 121.0 (58.7) N 236.7 (0.5) I	115.7	-	N/A ^a	N/A ^a
	M8	321	Cr 127.9 (56.4) N 232.5(0.6) I	104.6	-	N/A ^a	N/A ^a

^a The wavelength of absorbance and emission (optical properties) for M5 – M8 were not recorded in previous study by Karim et al.

LC properties of monomers **M1 - M4** and **M5 - M8** showed similar characteristic, in which all the monomers exhibited nematic phase except for the unsubstituted monomers **M1** and **M5**. Both of the unsubstituted LC monomers, **M1** and **M5**, exhibited smectic and nematic phases at lower and higher transitional temperatures during heating and cooling scans. According to Table 4.7, the decomposition temperature as well as the transition temperatures in **M1 - M4** were lower than those of **M5 - M8**, showing the mesomorphic character of Schiff base ester linked monomers are less stable compared to azo-ester bridged monomers. Moreover, the nematic mesophase ranges (ΔN) of **M1** (25.5 °C), **M2** (91.4 °C), **M3** (91.1 °C) and **M4** (85.0 °C) were also found to be smaller than azo-ester based LC monomers, i.e., **M5** (52.9 °C), **M6** (123.0 °C), **M7** (115.7 °C) and **M8** (104.6 °C).

The Schiff base and azo linkages in Series I and II showed a pronounced effect on mesomorphic properties as discussed above. Imine-ester based LC monomers demonstrated decrease in the decomposition temperature, transition temperatures as well as nematic phase stability when compared to monomers containing azo-ester bridged monomers. These observations may be attributed to the movement of electron in the system where electron density pulled by imine linkage in the central core lead to decrease in the transition temperature. In contrast, the azo linkage in the central core provides electron density towards the entire system that enhances the transition temperature (Selvarasu & Kannan, 2016).

4.6 Optical properties of M1 – M4

4.6.1 Effect of different solvents on monomers.

Table 4.8: Absorption and PL emission maxima spectra M1 – M4 in selected solvents.

Solvents	π^*	α	β	$E_T(30)$	Dielectric constant, ϵ	M1		M2		M3		M4	
						λ_{abs} (nm)	λ_{em} (nm)	λ_{abs} (nm)	λ_{em} (nm)	λ_{abs} (nm)	λ_{em} (nm)	λ_{abs} (nm)	λ_{em} (nm)
Chlorobenzene	0.71	0.00	0.07	36.80	5.62	352	408	361	421,	377	427,	381	428,
								492		498		500	
THF	0.82	0.13	0.10	37.40	7.52	349	404	357	441	368	416,	373	419,
										446			452
CHCl ₃	0.58	0.00	0.55	39.10	4.81	280,	405	279,	439	279,	455	281,	459
						351		360		378		379	
DCM	0.58	0.44	0.00	40.70	8.93	276,	406	279,	401,	282,	417,	279,	423,
						348		359	446	374	450	376	457
DMF	0.88	0.00	0.69	43.20	36.70	350	407	357	403,	373	420,	375	420,
								436		446			452

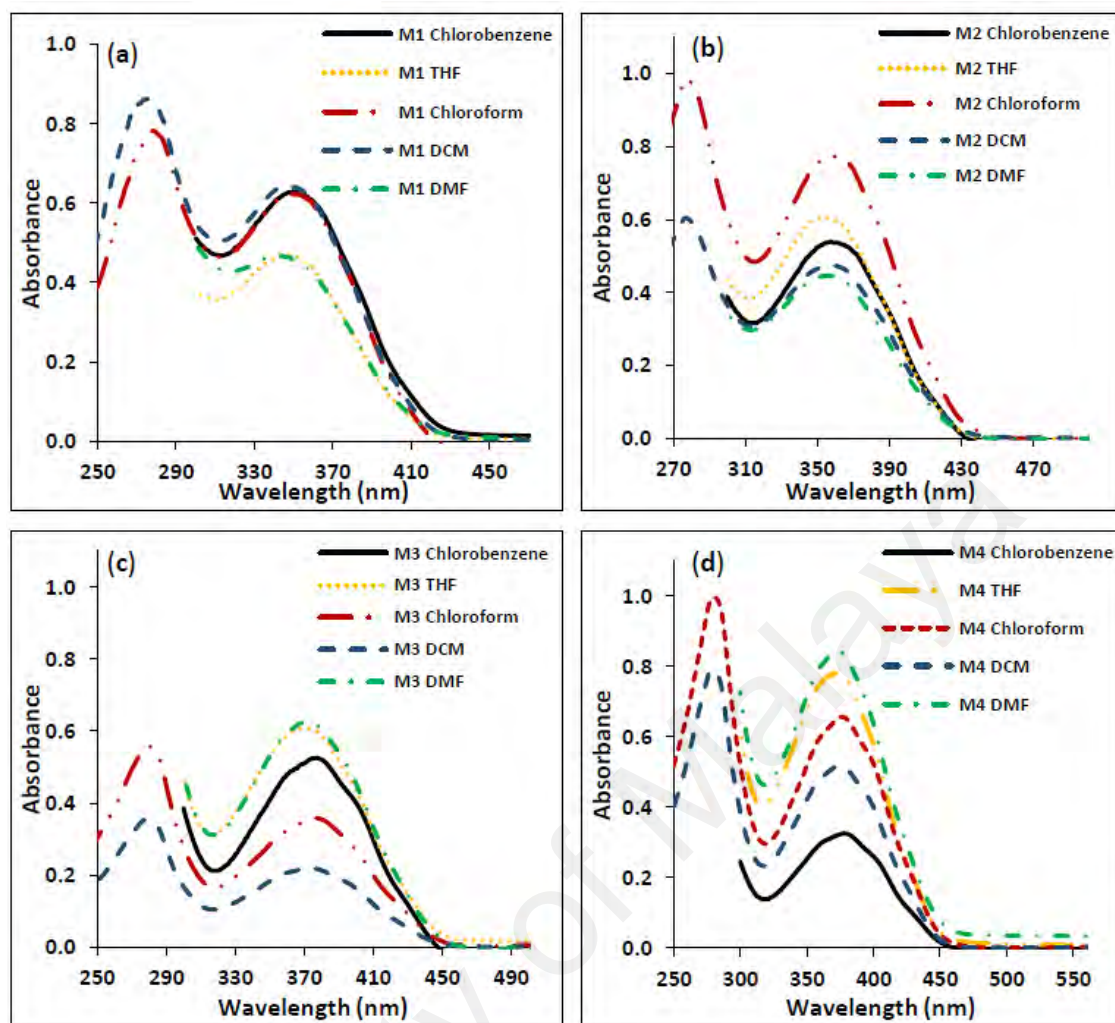


Figure 4.17: UV-Vis absorption spectra for M1 - M4 in different solvents.

According to Table 4.8 and Figure 4.17, absorption bands for **M1 – M4** demonstrate a slightly solvent dependence which did not show a regular variation with the solvent polarity ranging from 374-381 nm. The inconsistency plot indicates that these polymers display a polytonic character in all the employed solvents. This polytonic behavior cannot be explained on the basis of reciprocal polarization effects because wavelengths do not proportionally change by the change of media dielectric constant (Sidir et al., 2017) as well as the polarity of solvent. Bozic et al. (Božić et al., 2014) also observed a similar result for their studied compounds. They observed that azo dyes did not change significantly in all the employed solvents and the absorption maxima did not correlate with the polarity of the solvent.

Based on Figure 4.17, all the monomers revealed two absorption bands in non-polar solvents (DCM and CHCl_3): (i) a lower absorption band at 276-282 nm and (ii) a higher absorption band at 348-376 nm. The appearance of another band at lower wavelength is due to the electronic transition of $-\text{N}=\text{CH}$. Similar to the second band, the first band is also not affected significantly by changes in solvents (Sıdır & Sıdır, 2015).

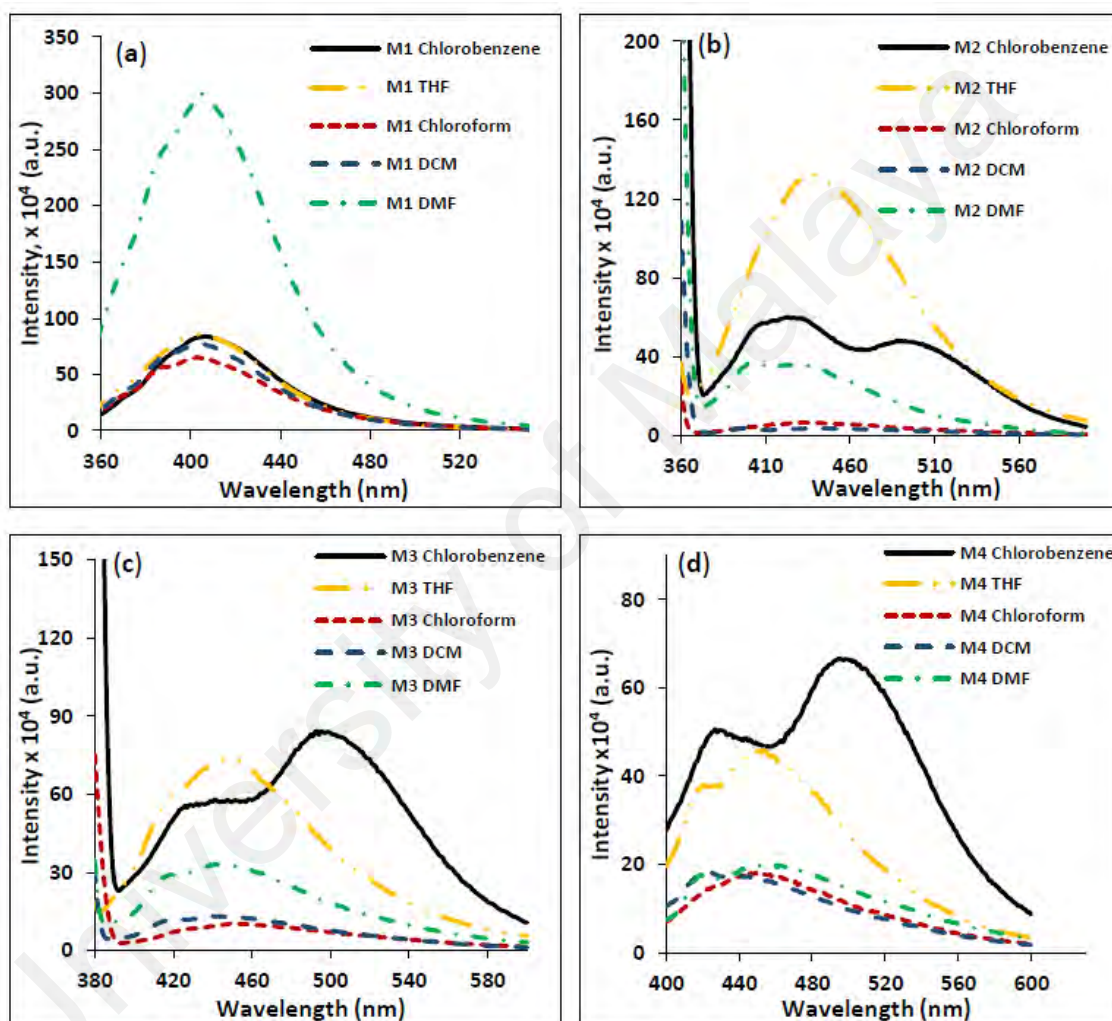


Figure 4.18: Photoluminescence emission spectra of M1 - M4 in various solvents.

To explain the effect of solvent polarity on the emission spectra of **M1** – **M4**, the emission maxima of the higher wavelength of the polymers in different solvents were taken as reference. As depicted in Figure 4.18, the emission maxima of **M1** – **M4** display a polytonic character and highly dependence on the solvent polarity ranging from 401-

500 nm, attributes to the independence on the change of polarity of solvent. As an example, monomer **M1** displayed the maxima emission wavelength (λ_{\max}) at 408 nm (in chlorobenzene), 404 nm (in THF), 405 nm (in CHCl_3), 406 nm (in DCM) and 407 nm (in DMF). This plot indicates that a polytonic character takes place in the emission studies for the investigated polymers. Rufchahi and co-worker (Rufchahi & Mohammadinia, 2014) also reported a similar observation for their studied compound, which is 6-butyl-4-hydroxyquinolin-2-(1H)-one.

The first emission peak corresponds to the π - π^* transition of the benzenoid rings while latter associated to the n - π^* transition of the quinoid rings (Hosseini & Mohammadi, 2009; Huang et al., 2002). The poor fluorescence intensities of **M2** and **M3** in DCM and CHCl_3 can be linked to small concentration of isomers that lead the solute and solvent could not interact properly due to large intermolecular distances (Bera et al., 2005). This means that the dye molecular structure, shape of spectrum and the peak position variations might be controlled by the solvent dye interactions (Gilani et al., 2012).

4.6.2 Correlation by solvent polarity scales

In order to explain the solvatochromic behavior of Schiff base benzothiazole monomers, their spectral properties have been correlated to different solvent polarity scales. The effect of solvent dipolarity/polarizability and hydrogen bonding on the absorption spectra has been interpreted by Reichardt-Dimroth solvent scales, $E_T(30)$ and Kamlet Taft solvent scales.

4.6.2.1 Reichardt-Dimroth solvent scale

Reichardt-Dimroth solvent scale is one of the examples of single parameter empirical scales of solvent polarity that only uses one parameter to describe the system. However, this solvent scale method is limited in the correlation analysis compared to other solvent-dependent processes because they respond to a combination of nonspecific and specific solute/solvent interactions, which are typical for the chemical structure of the probe molecule (Heger, 2006). Table 4.9 and Figure 4.19 depict the linear correlation maximum absorption wavenumber with Reichardt-Dimroth solvent $E_T(30)$ parameter.

Table 4.9: Data of linear correlations between the absorption wavenumbers ν_a (cm^{-1}) of M1– M4 and $E_T(30)$ values (cm^{-1}) for n different solvents, according to $\nu_a = \nu_0 + S \cdot E_T(30)$ as Eq. 1, with r as correlation coefficient.

Monomers	ν_a (cm^{-1})	Slope (S)	N^a
M1	27.846	0.018	5
M2	26.845	0.026	5
M3	26.685	0.001	5
M4	25.337	0.031	5

^a refer to the number of solvents used.

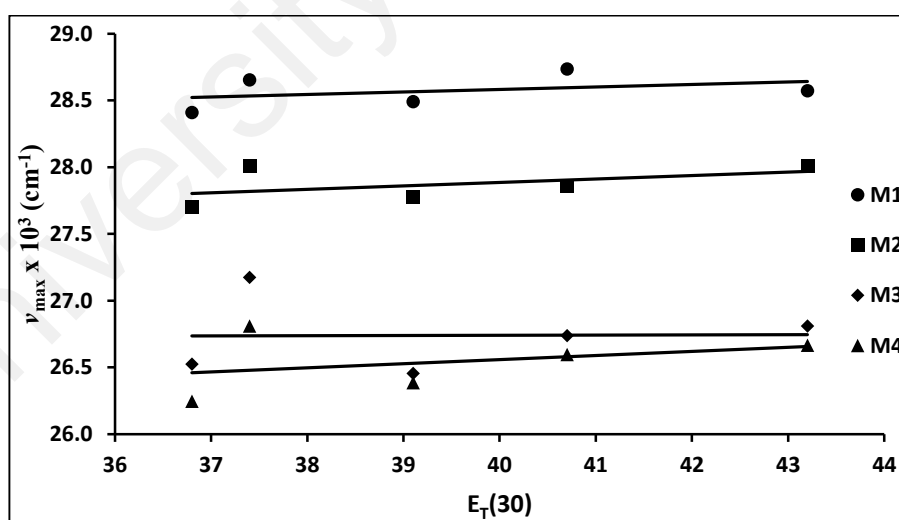


Figure 4.19: Plot of absorption frequency (ν_{\max} in 10^3 cm^{-1}) of M1 - M4 versus the $E_T(30)$ values in various solvents.

Figure 4.19 depicts the non-linear correlation of maximum absorption energy with Reichardt-Dimroth solvent $E_T(30)$ parameter. The application of $E_T(30)$ values show nonlinear relations indicating that the change in the position of the CT band is not due to

dielectric properties but can be considered as being the resultant of the different factors governed by the various solvent parameters. These may be additive, counter-acting or may even cancel each other (El-Wakiel et al., 2011). Thus, the plot elucidates that the specific solute solvent interaction plays an important role in determining the spectral position. This involves changes in the solution energies of the ground and excited states as well as solute solvent hydrogen bonding (Al-Shihry, 2005).

4.6.2.2 Kamlet-Taft solvent scale

Linear solvation energy relationship (LSERs) method is one of the most successful quantitative treatments of the solvent effects that has been used to determine and annotate the solute-solvent interactions on the solvent medium of molecules. LSERs have been interpreted by using statistical multiple linear regression analysis (MLRA) originated from Kamlet-Taft parameters in 1976. Generally, the correlation coefficient can be obtain with the following equation, Eq. (2):

$$v_{(\max)} = v_o + s\pi^* + a\alpha + b\beta \quad \text{Eq. (2)}$$

where π^* is a measure of the solvent dipolarity/polarizability, α is the scale of the solvent hydrogen bond donor (HBD) acidities, β is the scale of the solvent hydrogen bond acceptor (HBA) basicities and v_o represents the maximum absorption wavenumbers in gaseous phase (Lagalante et al., 1998). The regression coefficients s , b and a in Eq. (2) measure the relative susceptibilities of the solute property (such as absorption, fluorescence and other spectroscopic parameters) to the indicated solvent parameters (Zakerhamidi et al., 2010; Zakerhamidi et al., 2013).

According to Table 4.10, the dominant coefficient that affecting the absorption band of monomers **M1** and **M3** is the dipolarity/polarizability, due to larger value of s

coefficient compared to a and b coefficients. Meanwhile, the correlation coefficient for monomers **M2** and **M4** shows that b coefficient is the biggest compared to the other coefficients indicating that the solvent hydrogen bond acceptor (HBA) basicities, β , plays a crucial role on affecting the absorption band with respect to solvent polarities.

Table 4.10: Solvatochromic parameters for M1 - M4 using Kamlet-Taft approach.

Monomers	$\nu_o \times 10^3$ (cm^{-1})	$s \times 10^3$ (cm^{-1})	$a \times 10^3$ (cm^{-1})	$b \times 10^3$ (cm^{-1})	P_s (%)	P_a (%)	P_b (%)
M1	28.37	0.21	0.10	0.14	47	22	31
M2	27.72	0.00	0.18	0.47	0	28	72
M3	27.22	-0.82	-0.51	0.60	43	26	31
M4	26.45	-0.16	0.18	0.64	16	18	66

The positive sign of s coefficient for monomers **M1** and **M4** as well as b coefficient for monomer **M2** indicate a hypsochromic effect (blue shift) on the absorption spectra for these monomers according to the solvent polarity. This observation suggests that the ground state has better stabilization relative to the electronic excited state with increasing solvent polarity. Thus, molecules in the ground state possess higher dipolar properties compared to molecules in the excited state (Ajaj et al., 2015). In addition, the interaction of solvents with the lone pair of oxygen atom from the carbonyl group (C=O) could also lead to a negative solvatochromism with increasing solvent polarity (Stalin et al., 2006). In contrast, monomer **M3** undergoes a bathochromic effect (red shift) on the absorption band with respect to solvent polarity due to the negative sign of s coefficient that represents the dipolarity/polarizability.

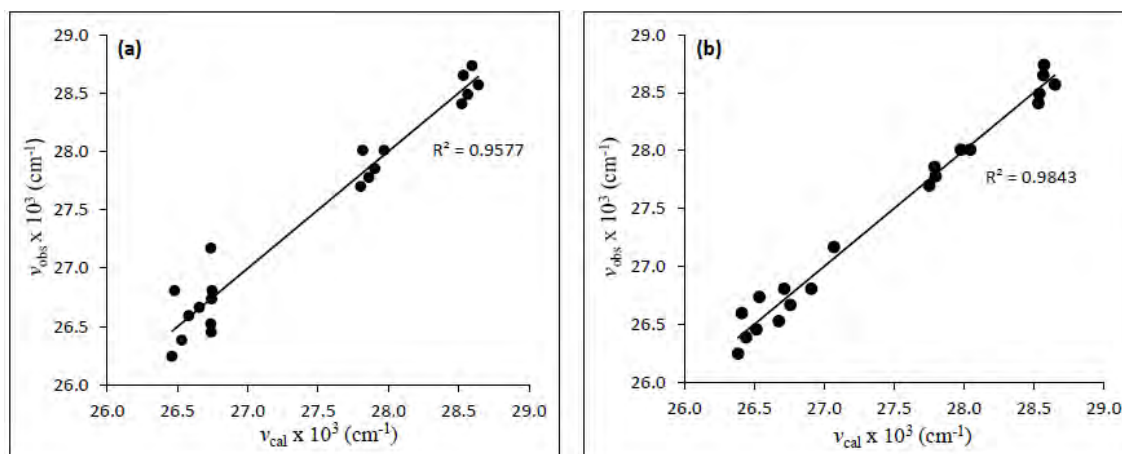


Figure 4.20: Experimental versus calculated values of ν_{max} for all investigated monomers using (a) Reichardt-Dimroth and (b) Kamlet Taft solvent scales.

The degree of success of Eqs. (1) and (2) are shown in Figure 4.20. An excellent linear relationship between the experimental values of ν_{max} and the predicted absorption maxima calculated with Eqs. (1) and (2) have been observed. Thus, in comparison between both solvent scales approaches, the use of Kamlet Taft ($R^2 = 0.9843$) gives a better regression than Reichardt-Dimroth solvent scales, $E_T(30)$ ($R^2 = 0.9577$). It is shown that correlations of spectral properties are significantly improved by such multi-parameter treatment as this method allows various independent interactions to be characterized implicitly between solvent and solute ground, transition and surrounding (Stock et al., 2016).

Table 4.11: Observed and calculated absorption maxima for all monomers in various solvents.

Monomers	Solvents	Observation value		Calculated by $E_T(30)$		Calculated by Kamlet Taft	
		λ_{\max} (nm)	ν_{\max} ($\times 10^3 \text{cm}^{-1}$)	λ_{\max} (nm)	ν_{\max} ($\times 10^3 \text{cm}^{-1}$)	λ_{\max} (nm)	ν_{\max} ($\times 10^3 \text{cm}^{-1}$)
M1	Chlorobenzene	352	28.41	351	28.52	350	28.53
	THF	349	28.65	350	28.53	350	28.57
	CHCl_3	351	28.49	350	28.57	350	28.54
	DCM	348	28.74	350	28.60	350	28.57
	DMF	350	28.57	349	28.64	349	28.65
M2	Chlorobenzene	361	27.70	360	27.80	360	27.75
	THF	357	28.01	359	27.82	357	27.98
	CHCl_3	360	27.78	359	27.86	360	27.80
	DCM	359	27.86	358	27.90	360	27.79
	DMF	357	28.01	358	27.97	357	28.04
M3	Chlorobenzene	377	26.53	374	26.74	375	26.67
	THF	368	27.17	374	26.74	369	27.10
	CHCl_3	378	26.46	374	26.74	377	26.51
	DCM	374	26.74	374	26.74	377	26.54
	DMF	373	26.81	374	26.75	372	26.91
M4	Chlorobenzene	381	26.25	378	26.46	379	26.38
	THF	373	26.81	378	26.48	374	26.71
	CHCl_3	379	26.39	377	26.53	378	26.44
	DCM	376	26.60	376	26.58	379	26.41
	DMF	375	26.67	375	26.66	374	26.76

4.6.3 Effect of different strengths of electron-donating groups

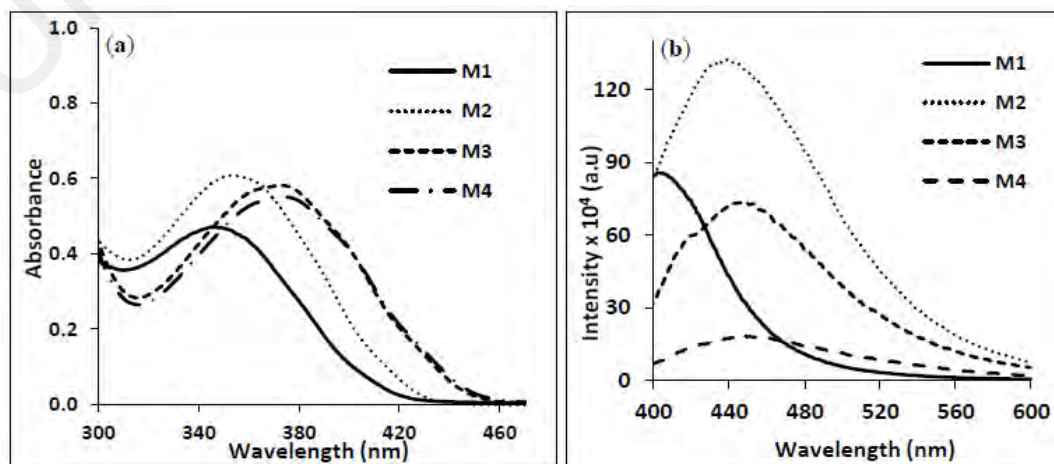


Figure 4.21: (a) Absorption and (b) emission spectra for M1 - M4 in dilute THF.

Figure 4.21(a) depicts the UV–vis absorption spectra of monomers **M1** - **M4** in dilute THF solvent at concentration 5×10^{-5} M in the wavelength range 200-500 nm. The absorption spectra of all compounds are very similar in shape because of their structural similarity. The broad absorption band in the investigated compounds appeared in the range of 348 - 381 nm. This may be assigned to π - π^* transition involving the conjugation between $-\text{N}=\text{CH}-$ and phenyl rings (Sıdır et al., 2016; Sıdır et al., 2011). The absorption maxima (λ_{max}) of the monomers in dilute THF were red shifted from **M1** to **M4** with increasing strength of electron pushing group ($-\text{CH}_3$, $-\text{OCH}_3$, $-\text{OC}_2\text{H}_5$) on benzothiazole unit in the mesogenic core. The same trend was also observed in CHCl_3 , DCM, DMF and chlorobenzene. These shifts of absorbance maxima (λ_{max}) may be ascribed to the presence of an electron-donor substituents in the benzothiazole that increase the absorption coefficient, thus enhances the polarization of the molecules (Paley et al., 1990). Issa and co-workers also observed a similar result for hydroxy 4-aminoantipyrine Schiff bases (Issa et al., 2005).

Figure 4.21(b) depicts the photoluminescent (PL) spectra of **M1** - **M4** in THF solution (5×10^{-5} M) and the emission spectra of the monomers show an identical pattern as in UV-vis spectra. This is due to the structural similarities in the mesogenic unit. The presence of broad band in the emission spectra could be due to π - π^* transition involving the π -electronic system throughout the whole molecule with a considerable charge transfer (CT) character (Božić et al., 2014). The fluorescence emission maxima of monomers are located in the range within the visible region of the spectrum and can be categorized as violet-blue emission. Like UV–Vis spectra, PL emission maxima also exhibited a significant bathochromic shifting due to highly polarizable π -conjugated structures (Karim et al., 2013).

4.6.4 Effect of temperature on monomers

To quantify the temperature sensing ability of all Schiff base ester monomers incorporating benzothiazole chromophore in dilute THF (5×10^{-5} M), emission spectra were recorded at different temperatures ranging from 20 °C to 55 °C. Figure 4.22 displays the emission fluorescence spectra of **M1** - **M4** in dilute THF at different temperatures.

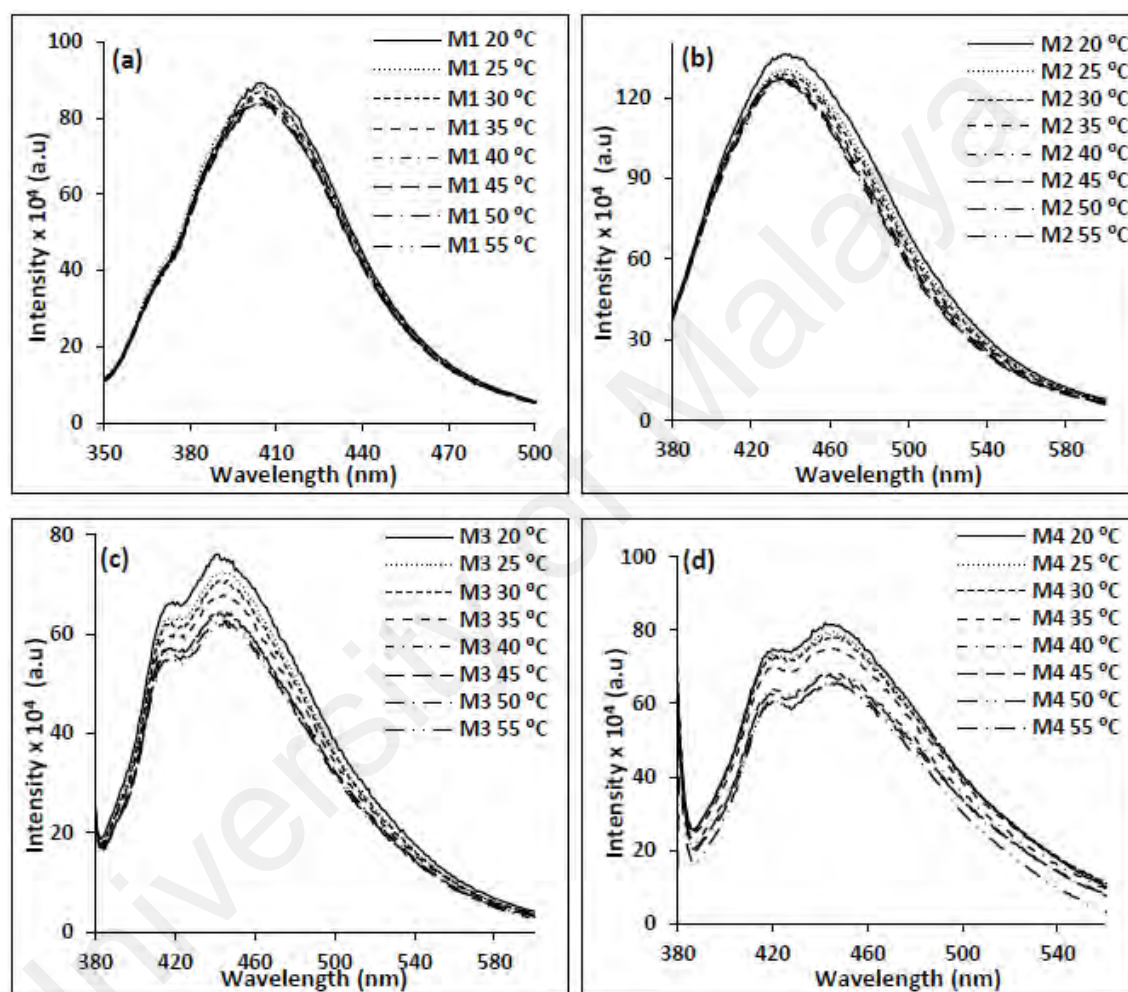


Figure 4.22: Emission fluorescence spectra of M1 – M4 in THF at different temperatures.

As illustrated in Figure 4.22, compounds with alkoxy groups, **M3** and **M4**, exhibit a double peak phenomenon of fluorescence spectra which may result from the marketed difference between the excited state and the ground state (Jian et al., 2016). In addition, the emission band for the reported monomers does not shift in response to the changes of

temperature in the fluorescent emission spectra. This shows that the temperature does not affect the excited states of these compounds (Hosseini & Mohammadi, 2009).

However, the emission bands for **M1 - M4** exhibited a significant decrease in the intensity as the temperature was varied. Based on the above results, it can be concluded that an increase in temperature will increase the molecular energy, charge delocalization and weakens the intermolecular hydrogen bonding, and consequently assists the solute–solvent dissociation (Alizadeh et al., 2009). This observation was also reported in a similar work by Rageh (Rageh, 2004). He suggested that this behavior could correspond to an association and dissociation processes of solute–solvent interaction. He further explained that increase in temperature leading to an increase in the rate of dissociation between the solute and the solvent. Thus, this will lead to decrease in the concentration of the complexed species as well as equilibrium of reaction: $HA + S \leftrightarrow [AH \cdots S]$, where HA and S is the solute and solvent respectively.

CHAPTER 5: CONCLUSIONS & SUGGESTIONS FOR FUTURE STUDIES

5.1 Conclusions

A series of methyl-methacrylate monomers containing Schiff base-ester as linkage was successfully synthesized via Schiff base reaction followed by Williamson etherification and esterification reactions. The investigated LC monomers were differentiated with each other by varying the terminal substituents attached on the sixth position of benzothiazole ring. The molecular structure for all monomers were identified using ^1H NMR, ^{13}C NMR, and FTIR spectroscopic techniques.

The thermal properties of investigated LC monomers was analyzed using TGA showed that monomer **M4** are the most thermally stable compared to the other monomers. The liquid crystalline behavior of monomers **M1** - **M4** was studied by DSC and POM showed monomer **M1** displayed both smectic and nematic mesophases upon heating and cooling cycles, whereas the other compounds, **M2** - **M4**, revealed only nematic mesophase with various textures at different temperatures. The nematic mesophase stability in **M3** and **M4** was shown to decrease due to the fact that the oxygen being in conjugation with the heteroaromatic core extend the length of the rigid core as well as enhanced the polarizability anisotropy.

It can be concluded that azo-ester series were found to have better thermal stabilities and broad nematic mesomorphic ranges compared to Schiff base ester monomers. This observation may be due to the nature of azo linker providing rich electron density towards the entire system that could enhance the transition temperature, while Schiff base linkage in the central core will pulled the electron density resulting to decrease in thermal temperatures.

The optical properties for all LC monomers was analyzed by UV-Vis and fluorescence spectroscopies showed absorption peaks from 348 to 381 nm and emission

bands from 401 to 500 nm, respectively. Both the absorption and emission bands are bathochromically shifted with the incorporation of electron-donating terminal substituents in the mesogen of the monomers. The UV-vis absorption maxima (λ_{max}) of investigated monomers also undergo a polytonic behavior with increasing solvent polarity. This observation was further confirmed using Reichardt-Dimroth solvent scale, $E_{\text{T}}(30)$, and Kamlet-Taft approach. The fluorescence intensity for all monomers were decreased with increase in temperature without shifting their bands.

5.2 Suggestions for future studies

Mesomorphic behavior of LC compounds is basically dependent on its molecular architecture, in which a slight change in the molecular geometry brings about considerable change in its mesomorphic properties. Thus, it is interesting to design and modified a similar LC compounds such as varying the flexible segments, rigid core, and polymerized units, or insertion of different lateral groups and study their thermal behavior as well as their mesomorphic properties. A rheological studies on the synthesized monomers can also lead to a new finding as this work is still limited for the low molecular weight of LC monomers. The continuation of this work will provide a wide range of choices for various practical applications.

In addition, the design and synthesis of LC compounds containing transitional metal in the center core known as metallomesogens has attracted a lot of attention in recent years as the association with the peculiar properties of metallic clusters could lead to great potential in the design of new electricity-to-light energy conversion system, optically based sensors and displays. It is also fascinating to observe the thermal and mesomorphic behaviors on LC materials incorporating metal ions as the complexes will revealed a variety of properties. Moreover, the synthesized Schiff base LC compounds

could be further investigated in biological study as Schiff base group is well known to possess anticancer, antifungal, antioxidant, antibacterial, and antiviral properties.

University of Malaya

REFERENCES

- Abraham, R. J., Fisher, J., & Loftus, P. (1988). *Introduction to NMR spectroscopy*. New Jersey, US: John Wiley & Sons.
- Ajaj, I., Assaleh, F. H., Markovski, J., Rančić, M., Brković, D., Milčić, M., & Marinković, A. D. (2015). Solvatochromism and azo-hydrazo tautomerism of novel arylazo pyridone dyes: Experimental and quantum chemical study. *Arabian Journal of Chemistry*, 1-16.
- Al-Shihry, S. S. (2005). Synthesis and spectral studies of Schiff bases of 2-amino-5-mercapto-1, 3, 4-thiadiazole. *Scientific Journal of King Faisal University (Basic and Applied Sciences)*, 6(2), 1426.
- Alizadeh, K., Seyyedi, S., Shamsipur, M., Rouhani, S., & Haghbeen, K. (2009). Solvatochromism and temperature effects on the electronic absorption spectra of some azo dyes. *Spectrochimica Acta Part A: Molecular and Biomolecular Spectroscopy*, 74(3), 691-694.
- Balaji, K., & Murugavel, S. (2012). Studies on synthesis and thermal characterisation of thermotropic liquid-crystalline poly (benzylidene-ether) s containing alkanones and methylene spacers in the main chain. *Liquid Crystals*, 39(6), 683-693.
- Batista, R. M., Costa, S. P., & Raposo, M. M. M. (2004). Synthesis of new fluorescent 2-(2', 2''-bithienyl)-1, 3-benzothiazoles. *Tetrahedron Letters*, 45(13), 2825-2828.
- Belmar, J. (1999). New liquid crystals containing the benzothiazol unit: amides and azo compounds. *Liquid Crystals*, 26(3), 389-396.
- Bera, R. N., Sakakibara, Y., Abe, S., Yase, K., & Tokumoto, M. (2005). Time-resolved photoluminescence study on concentration quenching of a red emitting tetraphenylchlorin dye for organic electroluminescent devices. *Synthetic Metals*, 150(1), 9-13.
- Boden, E. P., & Keck, G. E. (1985). Proton-transfer steps in Steglich esterification: A very practical new method for macrolactonization. *The Journal of Organic Chemistry*, 50(13), 2394-2395.
- Boussoualem, M., King, R. C. Y., Brun, J.-F., Duponchel, B., Ismaili, M., & Roussel, F. (2010). Electro-optic and dielectric properties of optical switching devices based on liquid crystal dispersions and driven by conducting polymer [poly (3, 4-ethylene dioxythiophene): polystyrene sulfonate (PEDOT: PSS)]-coated electrodes. *Journal of Applied Physics*, 108(11), 113526 (1) - 13526 (6).
- Božić, B. Đ., Alimmari, A. S., Mijin, D. Ž., Valentić, N. V., & Ušćumlić, G. S. (2014). Synthesis, structure and solvatochromic properties of novel dyes derived from 4-(4-nitrophenyl)-3-cyano-2-pyridone. *Journal of Molecular Liquids*, 196, 61-68.
- Brown, G. (2012). *Liquid crystals and biological structures*. New York, US: Academic Press.

- Chandran, A., Prakash, J., Joshi, T., & Biradar, A. M. (2014). Probing the effect of temperature and electric field on the low frequency dielectric relaxation in a ferroelectric liquid crystal mesogen. *Journal of Molecular Liquids*, 198, 280-285.
- Chia, W.-L., & Lin, X.-M. (2013). Synthesis and Thermotropic Studies of a New Series of Teraryl Liquid Crystals 2-(4'-Alkoxybiphen-4-yl)-5-Cyanopyridines. *International Journal of Molecular Sciences*, 14(9), 18809-18823.
- Collings, P. J. (2002). *Liquid crystals: nature's delicate phase of matter*. (2nd ed.). Princeton, NJ: Princeton University Press.
- Collings, P. J., & Hird, M. (2017). *Introduction to liquid crystals: chemistry and physics*. Florida, US: CRC Press, Taylor and Francis.
- Collyer, A. A. (2012). *Liquid crystal polymers: from structures to applications* (Vol. 1). Berlin, Germany: Springer Science & Business Media.
- Cordes, E. H., & Jencks, W. P. (1963). The mechanism of hydrolysis of Schiff bases derived from aliphatic amines. *Journal of the American Chemical Society*, 85(18), 2843-2848.
- Cristaldi, D. J., Pennisi, S., & Pulvirenti, F. (2009). *Liquid crystal display drivers: Techniques and circuits*. Berlin: Germany: Springer Science & Business Media.
- Critchley, J., Knight, G., & Wright, W. W. (2013). *Heat-resistant polymers: technologically useful materials*. Berlin, Germany: Springer Science & Business Media.
- De Feyter, S., & De Schryver, F. C. (2003). Two-dimensional supramolecular self-assembly probed by scanning tunneling microscopy. *Chemical Society Reviews*, 32(3), 139-150.
- Demus, D., Diele, S., Klapperstück, M., Link, V., & Zschke, H. (1971). Investigation of a smectic tetramorphous substance. *Molecular Crystals and Liquid Crystals*, 15(2), 161-174.
- Demus, D., Goodby, J. W., Gray, G. W., Spiess, H. W., & Vill, V. (2011a). *Handbook of liquid crystals, low molecular weight liquid crystals I: calamitic liquid crystals*. New Jersey, US: John Wiley & Sons.
- Demus, D., Goodby, J. W., Gray, G. W., Spiess, H. W., & Vill, V. (2011b). *Handbook of Liquid Crystals, Volume 2A: Low Molecular Weight Liquid Crystals I: Calamitic Liquid Crystals*. New Jersey, US: John Wiley & Sons.
- Dierking, I., & Al-Zangana, S. (2017). Lyotropic Liquid Crystal Phases from Anisotropic Nanomaterials. *Nanomaterials*, 7(10), 305 (1-28).
- Dumanli, A. G., & Savin, T. (2016). Recent advances in the biomimicry of structural colours. *Chemical Society Reviews*, 45(24), 6698-6724.

- Dutta, G. K., Guha, S., & Patil, S. (2010). Synthesis of liquid crystalline benzothiazole based derivatives: A study of their optical and electrical properties. *Organic Electronics*, 11(1), 1-9.
- El-Wakiel, N., El-Sayed, Y., & Gaber, M. (2011). Synthesis, characterization, and theoretical studies of Co (II) and Cu (II) complexes of 1-[(5-mercapto-[1, 3, 4]thiadiazol-2-ylimino)-methyl]-naphthalen-2-ol and its interaction with Cu nanoparticles. *Journal of Molecular Structure*, 1001(1), 1-11.
- Ermakov, S., Beletskii, A., Eismont, O., & Nikolaev, V. (2016). Brief Review of Liquid Crystals. In Ermakov, S. F., Beletskii, A., Eismont, O., Nikolaev, V. (Eds.), *Liquid Crystals in Biotribology* (pp. 37-56). Cham, Switzerland: Springer.
- Field, L. D., Sternhell, S., & Kalman, J. R. (2012). *Organic structures from spectra*. New Jersey, US: John Wiley & Sons.
- Findeisen-Tandel, S., Weissflog, W., Baumeister, U., Pelzl, G., Murthy, H. S., & Yelamaggad, C. V. (2012). Laterally substituted symmetric and nonsymmetric salicylideneimine-based bent-core mesogens. *Beilstein Journal of Organic Chemistry*, 8, 129-154.
- Foo, K.-L., Ha, S.-T., Lin, C.-M., Lin, H.-C., Lee, S.-L., Yeap, G.-Y., & Sastry, S. S. (2015). Synthesis, characterization and mesomorphic properties of new symmetrical dimer liquid crystals derived from benzothiazole. *Karbala International Journal of Modern Science*, 1(3), 152-158.
- Fuhrmann, E., & Talbiersky, J. (2005). Synthesis of alkyl aryl ethers by catalytic Williamson ether synthesis with weak alkylation agents. *Organic Process Research & Development*, 9(2), 206-211.
- Ghanem, E., & Al-Hariri, S. (2013). Synthesis and powder X-ray diffraction of new Schiff-base liquid crystal. *Liquid Crystals Today*, 22(4), 76-81.
- Ghoneim, P. S. N., & Suppan, P. (1997). *Solvatochromism*. Cambridge, England: The Royal Society of Chemistry.
- Ghosh, S., Begum, N., Turlapati, S., Roy, S. K., Das, A. K., & Rao, N. V. (2014). Ferroelectric-like switching in the nematic phase of four-ring bent-core liquid crystals. *Journal of Materials Chemistry C*, 2(3), 425-431.
- Gilani, A. G., Moghadam, M., Zakerhamidi, M., & Moradi, E. (2012). Solvatochromism, tautomerism and dichroism of some azoquinoline dyes in liquids and liquid crystals. *Dyes and Pigments*, 92(3), 1320-1330.
- Gray, G. W. (1962). *Molecular structure and the properties of liquid crystals*. Cambridge, US: Academic press.
- Gulbas, H. E., Ocak, H., Gursel, Y. H., & Bilgin-Eran, B. (2013). Synthesis and Mesomorphic Properties of New Side Chain Liquid Crystalline Oligomers Containing Salicylaldimine Mesogenic Groups. *Molecular Crystals and Liquid Crystals*, 574(1), 40-49.

- Günther, H. (2013). *NMR spectroscopy: basic principles, concepts and applications in chemistry*. New Jersey, US: John Wiley & Sons.
- Ha, S.-T., Koh, T.-M., Lee, S.-L., Yeap, G.-Y., Lin, H.-C., & Ong, S.-T. (2010). Synthesis of new schiff base ester liquid crystals with a benzothiazole core. *Liquid Crystals*, 37(5), 547-554.
- Ha, S.-T., Koh, T.-M., Lin, H.-C., Yeap, G.-Y., Win, Y.-F., Ong, S.-T., . . . Ong, L.-K. (2009). Heterocyclic benzothiazole-based liquid crystals: synthesis and mesomorphic properties. *Liquid Crystals*, 36(9), 917-925.
- Ha, S.-T., Koh, T.-M., Yeap, G.-Y., Lin, H.-C., Lee, S.-L., Win, Y.-F., & Ong, S.-T. (2010). Synthesis and mesomorphic properties of 6-methoxy-and 6-ethoxy-2-(2-hydroxy-4-alkanoyloxybenzylideneamino) benzothiazoles. *Molecular Crystals and Liquid Crystals*, 528(1), 10-22.
- Ha, S.-T., & Lee, T.-L. (2014). Synthesis and mesomorphic properties of new fluorinated Schiff base liquid crystals. *International Scholarly Research Notice Materials Science*, 2014, 1-7. <http://dx.doi.org/10.1155/2014/904657>.
- Ha, S. T., Foo, K. L., Lin, H. C., Ito, M. M., Abe, K., Kunbo, K., & Sastry, S. S. (2012). Mesomorphic behavior of new benzothiazole liquid crystals having Schiff base linker and terminal methyl group. *Chinese Chemical Letters*, 23(7), 761-764.
- Ha, S. T., Foo, K. L., Subramaniam, R. T., Ito, M. M., Sastry, S. S., & Ong, S. T. (2011). Heterocyclic benzoxazole-based liquid crystals: Synthesis and mesomorphic properties. *Chinese Chemical Letters*, 22(10), 1191-1194.
- Ha, S. T., Koh, T. M., Yeap, G. Y., Lin, H. C., Beh, J. K., Win, Y. F., & Boey, P. L. (2009). New mesogenic Schiff base esters comprising benzothiazole moiety: Synthesis and mesomorphic properties. *Chinese Chemical Letters*, 20(9), 1081-1084.
- Hamryszak, L., Janeczek, H., & Schab-Balcerzak, E. (2012). New thermotropic symmetrical and unsymmetrical azomethine with azobenzene unit and fluorinated alkyl chain: Synthesis and characterization. *Journal of Molecular Liquids*, 165, 12-20.
- Han, J., Chang, X. Y., Cao, B. N., & Wang, Q. C. (2009). Synthesis, single crystal structures and liquid crystal property of 2, 5-diphenyl-1, 3, 4-oxadiazoles/1, 3, 4-thiadiazoles. *Soft Materials*, 7(4), 342-354.
- Hoogboom, J., Elemans, J. A., Rowan, A. E., Rasing, T. H., & Nolte, R. J. (2007). The development of self-assembled liquid crystal display alignment layers. *Philosophical Transactions of the Royal Society of London A: Mathematical, Physical and Engineering Sciences*, 365(1855), 1553-1576.
- Hosseini, S. H., & Mohammadi, M. (2009). Preparation and characterization of new polypyrrole having side chain liquid crystalline moieties. *Materials Science and Engineering: C*, 29(5), 1503-1509.

- Huang, K., Qiu, H., & Wan, M. (2002). Synthesis of highly conducting polyaniline with photochromic azobenzene side groups. *Macromolecules*, 35(23), 8653-8655.
- Hudson, S. A., & Maitlis, P. M. (1993). Calamitic metallomesogens: metal-containing liquid crystals with rodlike shapes. *Chemical Reviews*, 93(3), 861-885.
- Hussein, M. A., Abdel-Rahman, M. A., Asiri, A. M., Alamry, K. A., & Aly, K. I. (2012). Review on: liquid crystalline polyazomethines polymers. Basics, syntheses and characterization. *Designed Monomers and Polymers*, 15(5), 431-463.
- Islam, S., Siddiki, A. N. A., Begum, S., & Salam, M. A. (2018). Synthesis, Spectral Characterization and Thermal Behavior of Newly Derived La (III), Co (III) and Mn (II) Complexes with Schiff Base Derived from Methionine and Salicylaldehyde. *Open Journal of Inorganic Chemistry*, 8(02), 55-69.
- Issa, R. M., Khedr, A. M., & Rizk, H. F. (2005). UV-vis, IR and ¹H NMR spectroscopic studies of some Schiff bases derivatives of 4-aminoantipyrine. *Spectrochimica Acta Part A: Molecular and Biomolecular Spectroscopy*, 62(1), 621-629.
- Jian, J., Hong, F., Xia, Z., Zhu, D., Wu, H., Liu, J., . . . Wang, H. (2016). New fluorescent N-heterocyclic liquid crystals with high birefringence. *Journal of Molecular Liquids*, 224, 909-913.
- Karim, M. R., Sheikh, M. R. K., Salleh, N. M., Yahya, R., Hassan, A., & Hoque, M. A. (2013). Synthesis and characterization of azo benzothiazole chromophore based liquid crystal macromers: Effects of substituents on benzothiazole ring and terminal group on mesomorphic, thermal and optical properties. *Materials Chemistry and Physics*, 140(2), 543-552.
- Karim, M. R., Sheikh, M. R. K., Yahya, R., Salleh, N. M., & Azzahari, A. D. (2015). Synthesis of polymerizable liquid crystalline monomers and their side chain liquid crystalline polymers bearing azo-ester linked benzothiazole mesogen. *Colloid and Polymer Science*, 293(7), 1923-1935.
- Kaya, İ., Öksüzgülmez, S., & Güzel, H. (2008). Synthesis, characterization, thermal degradation and electrical conductivity of poly-4-[(pyridin-2-yl-imino) methyl] benzene-1, 3-diol and polymer-metal complexes. *Bulletin of the Chemical Society of Ethiopia*, 22(2). 237-246.
- Kelker, H., & Scheurle, B. (1969). A Liquid-crystalline (Nematic) Phase with a Particularly Low Solidification Point. *Angewandte Chemie International Edition*, 8(11), 884-885.
- Khoo, I.-C. (2007). *Liquid crystals: physical properties and nonlinear optical phenomena* (Vol. 64). New Jersey, US: John Wiley & Sons.
- Kumar, S. (2001). *Liquid crystals: experimental study of physical properties and phase transitions*. England, UK: Cambridge University Press.
- Kumar, S. (2016). *Chemistry of discotic liquid crystals: from monomers to polymers*. Florida, US: CRC press, Taylor and Francis.

- Kumar, S., & Pal, S. K. (2005). Ionic discotic liquid crystals: synthesis and characterization of pyridinium bromides containing a triphenylene core. *Tetrahedron Letters*, 46(23), 4127-4130.
- Lagalante, A. F., Hall, R. L., & Bruno, T. J. (1998). Kamlet– Taft solvatochromic parameters of the sub-and supercritical fluorinated ethane solvents. *The Journal of Physical Chemistry B*, 102(34), 6601-6604.
- Lim, Y.-W. C., Ha, S.-T., Yeap, G.-Y., & Sastry, S. S. (2015). Synthesis and mesomorphic properties of new heterocyclic liquid crystals with Central Ester–Chalcone linkages. *Journal of Taibah University for Science*, 11(1), 133-140.
- Liu, J.-H., Wang, Y.-K., Chen, C.-C., Yang, P.-C., Hsieh, F.-M., & Chiu, Y.-H. (2008). Synthesis and characterization of optically active liquid crystalline polyacrylates containing mesogenic phenylbenzoate groups. *Polymer*, 49(18), 3938-3949.
- Lorenz, A., & Kitzerow, H.-S. (2011). Efficient electro-optic switching in a photonic liquid crystal fiber. *Applied Physics Letters*, 98(24), 241106(1)-241106(3).
- Medvidović-Kosanović, M., Balić, T., Marković, B., & Šter, A. (2015). Comparison of the electrochemical properties of two structurally different novel bis-Schiff bases. *International Journal of Electrochemical Science*, 10(1), 63-83.
- Misra, A. K., Tripathi, P. K., & Manohar, R. (2015). Fluorescence, UV absorbance and dielectric studies of fluorescent dye doped ferroelectric liquid crystal. *Journal of Non-Crystalline Solids*, 412, 1-4.
- Mohammad, A.-T., Srinivasa, H., Hariprasad, S., & Yeap, G.-Y. (2016). Enhanced liquid crystal properties in symmetric ethers containing the oxazepine core: synthesis and characterization of seven member heterocyclic dimers. *Tetrahedron*, 72(27), 3948-3957.
- Müller, M., & Chentanez, N. (2011). Solid simulation with oriented particles. *ACM Transactions on Graphics (TOG)*, 30(4), 1-9. <http://doi.acm.org/10.1145/1964921.1964987>.
- Muniprasad, M., Srinivasulu, M., Chalapathi, P., & Potukuchi, D. (2012). Influence of chemical moieties and the flexible chain for the tilted smectic phases in linear hydrogen bonded liquid crystals with Schiff based pyridene derivatives. *Journal of Molecular Structure*, 1015, 181-191.
- Nagaveni, N., Roy, A., & Prasad, V. (2012). Achiral bent-core azo compounds: effect of different types of linkage groups and their direction of linking on liquid crystalline properties. *Journal of Materials Chemistry*, 22(18), 8948-8959.
- Naoum, M., Fahmi, A., Alaasar, M., & Ahmed, N. (2011). Effect of exchange of terminal substituents on the mesophase behavior of laterally methyl substituted phenyl azo benzoates in pure and mixed systems. *Thermochimica Acta*, 525(1), 78-86.
- Nourmohammadian, F. (2013). Novel aza-substituted benzothiazol and 1, 2, 4-Triazol dyes: synthesis, characterization and properties. *Prog. Color Colorants Coating*, 6, 37-49.

- Ooi, Y.-H., Yeap, G.-Y., & Takeuchi, D. (2013). Synthesis, mesomorphic properties and structural studies on 1, 3, 5-trisubstituted benzene-based star-shaped derivatives containing Schiff base ester as the peripheral arm. *Journal of Molecular Structure*, *1051*, 361-375.
- Paley, M. S., McGill, R. A., Howard, S. C., Wallace, S. E., & Harris, J. M. (1990). Solvatochromism: A new method for polymer characterization. *Macromolecules*, *23*(21), 4557-4564.
- Parra, M., Hernandez, S., & Alderete, J. (2003). Metallomesogens derived from chelating schiffs bases containing 1, 3, 4-oxadiazole and 1, 3, 4-thiadiazole: synthesis, characterization and study of mesomorphic properties. *Journal of the Chilean Chemical Society*, *48*(1), 57-60.
- Pavia, D. L., Lampman, G. M., Kriz, G. S., & Vyvyan, J. A. (2008). *Introduction to spectroscopy*. Boston, US: Cengage Learning.
- Pavluchenko, A., Smirnova, N., Titov, V., Kovshev, E., & Djumaev, K. (1976). Nematic liquid crystals containing pyridine and benzazole rings. *Molecular Crystals and Liquid Crystals*, *37*(1), 35-46.
- Pietsch, C., Hoogenboom, R., & Schubert, U. S. (2010). PMMA based soluble polymeric temperature sensors based on UCST transition and solvatochromic dyes. *Polymer Chemistry*, *1*(7), 1005-1008.
- Prajapati, A., & Bonde, N. (2006). Mesogenic benzothiazole derivatives with methoxy substituents. *Journal of Chemical Sciences*, *118*(2), 203-210.
- Praveen, P. L., & Ojha, D. P. (2012). Calculation of spectral shifts in UV–visible region and photo stability of thermotropic liquid crystals: Solvent and alkyl chain length effects. *Journal of Molecular Liquids*, *169*, 110-116.
- Qaddoura, M. A., & Belfield, K. D. (2009). Synthesis, characterization and texture observations of calamitic liquid crystalline compounds. *International Journal of Molecular Sciences*, *10*(11), 4772-4788.
- Rageh, N. M. (2004). Electronic spectra, solvatochromic behavior and acid–base properties of some azo cinnoline compounds. *Spectrochimica Acta Part A: Molecular and Biomolecular Spectroscopy*, *60*(1), 103-109.
- Reddy, G. S. M., Narasimhaswamy, T., & Raju, K. M. (2014). Synthesis and mesophase characterization of novel methacrylate based thermotropic liquid crystalline monomers and their polymers. *New Journal of Chemistry*, *38*(9), 4357-4364.
- Rufchahi, E. M., & Mohammadinia, M. (2014). 6-Butyl-4-hydroxyquinolin-2-(1H)-one as an enol type coupling component for the synthesis of some new azo disperse dyes. *Journal of Molecular Liquids*, *199*, 393-400.
- Sackmann, H., & Demus, D. (1966). The polymorphism of liquid crystals. *Molecular Crystals and Liquid Crystals*, *2*(1-2), 81-102.

- Sakthivel, P., & Kannan, P. (2005). Thermotropic main-chain liquid-crystalline photodimerizable poly (vanillylidenealkoxy alkylphosphate ester) s containing a cyclopentanone moiety. *Polymer International*, 54(11), 1490-1497.
- Salleh, N. M., Sheikh, M. R. K., Yahya, R., Karim, M. R., Azzahari, A. D., & Hassan, A. (2013). Effect of the lateral substituent on the mesomorphic behavior of side-chain liquid-crystalline polymers containing a Schiff base ester. *Journal of Polymer Research*, 20(12), 1-11.
- Sarkar, S. K., & Das, M. K. (2014). Critical behavior of optical birefringence at the nematic–smectic A phase transition in a binary liquid crystal system. *Journal of Molecular Liquids*, 199, 415-418.
- Schmidt-Mende, L., Fechtenkötter, A., Müllen, K., Moons, E., Friend, R. H., & MacKenzie, J. (2001). Self-organized discotic liquid crystals for high-efficiency organic photovoltaics. *Science*, 293(5532), 1119-1122.
- Selvarasu, C., & Kannan, P. (2016). Effect of azo and ester linkages on rod shaped Schiff base liquid crystals and their photophysical investigations. *Journal of Molecular Structure*, 1125, 234-240.
- Senyuk, B. (2011). General Remarks: Building blocks. In *Liquid crystals: a simple view on a complex matter*. Retrieved from <http://www.personal.kent.edu/~bisenyuk/liquidcrystals/maintypes.html>.
- Seou, C.-K., Ha, S.-T., Win, Y.-F., Lee, S.-L., & Yeap, G.-Y. (2014). Synthesis and phase transition behaviours of new non-symmetric liquid crystal dimers. *Liquid Crystals*, 41(11), 1627-1634.
- Sıdır, İ., Sıdır, Y. G., Berber, H., & Türkoğlu, G. (2016). Specific and non-specific interaction effect on the solvatochromism of some symmetric (2-hydroxybenzilydeamino) phenoxy Schiff base derivatives. *Journal of Molecular Liquids*, 215, 691-703.
- Sıdır, Y. G., & Sıdır, İ. (2015). Solvatochromic fluorescence of 4-alkoxybenzoic acid liquid crystals: Ground and excited state dipole moments of monomer and dimer structures determined by solvatochromic shift methods. *Journal of Molecular Liquids*, 211, 591-603.
- Sıdır, Y. G., Sıdır, İ., Berber, H., & Taşal, E. (2011). UV-spectral changes for some azo compounds in the presence of different solvents. *Journal of Molecular Liquids*, 162(3), 148-154.
- Sıdır, Y. G., Sıdır, İ., Berber, H., & Türkoğlu, G. (2015). Solvatochromism and electronic structure of some symmetric Schiff base derivatives. *Journal of Molecular Liquids*, 204, 33-38.
- Sıdır, Y. G., Sıdır, İ., & Demiray, F. (2017). Dipole moment and solvatochromism of benzoic acid liquid crystals: Tuning the dipole moment and molecular orbital energies by substituted Au under external electric field. *Journal of Molecular Structure*, 1137, 440-452.

- Singh, S. K., Singh, H. K., Nandi, R., Kumar, V., Tarcea, N., Popp, J., . . . Singh, B. (2014). Synthesis, characterization and mesomorphic investigations of ester-substituted aroylhydrazones possessing a lateral hydroxyl group. *Polyhedron*, *74*, 99-112.
- Singh, S. K., Vikram, K., & Singh, B. (2011). Synthesis, characterisation and mesomorphic properties of ester containing aroylhydrazones and their nickel (II) complexes. *Liquid Crystals*, *38*(9), 1117-1129.
- Smith, B. C. (2011). *Fundamentals of Fourier transform infrared spectroscopy*. Florida, US: CRC press, Taylor and Francis.
- Solomons, T. G., & Fryhle, C. B. (2000). *Organic chemistry* (7th ed.). New York, US: John Wiley and Sons.
- Stalin, T., Sivakumar, G., Shanthi, B., Sekar, A., & Rajendiran, N. (2006). Photophysical behaviour of 4-hydroxy-3, 5-dimethoxybenzoic acid in different solvents, pH and β -cyclodextrin. *Journal of Photochemistry and Photobiology A: Chemistry*, *177*(2), 144-155.
- Stock, R. I., Schramm, A. D., Rezende, M. C., & Machado, V. G. (2016). Reverse solvatochromism in solvent binary mixtures: a case study using a 4-(nitrostyryl) phenolate as a probe. *Physical Chemistry Chemical Physics*, *18*(30), 20266-20269.
- Thaker, B., & Kanojiya, J. (2011). Synthesis, characterization and mesophase behavior of new liquid crystalline compounds having chalcone as a central linkage. *Molecular Crystals and Liquid Crystals*, *542*(1), 84-98.
- Thaker, B., Kanojiya, J., & Tandel, R. (2010). Effects of different terminal substituents on the mesomorphic behavior of some azo-schiff base and azo-ester-based liquid crystals. *Molecular Crystals and Liquid Crystals*, *528*(1), 120-137.
- Thaker, B., Patel, B., Dhimmari, Y., Chothani, N., Solanki, D., Patel, N., . . . Makawana, U. (2013). Mesomorphic studies of novel azomesogens having a benzothiazole core: synthesis and characterisation. *Liquid Crystals*, *40*(2), 237-248.
- Tokunaga, K., Iino, H., & Hanna, J.-i. (2009). Charge carrier transport properties in liquid crystalline 2-phenylbenzothiazole derivatives. *Molecular Crystals and Liquid Crystals*, *510*(1), 241-249.
- Tokunaga, K., Takayashiki, Y., Iino, H., & Hanna, J.-i. (2009). One-dimensional to three-dimensional electronic conduction in liquid crystalline mesophases. *Molecular Crystals and Liquid Crystals*, *510*(1), 250-258.
- Tsakos, M., Schaffert, E. S., Clement, L. L., Villadsen, N. L., & Poulsen, T. B. (2015). Ester coupling reactions—an enduring challenge in the chemical synthesis of bioactive natural products. *Natural Product Reports*, *32*(4), 605-632.
- Vančik, H. (2014). *Basic Organic Chemistry for the Life Sciences*. Cham, Switzerland: Springer International Publishing.

- Vasanthi, B. J., & Ravikumar, L. (2007). Synthesis and characterization of new poly (azomethine ester)s having phenylthiourea units. *European Polymer Journal*, 43(10), 4325-4331.
- Vertogen, G., & de Jeu, W. H. (2012). *Thermotropic liquid crystals, fundamentals* (Vol. 45). Berlin, Germany: Springer Science & Business Media.
- Wei, Q., Shi, L., Cao, H., Wang, L., Yang, H., & Wang, Y. (2008). Synthesis and mesomorphic properties of two series of new azine-type liquid crystals. *Liquid Crystals*, 35(5), 581-585.
- Williamson, A. W. (1852). XXII.—On etherification. *Quarterly Journal of the Chemical Society of London*, 4(3), 229-239.
- Xiang, T. (2012). *Synthesis and Characterization of Polymeric Schiff Bases from 2, 5-Diformylfuran (University of Akron)*, 1-76 (Master's thesis). Available from Electronic Thesis & Dissertation database. (UMI No. akron1353710697).
- Yam, W. S., & Yeap, G. Y. (2011). Nematogenic and smectogenic liquid crystals from new heterocyclic isoflavone derivatives: Synthesis, characterization and X-ray diffraction studies. *Chinese Chemical Letters*, 22(2), 229-232.
- Yan, J., Guo, Y., Altawashi, A., Moosa, B., Lecommandoux, S., & Khashab, N. M. (2012). Experimental and theoretical evaluation of nanodiamonds as pH triggered drug carriers. *New Journal of Chemistry*, 36(7), 1479-1484.
- Yeap, G.-Y., Hng, T.-C., Yeap, S.-Y., Gorecka, E., Ito, M. M., Ueno, K., . . . Imrie, C. T. (2009). Why do non-symmetric dimers intercalate? The synthesis and characterisation of the α -(4-benzylidene-substituted-aniline-4'-oxy)- ω -(2-methylbutyl-4'-(4''-phenyl) benzoateoxy) alkanes. *Liquid Crystals*, 36(12), 1431-1441.
- Yeap, G.-Y., Lee, H.-C., Mahmood, W. A. K., Imrie, C. T., Takeuchi, D., & Osakada, K. (2011). Synthesis, thermal and optical behaviour of non-symmetric liquid crystal dimers α -(4-benzylidene-substituted-aniline-4'-oxy)- ω -[pentyl-4-(4'-phenyl) benzoateoxy] hexane. *Phase Transitions*, 84(1), 29-37.
- Yeap, G.-Y., Mohammad, A.-T., & Osman, H. (2010). Synthesis, spectroscopic and mesomorphic studies on heterocyclic liquid crystals with 1, 3-oxazepine-4, 7-dione, 1, 3-oxazepane-4, 7-dione and 1, 3-oxazepine-1, 5-dione cores. *Journal of Molecular Structure*, 982(1), 33-44.
- Yeap, G.-Y., Osman, F., & Imrie, C. T. (2015). Non-symmetric dimers: effects of varying the mesogenic linking unit and terminal substituent. *Liquid Crystals*, 42(4), 543-554.
- Zakerhamidi, M., Keshavarz, M., Tajalli, H., Ghanadzadeh, A., Ahmadi, S., Moghadam, M., . . . Hooshangi, V. (2010). Isotropic and anisotropic environment effects on the UV/vis absorption spectra of three disperse azo dyes. *Journal of Molecular Liquids*, 154(2), 94-101.

- Zakerhamidi, M., Nejati, K., Sorkhabi, S. G., & Saati, M. (2013). Substituent and solvent effects on the spectroscopic properties and dipole moments of hydroxyl benzaldehyde azo dye and related Schiff bases. *Journal of Molecular Liquids*, *180*, 225-234.
- Zhou, X. (2014). *Multi-scale simulations of the UV-vis absorption spectra of organic chromophores in condensed phases* (Doctoral thesis, University of Geneva, Switzerland). Retrieved from <https://archive-ouverte.unige.ch/unige:40428>.

University of Malaya

LIST OF PUBLICATIONS AND PAPERS PRESENTED

Publications

Dzulkharnien, N. S. F., Salleh, N. M., Yahya, R., & Karim, M. R. (2017). Synthesis of imine-ester-linked benzothiazole mesogen containing liquid crystalline monomers with different terminal substituents. *Soft Materials*, 15(4), 292-301.

Presentation

Oral

- (a) Solvatochromism and thermochromism of side chain liquid crystalline polymers bearing azo-benzothiazole chromophore in the mesogen, The 1st Asian Researcher Symposium 2016, 25th-26th April 2016, Universitas Indonesia, Depok, Indonesia.

University of Malaya